NSF Grant ATM-0002256
National Science Foundation

A RADAR PERSPECTIVE ON THE VARIABILITY OF TROPICAL CONVECTION CHARACTERISTICS OVER THE SOUTHWESTERN AMAZON AND EASTERN PACIFIC REGIONS

by Luis Gustavo Pereira and Steven A. Rutledge

Colorado State University

DEPARTMENT OF ATMOSPHERIC SCIENCE

PAPER NO. 739

A RADAR PERSPECTIVE ON THE VARIABILITY OF TROPICAL CONVECTION CHARACTERISTICS OVER THE SOUTHWESTERN AMAZON AND EASTERN PACIFIC REGIONS

by

Luis Gustavo Paiva Pereira

and

Steven A. Rutledge

Department of Atmospheric Science

Colorado State University

Fort Collins, CO 80523

Research Supported by

National Science Foundation

under Grant ATM-0002256

Spring 2003

Atmospheric Science Paper No. 739

COLORADO STATE UNIVERSITY

March 25, 2003

WE HEREBY RECOMMEND THAT THE THESIS PREPARED UNDER OUR SUPERVISION BY LUIS GUSTAVO PAIVA PEREIRA ENTITLED A RADAR PERSPECTIVE ON THE VARIABILITY OF TROPICAL CONVECTION CHARACTERISTICS OVER THE SOUTHWESTERN AMAZON AND EASTERN PACIFIC REGIONS BE ACCEPTED AS FULFILLING IN PART REQUIREMENTS FOR THE DEGREE OF MASTER OF SCIENCE.

Committee on Graduate Work

Advisor

Department Head

ABSTRACT OF THESIS

A RADAR PERSPECTIVE ON THE VARIABILITY OF TROPICAL CONVECTION CHARACTERISTICS OVER THE SOUTWESTERN AMAZON AND EASTERN PACIFIC REGIONS

The focus of this study is to evaluate the intra-regional and inter-regional variability of tropical convection characteristics in the southwestern Amazon and eastern Pacific warm-pool regions. Convection is examined using radar data collected during two tropical field experiments: TRMM-LBA (Tropical Rainfall Measuring Mission – Large Scale Biosphere-Atmosphere in Amazonia) and EPIC (Eastern Pacific Investigation of Climate Processes in the Coupled Ocean-Atmosphere System).

In each of the two tropical regions studied, two distinct wind regimes have been observed to occur. In the southwest Amazon, one wind regime was called easterly regime and the other westerly regime. These changes in wind regime have been previously shown to be associated with the passage of baroclinic waves in the subtropical parts of Brazil and the formation of a synoptic-scale feature known as the South Atlantic Convergence Zone. In the east Pacific, one wind regime was called the northerly regime and the other southerly regime. The changes in wind regime over the east Pacific have been observed to be associated with the passage of easterly waves.

The variability of the convective characteristics is evaluated in each region as a function of time of day and wind circulation. Some of the features used to evaluate the characteristics of convection include convective area, convective fraction, reflectivity profiles, rain rates, warm rain statistics and ice fraction.

The results presented in this thesis showed that the easterly and northerly wind regimes more frequently featured characteristics of stronger convection: greater rain rates, greater reflectivities and convective fractions, deeper convective cores and smaller fractions of warm-rain-producing areas. The results also showed that the easterly regime was associated with higher ice fractions. The diurnal cycle results indicated that convection initiates in the morning and peaks in the afternoon over the southwest portion of the Amazon, whereas in the east Pacific the convection initiates after sunset and peaks just before sunrise. Variations associated with wind regime were shown to be more intense in the southwest Amazon. It was also found that the east Pacific region presented larger convective areas and convective fractions than the southwest portion of the Amazon. The eastern Pacific region was also associated with larger fractions of warm rain areas, but overall the fraction of rainfall owed to warm processes was very small and approximately the same in both regions.

Luis Gustavo Paiva Pereira
Atmospheric Science Department
Colorado State University
Fort Collins, CO 80523
Spring 2003

ACKNOWLEDGEMENTS

My deepest appreciation goes to Maria Assuncao Faus da Silva Dias, who initiated me in the scientific community, gave me the opportunity to take part in the LBA field program, and without whom I would have never been able to achieve my professional goals. Further thanks goes to Drs. Walt Petersen, Rob Cifelli, Larry Carey, Tom Rickenbach and Ali Tokay for their assistance, numerous discussions and valuable criticism. I would also like to thank Paul Hein for his computing guidance and patience throughout my research. Thanks to Margi Cech, Andrea Williams, Sarah Tessendorf, Laura Ciasto and Tracy Depue for their support. This research was also supported under National Science Foundation Grant ATM-0002256.

TABLE OF CONTENTS

LIST OF TABLES

LIST OF FIGURES

CHAPTER ONE

Introduction

1.1 Motivation and Objectives

Tropical meteorology has become an area of increasing interest and importance in the field of atmospheric science. Despite the fact that forty to fifty percent of Earth is in the tropics, most atmospheric-related research used to be focused in the middle-latitudes. The limiting factor to the development of tropical meteorology rested mostly in the fact that there were little or no atmospheric data available in tropical regions. Tropical observations and measurements were very difficult to obtain, since uninhabited regions, like vast ocean areas and rain forests, cover most of the tropics. In the last twenty-five years, our knowledge about the tropics has dramatically increased with the availability of tropical datasets collected during several field experiments. Some important tropical datasets include GATE (GARP Atlantic Tropical Experiment), EMEX (Equatorial Monsoon Experiment), DUNDEE (Down Under Doppler and Electricity Experiment), ABLE (Amazon Boundary Layer Experiment), TOGA-COARE (Tropical Ocean Global Atmosphere - Coupled Ocean Atmosphere Response Experiment), MCTEX (Maritime Continent Thunderstorm Experiment), TRMM (Tropical Rainfall Measuring Mission), LBA (Large Scale Biosphere-Atmosphere Experiment in Amazonia), TEPPS (Tropical Eastern Pacific Process Study) and EPIC (Eastern Pacific Investigation of Climate Processes in the Coupled Ocean-Atmosphere System).

The understanding of convection, and its temporal and spatial variability at different scales, is of paramount importance to comprehend how the tropics interact with the rest of the globe. Convection in the tropics tends to occur over the three continents that are intersected by the equator, i.e., South America, Africa and the Indonesian maritime continent (Krishnamurti *et al.*, 1973; DeMaria, 1985), and also in oceanic regions along the ITCZ (Intertropical Convergence Zone). It is also known that zonal variations in convection intensity are associated with asymmetries in the zonal atmospheric circulation (Bjerknes, 1969; Krishnamurti, 1971; Silva Dias *et al.*, 1983). The primary role of shallow cumulus clouds in the trade wind regime is to transport moisture upward toward the trade inversion layer to offset subsidence drying (Riehl *et al.*, 1951; Augstein *et al.*, 1973; Holland and Rasmussen, 1973; Nitta and Esbensen, 1974; Betts, 1975; Johnson *et al.*, 1999). The water vapor from the trade wind layer converges in the tropics to become the fuel for hot towers (Riehl and Malkus, 1958). Three-fourths of the energy that drives the atmospheric wind circulation comes from the latent heat release by tropical precipitation (Kummerow *et al.*, 2000). Convective intensity and/or rainfall measurements can be used to evaluate the distribution of systems that produce the bulk of the heat, momentum and moisture in the tropics and subtropics (Nesbitt *et al.*, 2000).

The objective of this study is to provide a comprehensive analysis of convective characteristics for two tropical regions using radar data. Analyzing the diurnal cycle and the wind-regime-dependent intraseasonal variations in convection in the Amazon and in the eastern Pacific warm pool region, this study focuses on identifying differences in convection between these two regions. Quantitative radar data is the prime tool for our

analyses used to characterize convection. Rainfall, cloud microphysical characteristics (as inferred from available polarimetric data) and the vertical and horizontal structures of convection are examined in this study.

1.2 TRMM/LBA Campaign Overview

The Tropical Rainfall Measuring Mission (TRMM) is a joint mission between the National Aeronautics and Space Administration (NASA) in the United States and the National Space Development Agency (NASDA) in Japan. It was created to diagnose tropical rainfall and the latent heat release associated with this rainfall to better understand the global atmospheric circulation. TRMM provides a comprehensive dataset on the spatial and temporal variation of rainfall over undersampled ocean and tropical regions.

The Large Scale Biosphere-Atmosphere Experiment in the Amazon (LBA) is an international research project led by Brazil. It was designed to understand the climatological, ecological, biogeochemical and hydrological functioning of the Amazon and how these functions are affected by land use change. It was also designed to study how the Amazon works as a regional entity and its influence on the global climate (Silva Dias *et al.*, 2002).

The TRMM/LBA was a major component of the NASA TRMM ground validation. It was conducted during the wet season months (Rao and Hada, 1990; Horel *et al.*, 1989) of January and February of 1999 in the State of Rondonia, Brazil. The area of intense measurements was located in the southwest portion of the Amazon between latitudes 9° S and 13° S and between longitudes 60° W and 64° W. Figure 1.1 depicts the

region where TRMM/LBA took place. This region was covered by an extensive array of instruments, including multiple radiosonde and tethered balloon sites, a lightning detection network, a rain gauge and disdrometer network, a dual-wavelength profiler, surface observing stations, micrometeorological towers, sodars, surface radiation measurements, two Doppler radars (one C-band, and one S-band with polarimetric capabilities) and also two aircraft, one of them carrying a third radar (X band).

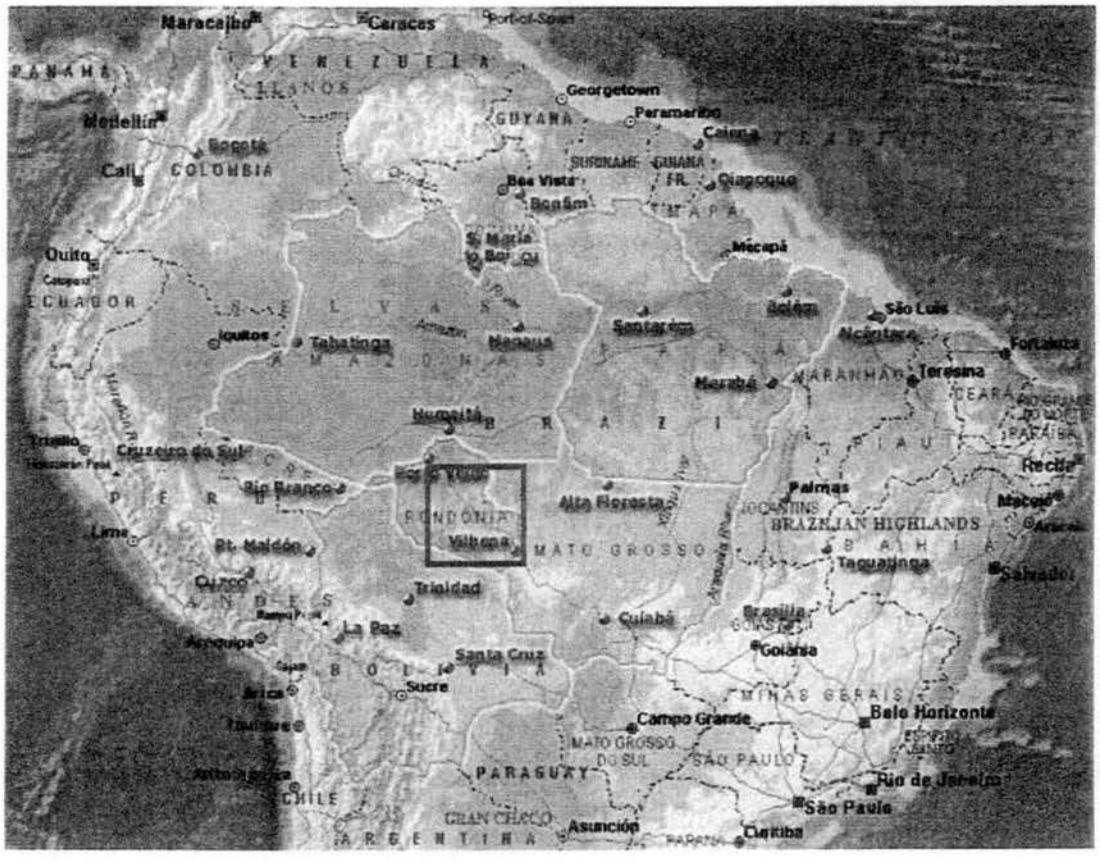

Figure 1.1 – South America Map. The box indicates the TRMM/LBA region.

Two distinct wind regimes were identified in the region during TRMM/LBA. The prevailing direction of the low-level zonal wind component switched five times during the campaign (Petersen *et al.*, 2002). Figure 1.2 depicts the 700-mb mean wind vectors

for two days during the TRMM/LBA, each one showing a different wind regime circulation pattern. The duration of each wind regime period varied between two and fourteen days. Petersen *et al.* (2002) determined the wind regime periods using radiosonde information collected during the TRMM/LBA. Table 1.1 summarizes the periods found for each wind regime circulation. The regime depicted in Figure 1.2a was called easterly regime and the regime depicted in Figure 1.2b was called westerly regime.

Two radars continually collected data, but the present study is based solely in the data collected by the S-pol radar. S-pol was developed by NCAR to provide an easy-to-transport Doppler polarimetric radar to the research community. The radar was located at 11.22° S and 62.00° W. The radar operating parameters can be found in Table 1.2.

Table 1.1 – TRMM/LBA wind regime periods (Petersen *et al.*, 2002).

Wind Regime	**Start Date**	**End Date**
Easterly	11 January, 1999	13 January, 1999
Westerly	14 January, 1999	18 January, 1999
Easterly	19 January, 1999	28 January, 1999
Westerly	29 January, 1999	07 February, 1999
Easterly	08 February, 1999	21 February, 1999
Westerly	22 February, 1999	28 February, 1999

a)

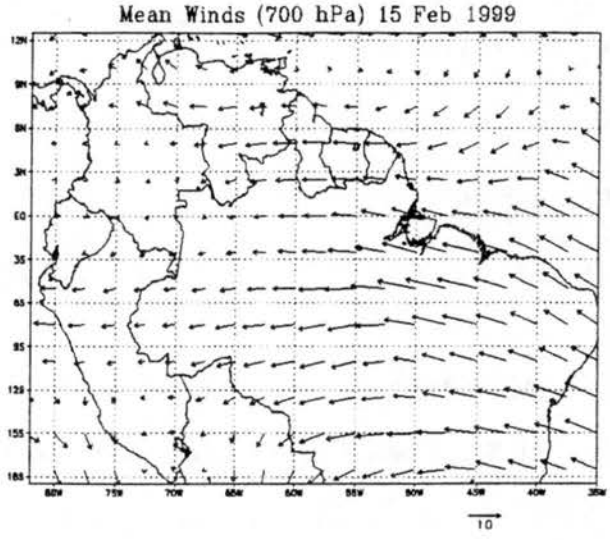

b)

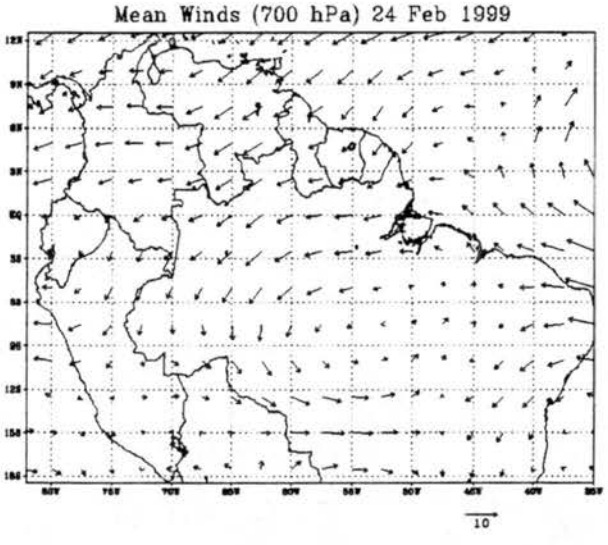

Figure 1.2 – TRMM/LBA Wind Circulation Patterns in a) an easterly regime day, and b) a westerly Regime.

Table 1.2: Operating specifications for radars in TRMM/LBA and EPIC campaigns.

Operating Specification	**TRMM/LBA (S-pol)**	**EPIC**
Wavelength	11 cm	5.4 cm
Pulse width	0.3 – 1.4 μs	1.2 - 2 μs
PRF	0 – 1300 Hz	500 – 910 Hz
Peak power	> 1 Mw	250 kW
Receivers	H & V simultaneously	H only
Beam width	0.91 °	0.95 °
Min. Detectable Signal	0 dBZ at 30 km	-12 dBZ at 30 km
Scan rate	Up to 18 °/sec each axis; 30 °/sec with pulley change	18 °/sec

1.3 EPIC Campaign Overview

The East Pacific Investigation of Climate Processes in the Coupled Ocean-Atmosphere System (EPIC) had two main components. The first component focused on the observation and understanding of the ocean-atmosphere processes responsible for the structure and evolution of the large-scale atmospheric heating gradients in the equatorial and northeastern Pacific portions of the cold tongue/ITCZ complex. This component would include the understanding of: a) the mechanisms governing the temperature and salinity field evolution in the region, b) the atmospheric planetary boundary layer

structure and evolution between the Equator and the ITCZ and c) the processes determining the existence, character and strength of the deep convection in the northeast Pacific ITCZ. The second component focused in understanding the dynamical, radiative and microphysical properties of the extensive boundary layer cloud decks in the southeasterly tradewind and cross-equatorial flow regime and their interactions with the ocean below (Weller *et al.*, 1999). The present study focus in the first component of EPIC, with an emphasis over the third aspect mentioned previously.

The first component of the EPIC campaign took place in September and October of 2001, between the Equator and 10° N along the 95°-W-meridian, where we focus our study. This region is located in the east Pacific warm pool region near the Central American coast, as illustrated by Figure 1.3. The observational platforms used in this campaign included the NOAA research vessel Ronald H. Brown, the NSF research vessel Horizon, a NOAA P-3 and the NCAR C-130 aircraft. The Ronald H. Brown was equipped with a C-band Doppler radar (operating specifications shown in Table 1.2), Doppler lidar, radiation instruments, sea surface thermometers, rain gauges, a wind profiler, air-sea flux system, standard surface meteorological instrumentation and also oceanographic instrumentation.

Three distinct easterly wave passages occurred during the EPIC campaign and, following the work of Petersen *et al.* (2003), we divide the days according to the meridional wind phase of the easterly wave. Different from previous studies, where the easterly wave was divided in eight phases (Reed and Recker, 1971) and four phases (Petersen *et al.*, 2003), here we chose to only use two phases to increase the statistical significance of the results in each period. The two phases used were named northerly

regime and southerly regime. The periods for each phase were determined using the meridional winds at 700 hPa, obtained from radiosonde data collected every 4 hours during the field campaign. The periods used in this study are shown in Table 1.3.

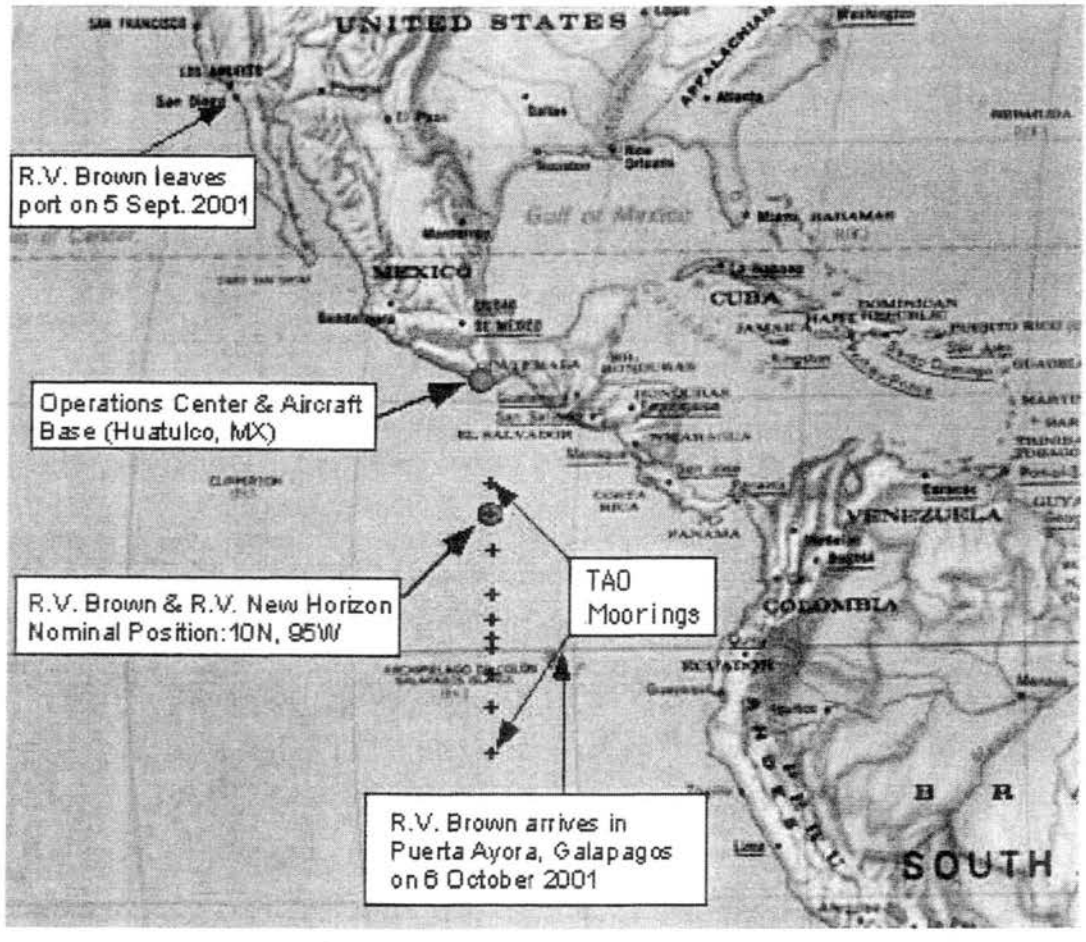

Figure 1.3 – Map depicting the EPIC intensive field campaign region.

Table 1.3 – EPIC wind regime periods (Dr. Walter Petersen, personal communication).

Wind Regime	Start Date	End Date
Northerly	12 September, 2001 - 00:00	16 September, 2001 - 11:59
Southerly	16 September, 2001 - 12:00	18 September, 2001 - 21:59
Northerly	18 September, 2001 - 22:00	21 September, 2001 - 03:39
Southerly	21 September, 2001 - 03:40	24 September, 2001 - 19:09
Northerly	24 September, 2001 - 19:10	28 September, 2001 - 02:29
Southerly	28 September, 2001 - 02:30	01 October, 2001 - 23:59

1.4 Scientific Background

Field experiments over different tropical regions have given a better insight into the variability and characteristics of tropical convection. This section describes some of the findings related to tropical convection characteristics that are pertinent to this study.

Using a coarse (i.e. 4 x 4 km) gridded radar dataset from GATE and subjective guidelines to partition convective and stratiform echoes, Cheng and Houze (1979) found that approximately 40% of the rainfall during the experiment was generated by stratiform features over the GATE oceanic region. They also found that convective clouds less than 5 km in depth produced a very small portion of the convective rainfall. Convective clouds that extended well above the freezing level, generally with echo tops heights between 10 and 13 km, generated the majority of the convective rainfall. Leary (1984) used the same set of partitioning guidelines defined by Cheng and Houze (1979) and also found that about 40% of the rainfall was generated by stratiform features. LeMone and Zipser (1980) and Zipser and LeMone (1980) found that only 10% of the updraft cores within GATE mesoscale convective systems (MCSs) had mean vertical velocities greater than 5 m/s, much weaker than convective updrafts over continental regions. Lucas *et al.* (1994) found similar vertical velocities during EMEX. Zipser and LeMone (1980) attributed these weak updrafts to smaller convective available potential energy (CAPE) values, found to be approximately 1500 J/kg in the GATE region. On the other hand, Szoke *et al.* (1986) suggested that differences between continental and maritime updraft strengths are more likely due to differences in the distribution of buoyancy with height. Zipser and LeMone (1980) found that the strongest updrafts would require one hour for a parcel to

travel from the lifting condensation level (i.e. cloud base) to the freezing level. This amount of time would be long enough for the collision-coalescence process to dominate droplet growth, in such a way that fall speeds become greater than the updraft before the droplet can reach the freezing levels.

Rutledge *et al.* (1992) used lightning data from DUNDEE to show that convective clouds produced during monsoonal circulation frequently lacked mixed-phase microphysical conditions to produce lightning. Monson circulation was associated with lower CAPE values, which was generally insufficient to result in updrafts of sufficient strength to allow cold cloud processes (e.g. riming, aggregation and deposition) to occur in the cloud. Lightning is thought to be more efficient in environments where ice crystals and supercooled droplets coexist. The convective clouds that formed during the DUNDEE experiment in the so-called break (i.e. non-monsoonal) period were associated with higher CAPE values, so updrafts were strong enough to allow mixed microphysical processes to occur. Lightning flash rates were observed to be more frequent during the break period (Rutledge *et al.*, 1992).

In the western Pacific warm-pool region, Lin and Johnson (1996) used sounding data from TOGA-COARE (Webster and Lukas, 1992) to describe the synoptic conditions over the experiment area. They identified three passages of the intraseasonal oscillation (ISO; Madden and Julian, 1994) during the intensive observing period of TOGA-COARE. Lin and Johnson (1996) showed that different characteristics of the ISO could be identified in the wind speed, rainfall and mean vertical motion time series. The inactive phase of the oscillation was characterized by weak winds. As the convective phase approached, the surface easterly winds increased in speed. Following the passage

of the convective phase, the winds would become westerly and increase their intensity. Three cruises took place during TOGA-COARE, each characterized by different phases of the ISO. DeMott and Rutledge (1998a, 1998b) described the differences in convective characteristics for each of the three cruises. The first cruise, which occurred during the inactive phase of the ISO, was characterized by shallow convection, but with intense cores, producing intense rain rates. The second cruise, which occurred during the convective phase of the ISO, was characterized by deep convection, though not particularly vertically intense, which produced light rain rates. The third cruise, which was dominated by convection associated with surface westerly winds, was characterized by intermediate echo top heights. Similar results were obtained by Rickenbach and Rutledge (1998).

During TRMM/LBA, convection was characterized in most studies according to the wind regime. Higher CCN concentrations (Williams *et al.*, 2002), larger droplet sizes (Tokay *et al.*, 2002), larger CAPE and CIN values (Cifelli *et al.*, 2002; Halverson *et al.*, 2002), higher ratios of convective precipitation, less cloud cover (Rickenbach *et al.*, 2002) and higher lightning activity (Williams *et al.*, 2002) were characteristics of the easterly regime. In the easterly regime, the predominant synoptic pattern was the development of isolated convective cells and also the propagation, across the Amazon, of squall lines (Pereira *et al.*, 2002) and instability waves that formed in the northern coast of Brazil, near the State of Para (Greco *et al.*, 1990; Cohen *et al.*, 1995). The westerly regime was characterized by less robust convection. It was associated with larger cloud cover and stratiform fraction (Rickenbach *et al.*, 2002), smaller droplets (Tokay *et al.*, 2002), smaller CAPE and CIN values (Cifelli *et al.*, 2002; Halverson *et al.*, 2002), lower

CCN concentrations and lower lightning activity (Williams *et al.*, 2002). In the westerly regime, the predominant synoptic pattern was the occurrence of convective cells embedded in large stratiform formations.

EPIC was also characterized according to the phase of the easterly wave. Petersen *et al.* (2003) showed that the northerly regime was characterized by CAPE values near 2000 J/Kg and smaller CIN (Convective Inhibition) values near - 5 J/Kg. The southerly regime indicated CAPE values near 1400 J/Kg and CIN values near –11 J/Kg. Atmospheric shear was strongest through the troposphere in the southerly regime. The northerly phase was also observed to be associated with a more vertically developed population of convective clouds and cloud-to-ground (CG) lightning (Petersen *et al.*, 2003). Boccippio *et al.* (2002) indicated that convection appeared to have a diurnal cycle that initiated after dusk and peaked overnight, consistent with the diurnal cycle observed over other oceanic regions (Nesbitt and Zipser, 2003). Petersen *et al.* (2003) also observed peaks in conditional rain rates, echo-top heights and vertical intensity of convection during the northerly phase of the easterly wave, and increased frequency of light precipitation in the southerly regime.

CHAPTER TWO

Data and Methodology

2.1 Data

Radar data from TRMM/LBA and EPIC field campaigns are used in this study. The TRMM/LBA dataset is composed of Plan Position Indicator (PPI) radar scans taken between 11 January 1999 and 28 February 1999. The EPIC dataset is composed of PPI radar scans obtained between 11 September 2001 and 1 October 2001. Surveillance and Range Height Indicator (RHI) scans were collected in both projects, but not used here.

2.2 Gridding Methodology

Radar volume scans from both campaigns (i.e. TRMM/LBA and EPIC) were interpolated to a Cartesian grid using NCAR's software REORDER. For TRMM/LBA three variables were interpolated: reflectivity (Z), differential reflectivity (Z_{dr}) and difference reflectivity (Z_{dp}). In the EPIC dataset, the only field to be interpolated was reflectivity, since the radar used during the EPIC campaign did not possess dual-polarimetric capabilities. Interpolation was done using a Cressman weighting function (Cressman, 1959) with a radius of influence of 1.5 km in the horizontal and 1.0 km in the vertical. The variables were interpolated horizontally to a 2-km grid and vertically to a 0.5-km grid, generating a total of 10201 grid points in the horizontal (i.e. 101 x 101) and 40 vertical levels. The interpolation methodology was chosen to be consistent with the

methodology used by Dr. Charlotte DeMott so the results presented here may be compared with those obtained for TOGA-COARE (DeMott and Rutledge, 1998a, DeMott and Rutledge, 1998b).

2.3 Convective and Stratiform Partitioning

In order to study various characteristics of tropical convection, a partitioning algorithm is often used to separate convective from stratiform precipitation. The method selected for our study is presented in Steiner and Houze (1993) and Steiner et al. (1995). This technique makes use of two criteria to determine if a given grid point is convective or stratiform. The procedure uses the 2-km level reflectivity field to run the algorithm. The first criterion, also called the absolute criterion, uses a fixed threshold of 40 dBZ, and assigns as convective any grid point with a reflectivity value greater or equal to this threshold. The second criterion, called the gradient criterion, uses the background reflectivity to determine if a grid point, with a reflectivity less than the absolute threshold, has convective characteristics. The background reflectivity is considered to be the region within an 11-km radius from the grid point. Therefore, if the grid point has a reflectivity value less than 40 dBZ, but 4.5 dBZ higher than the mean background reflectivity, the grid point is also tagged as convective. When the algorithm determines that a given a grid point is convective, all grid points in that column (above and below) are also considered convective. This assumption could cause some misclassification in regions of strong vertical shear, but we chose to not make any modifications to be consistent with other studies that made use of the same algorithm, such as DeMott and Rutledge (1998a, 1998b).

2.4 Reflectivity

The reflectivity is a measurement of the power that is backscattered to the radar. The reflectivity is a function of the power received by the radar (P_r), the distance to the target, the dielectric factor (K) of the target and the radar constant (C), as shown by equation 2.1.

$$Z = C\frac{P_r r^2}{|K|^2} \tag{2.1}$$

The value of $|K^2|$ for pure water is 0.93 (0.197 for ice). The radar constant is a function of several radar specifications, such as wavelength, beam width, pulse width, losses within the radar hardware, antenna gain and transmitter power. The relationship between reflectivity and target size depends on the radar wavelength. Most hydrometeors are much smaller than the radar wavelength and in these cases a relationship known as the Rayleigh approximation is used (Rayleigh valid for $r \leq 0.1\lambda$; where r is the radius of the hydrometeor). For this approximation, reflectivity is a function of the sixth power of the hydrometeor size, as it can be seen in equation 2.2.

$$Z = \int_0^\infty N(D)D^6 dD \qquad [mm^6/m^3] \tag{2.2}$$

where N(D) is the number density and D is the diameter of the targets. The equation above shows the importance of drop size distribution in the reflectivity value. Given a volume of 1 m^3, it takes 10^6 droplets with a diameter of 1 mm to produce the same reflectivity of one single droplet with a diameter of 10 mm.

The power transmitted by meteorological radars varies from several hundred kW to over 1 MW. The power received by the radar is typically many orders of magnitude less (e.g. 10^{-14} W). Therefore, reflectivity measurements are distributed in a large range of values. In order to simplify this reflectivity range a logarithmic scale is used, as indicated by equation 2.3. The unit used for the reflectivity is dBZ.

$$dBZ = 10\log_{10} Z \qquad \text{[dBZ]} \qquad (2.3)$$

Equation 2.3 normally yields values ranging from –30 to 70 dBZ. Values near the upper range are associated with intense convection and hail. Light rain is observed at reflectivity values near 10-20 dBZ.

In the present study, reflectivity is analyzed in two ways. The first analysis is the three-dimensional frequency distribution of reflectivities for each vertical level. Reflectivities were grouped in 5-dBZ intervals, and the frequency indicates the total number of occurrences of reflectivity values within that range. Analyses of this kind have also been used by Petersen and Rutledge (2001). The second type of reflectivity analysis is the diurnal variation of 45, 40, 35, 30, 25, 20, 15, 10, 5 and 0 dBZ heights. A dBZ height is the highest vertical level where that particular reflectivity value (± 2.5 dBZ) was observed in each grid point. Both analyses computed values only from grid points tagged as convective by the partitioning algorithm.

2.5 Rain rate (Z-R relationship)

Several techniques have been used to study raindrop size distributions (including disdrometers and aircraft measurements). Drop size distribution (DSD) is a fundamental quantity in radar meteorology since quantities are derived from moments of the DSD.

Reflectivity (as described in section 2.3) is a function of number density and drop diameter. If a certain drop size distribution is associated with a given rain rate, and also associated with a given reflectivity, we may calculate relationships linking the reflectivity to rain rate. Such relationships are known as Z-R relationships, and have the following general form:

$$Z = aR^b \qquad [\text{mm}^6/\text{m}^3] \qquad (2.4)$$

where Z is the reflectivity (mm^6/m^3); R is the rain rate (mm/h), and a and b are empirical constants.

Many Z-R relationships have been determined (Battan, 1973). One of the most commonly used Z-R relationships is known as the Marshall-Palmer relationship and is given by:

$$Z = 200R^{1.6} \qquad [\text{mm}^6/\text{m}^3] \qquad (2.5)$$

This Z-R relationship uses a DSD of the form, $N(D) = N_0 e^{-\lambda D}$ where N(D) is the number of drops per unit volume per size interval, N_0 is the slope intercept (cm^{-4}) and λ is the slope of the distribution (cm^{-1}). N_0 has a value of 8×10^{14} cm^{-4} for the so-called Marshall-Palmer distribution.

In this study we make use of 3 Z-R relationships. The first two were calculated using TRMM/LBA data (Carey *et al.*, 2000), one using easterly regime days (Equation 2.6a) and one using westerly regime days (Equation 2.6b). The other relationship (Equation 2.6c) was calculated using radar and aircraft data during EPIC (Dr. Robert Cifelli, personal communications) using all days regardless of the wind regimes described in the first chapter.

$$Z = 531R^{1.08} \qquad [\text{mm}^6/\text{m}^3] \qquad (2.6a)$$

$$Z = 426R^{1.11} \qquad [\text{mm}^6/\text{m}^3] \qquad (2.6b)$$

$$Z = 218R^{1.6} \qquad [\text{mm}^6/\text{m}^3] \qquad (2.6c)$$

Rain rate information is used to create cumulative relative frequency plots of rain rate. The cumulative frequency was calculated for 25 rain rate intervals, using 1.0 mm/h intervals, ranging from 0 mm/h to 25 mm/h. The rain rate was calculated only at convective grid points.

2.6 Differential Reflectivity (Z_{dr})

Polarimetric radars, like S-pol, are capable of transmitting and receiving both horizontally and vertically polarized radiation. This capability allows the radar to measure the reflectivity in each of these two components. One useful parameter that can be calculated from horizontal and vertical reflectivities is the Differential Reflectivity (Z_{dr}). The Differential Reflectivity represents the ratio between the horizontal and vertical

returned power. As in the case of reflectivity, this ratio also generates numbers in a wide range of values, so a logarithmic scale is also used (Equation 2.7).

$$Z_{dr} = 10\log_{10}\left(\frac{Z_h}{Z_v}\right) \qquad \text{[dB]} \qquad (2.7)$$

As it has been discussed before, reflectivity is a measure of the power backscattered by targets (e.g. droplets, ice crystals and hail), and larger targets reflect more power. Since the reflectivity is proportional to the diameter of the particle, if the vertical and horizontal diameters are equal, then the vertical and horizontal reflectivities will also be equal. Therefore, the ratio of the reflectivities will be 1.0, yielding a Z_{dr} of 0 dB. Thus, spherical targets (e.g. hailstones) will be identified in the Z_{dr} field by values near zero (Aydin *et al.*, 1984). Raindrops with diameters greater than 1 mm deform into oblate spheroids (Pruppacher and Beard, 1970). Hence, the ratio between the reflectivities will be greater than 1.0, yielding positive Z_{dr} values. The larger the raindrop, the more oblate it becomes, and thus, the greater is the corresponding Z_{dr}. Negative Z_{dr} values would be observed when the horizontal reflectivity (cross-section) is less (smaller) than the vertical reflectivity (cross-section). These values can be produced by some ice crystal shapes and certain hail types (Aydin and Zhao, 1990; Zrnić *et al.*, 1993; Hubbert *et al.*, 1998). Therefore, differential reflectivity provides a measure of the shape of meteorological targets. Z_{dr} was used in this study only to calculate the median drop diameter (D_o) described in the next section. No attempt was made to analyze the Z_{dr} statistics.

2.7 Median Drop Diameter (D_0)

The median drop diameter, also known as D_0, is defined as the drop size such that droplets less than this value contribute to half the total rainwater content (W).

$$\frac{\pi}{6}\rho_w \int_0^{D_0} D^3 N(D) dD = \frac{1}{2} W \qquad (2.8)$$

D_0 can be determined from the slope of an exponential drop size distribution Λ (Bringi and Chandrasekar, 2001). Since Z_{dr} is also a function of Λ (Seliga and Bringi, 1976; 1978), Z_{dr} can be expressed as a function of D_0. For an exponential drop size distribution, $\Lambda D_0 = 3.67$ (Marshall-Palmer distribution). However, the exponential drop size distribution form is not representative of instantaneous drop size distributions (Bringi and Chandrasekar, 2001). Ulbrich (1983) showed that $\Lambda D_0 = 3.67 + \mu$, where μ is the shape parameter.

Using a family of observed gamma drop size distributions, it is possible to obtain a $Z_{dr} - D_0$ relationship. In this study, two relationships are used (equations 2.9a and 2.9b) obtained, respectively, by Bringi and Chandrasekar (2001) and Dr. Ali Tokay (personal communications).

$$D_0 = 1.529(Z_{dr})^{0.467} \quad \text{[mm]} \qquad (2.9a)$$

$$D_0 = 1.877(Z_{dr})^{0.880} \quad \text{[mm]} \qquad (2.9b)$$

D_0 is calculated in the upper core region of the cloud (i.e. the region of the cloud above 5 km with reflectivity values greater than 30 dBZ). In this region, a mixture of different hydrometeors types is found (e.g. supercooled droplets, ice crystals and hail). The mixed phase region of a cloud can be idealized as a mixture of oriented oblate raindrops and isotropically oriented ice particles (Bringi and Chandrasekar, 2001). Even when ice particles tend to deviate from the spherical assumption, this is mitigated by the fact that they tend to tumble as they fall (Pruppacher and Klett, 1997) and they have a significantly lower dielectric constant than water (Seliga and Bringi, 1976; Herzegh and Jameson, 1992). Since ice crystals are either isotropically oriented or tumble as they fall, the values of the vertical and horizontal reflectivity values for ice can be assumed equal. That is:

$$Z_h^{ice} = Z_v^{ice} \qquad [\text{mm}^6/\text{m}^3] \qquad (2.10)$$

Thus, if we substitute equation 2.10 into equation 2.7 we will find out that ice produces a Z_{dr} value equal to zero. Therefore, negative and near-zero Z_{dr} values will be usually associated with some ice crystal shapes and certain hail types (Aydin and Zhao, 1990; Zrnić *et al.*, 1993; Hubbert *et al.*, 1998). The positive Z_{dr} values in the upper core region will be associated with supercooled droplets and ice crystals. Supercooled droplets will usually be associated with greater Z_{dr} values than ice crystals.

In this study, the diurnal and wind-regime variability of the median drop diameter of supercooled droplets is investigated in the upper core region of convective of

convective clouds in the TRMM/LBA region. Differential reflectivity information was not available during EPIC, thus no D_0 statistics are possible.

2.8 Difference Reflectivity (Z_{dp})

The difference reflectivity (Z_{dp}) is another useful parameter that can be calculated from horizontal and vertical reflectivities. The difference reflectivity represents the difference between the horizontal and vertical returned power. Like in the case of reflectivity, this difference also generates numbers in a wide range of values, so a logarithmic scale is also used (Equation 2.11).

$$Z_{dp} = 10\log_{10}\left(Z_h - Z_v\right) \qquad \text{[dB]} \qquad (2.11)$$

In equation 2.11, each reflectivity component represents the total reflectivity produced by raindrops and all other hydrometeor types. So they may be written as:

$$Z_h = Z_h^{rain} + Z_h^{ice} \qquad [\text{mm}^6/\text{m}^3] \qquad (2.12a)$$

$$Z_v = Z_v^{rain} + Z_v^{ice} \qquad [\text{mm}^6/\text{m}^3] \qquad (2.12b)$$

As mentioned in the previous section, the mixed phase region of a cloud can be idealized as a mixture of oriented oblate raindrops and isotropically oriented ice particles (Bringi and Chandrasekar, 2001). Under this assumption, equation 2.10 showed that the values of the vertical and horizontal reflectivities for ice could be assumed equal.

Therefore, if we substitute equation 2.10 into equation 2.12a, and then substitute this result and equation 2.12b into equation 2.11, we find that:

$$Z_{dp} = 10\log_{10}\left(Z_h^{rain} - Z_v^{rain}\right) \qquad \text{[dB]} \qquad (2.13)$$

Equation 2.13 shows that Z_{dp}, as opposed to the reflectivity itself, is a parameter that is only sensitive to raindrops. So, for regions where only rain is present, the horizontal reflectivity and the difference reflectivity will be highly correlated. Figure 2.4 shows a scatterplot of horizontal reflectivities and their corresponding difference reflectivities (Bringi and Chandrasekar, 2001). As it can be seen, there is a very tight clustering of points, so we may find a representative linear equation for these points using a least-squares fit. The resulting line is also known as rain line, and it has the general form of:

$$Z_{dp} = aZ_h - b \qquad \text{[dB]} \qquad (2.14)$$

Previous works have found the coefficients a and b to be, respectively, 1.2 and 15.4 (Golestani *et al.*, 1989), 1.13 and 9.1 (Conway and Zrnic, 1993) and 1.10 and 9.4 (Carey and Rutledge, 1996).

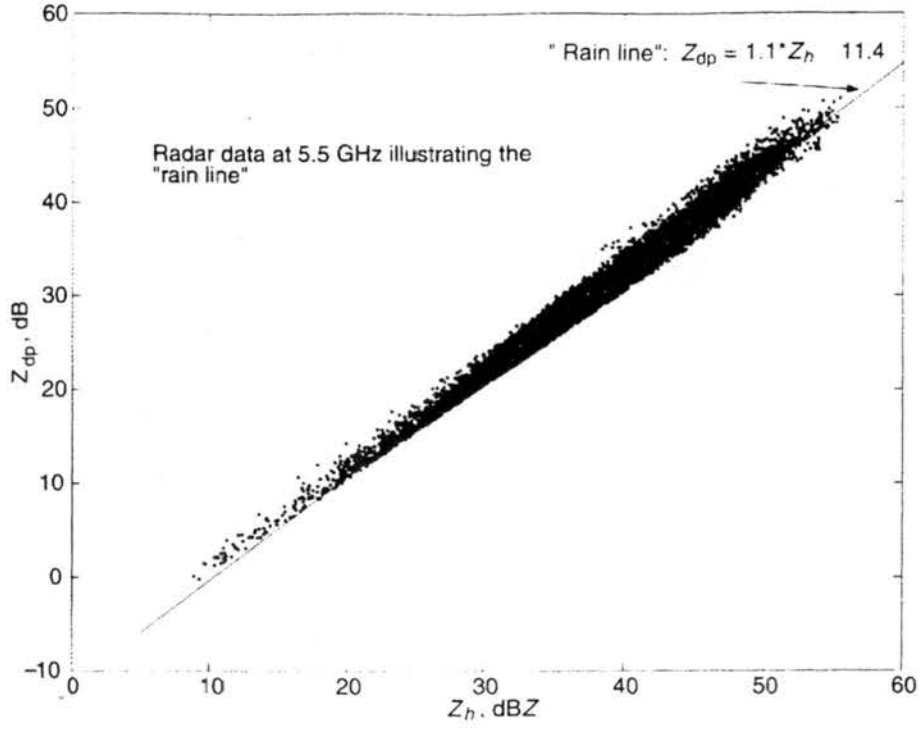

Figure 2.1 – Z_h – Z_{dp} relationship showing the rain line (Bringi and Chandrasekar, 2001)

For radar volumes containing a mixture of raindrops and ice particles, the total horizontal reflectivity will be higher than the horizontal reflectivity of rain only. However, the difference reflectivity should be the same since it is arguably insensitive to ice. Hence, the corresponding points in Figure 2.1 would lie to the right of the rain line (since in the mixed region, Z_{dp} would be the same of rain, but Z_h would be greater). Points lying to the left of the line are probably associated with ice crystals that are not isotropically oriented. For a given Z_{dp} value, let ΔZ be the difference between the reflectivity in the mixed region and the reflectivity of the rain line. After algebraic manipulation, it can easily be shown that:

$$f = \frac{Z_h^{ice}}{Z_h} = 1 - 10^{-0.1(\Delta Z_h)} \qquad (2.15)$$

where f is the ice fraction or the ratio of the equivalent ice reflectivity to the total equivalent reflectivity. Therefore, difference reflectivity can be used to determine ice fractions in the upper mixed regions of the clouds. Difference reflectivity was used only to calculate the water and ice masses. No attempt is made in this study to evaluate the Z_{dp} variability.

2.9 Water Mass and Ice Mass calculations

Water and ice masses can be calculated once the ice fraction is determined using power law relations. The ice water content relationship has the following form:

$$IWC = a(fZ_h)^b \qquad [g/m^3] \qquad (2.16)$$

In Equation 2.16, the coefficient *a* is associated with the drop size distribution, and given as 0.57, whereas the coefficient *b* can be established either empirically or through coordinated radar and aircraft data. The water and ice masses used in this study were calculated in the same way as in Cifelli *et al.* (2002). The ice mass was calculated using equation 2.17.

$$M_{ice} = 1000\pi \left(\frac{\rho_i}{\rho_a} \right) N_o^{3/7} \left(\frac{5.28x10^{-18} Z_h^{ice}}{720} \right)^{4/7} \quad \text{[g/kg]} \qquad (2.17)$$

where ρ_i is the ice density (0.917 kg/m^3), ρ_a is the air density in kg/m^3; N_0 ($4x10^6$ m^{-4}) is the intercept parameter of an assumed inverse exponential distribution for ice (Carey and Rutledge, 2000); Z_h^{ice} is the horizontal reflectivity of ice crystals in mm^6/m^3.

The water mass was calculated depending on the existence or not of mixed precipitation in the volume. The ΔZ (as described in section 1.4.5) standard error (1.1 dB) is multiplied by a constant that increases linearly with increased distance below the melting level. If ΔZ is greater than this parameter, then mixed precipitation is assumed and the water mass was calculated using equation 2.18.

$$M_{water} = 3.44x10^{-3} \left(Z_h^{rain} \right)^{4/7} \quad \text{[g/kg]} \qquad (2.18)$$

If ΔZ is less than this parameter, then pure rain is assumed and the water mass was calculated using equation 2.19.

$$M_{water} = 0.7x10^3 \left(\frac{Z_v^{4.159}}{Z_h^{3.273}} \right) \quad \text{[g/kg]} \qquad (2.19)$$

Water and ice mass were only calculated from the TRMM/LBA using S-pol data. Difference reflectivity was not available in the EPIC dataset. In TRMM/LBA the

instantaneous ratio of ice to total (water + ice) mass is evaluated. Analysis is done through a relative frequency plot of ice fraction. This analysis only takes into account information from the upper core region of the cloud. By upper core region is meant the grid points at or above the 5-km level with reflectivities greater or equal to 30 dBZ. Only convective grid points were used in these analyses.

2.10 Warm and Mixed Rain

In order to gain insight into the microphysical processes dominating raindrop formation and precipitation in general, precipitation may be separated into two groups: warm and mixed. Warm rain is produced by raindrops that grow by condensation followed by collision and coalescence. Mixed precipitation, on the other hand, involves both warm and cold cloud processes, the latter consisting of processes such as aggregation, riming and deposition. In the tropics, cold cloud processes are only observed when the cloud has a significant vertical growth, where parts of the cloud are above the freezing level.

Echo top information can be used to determine if a cloud has grown past the freezing level. The freezing level in both tropical regions studied here is found near 5 km. Hence, if a convective grid point shows an echo top below 5 km, the rain associated with it is assumed to be warm, otherwise the precipitation is tagged as mixed. For this study, the echo top threshold was chosen to be 5 dBZ. Attempts to use lower thresholds failed because the interpolation process smoothed the data, and 0 dBZ grid points were not very common, causing the rain type information to be thrown out. The rain type analysis was

done by evaluating the fraction of rain-producing areas and rain volume associated with warm rain processes.

2.11 Instantaneous Convective and Stratiform Areas

Convective and stratiform areas may be calculated by assuming that all the area surrounding a grid point also possesses the same characteristics. Since the grid points are horizontally spaced every 2 km, the "area of influence" of each grid point is 4 km^2. Therefore, for every grid point tagged as convective, a convective area of 4 km^2 is assumed. The total convective and stratiform areas were calculated based on the number of convective and stratiform grid points at the 2-km level.

Two analyses are made using convective and stratiform area information. The first analysis is the cumulative relative frequency of convective areas. The second analysis is the relative frequency of convective fraction, or convective-to-total echo area.

CHAPTER THREE

TRMM/LBA Intra-regional Variability

3.1 Overview

Radar-determined characteristics of convection in the southwestern portion of the Amazon are described in this chapter. We chose to evaluate convection by examining four main features: horizontal structure, vertical structure, precipitation characteristics (i.e. rain rate and rain type) and the upper core characteristics (i.e. ice fraction and diameter of supercooled droplets). These four components are analyzed by examining the variability associated with wind regime and with the diurnal cycle.

The variability associated with the diurnal cycle is investigated by dividing the day into six periods of four hours, with the first period beginning at 00:00 and ending at 03:59 (local time). The variability associated with wind regime is investigated by using the predominant zonal wind circulation, easterly and westerly regimes. The periods for each wind regime have been previously shown in Chapter One. More information about the TRMM/LBA campaign may be found at Silva Dias *et al.* (2002) and Cifelli *et al.* (2002).

3.2 Convective Horizontal Structure

In this section the horizontal characteristics of convection are evaluated by examining two reflectivity-derived products: convective area and convective fraction.

The convective area is the instantaneous total area covered by all convective features at any given time. The convective area is determined in the 10,000-km^2 domain using twenty-five 100-km^2 intervals, the relative frequency of observations within each of these intervals is calculated for each time period and wind regime. The convective area plots are shown in terms of cumulative relative frequency. The convective area is affected by the number of convective features within the domain as well as the size of individual convective features. Hence, smaller convective areas are associated with either a smaller number of individual convective systems and/or the occurrence of smaller convective systems. The convective fraction uses information from the convective and stratiform areas. The convective fraction shows the instantaneous ratio of the area occupied by all convective features to the area covered by precipitation (i.e. both convective and stratiform precipitation features). The relative frequency of the convective fraction is calculated for ten decimal intervals ranging from 0 to 1.

3.2.1 Convective Area

Figure 3.1a shows the convective area variability associated with the wind regimes. Since the easterly curve is always above the westerly curve, a higher frequency of larger convective areas occurred in the westerly regime. In the easterly regime 56% of observations indicated convective areas less than 100 km^2, whereas in the westerly regime this same range of areas represents 36% of all observations in this regime. The greatest difference between the easterly and westerly curves occurred for convective areas less than 800 km^2, where this difference is greater than 20%. In the easterly regime, each convective area interval beyond 800 km^2 accounts for less than 1% of observations,

whereas in the westerly regime the same occurs only for convective area intervals beyond 1600 km^2. In the easterly regime, a greater relative frequency (not cumulative) occurred only in the four smallest intervals (i.e. < 100, 100-200, 200-300 and 300-400 km^2). These results indicate that the westerly regime is associated with larger convective areas, which may be caused by either a greater number of individual convective systems or larger convective features.

Figure 3.1b shows the convective area variability associated with the diurnal cycle. It can be seen that the most sloped curves are the afternoon (12-16) and early evening (16-20) curves. These curve are associated with lower frequencies in the lowest intervals and higher frequencies in the intermediate intervals. Hence, the convection is more widespread in the afternoon and early evening, with 64% of observations between 13:00 and 13:59 indicating convective areas greater than 100 km^2, regardless of wind regime.

Figure 3.2a (b) shows the convective area variability associated with the diurnal cycle during the easterly (westerly) regime. These two plots are a combination of the effects of diurnal cycle and wind regime and should show a mixture of the characteristics observed in Figure 3.1. The easterly regime diurnal variability (Figure 3.2a) shows the lowest frequency of small convective areas (i.e. less than 100 km^2) occurring in the late afternoon and early evening period (16-20). Between midnight and noon, the total convective area was less than 100 km^2 in more than 60% of observations, whereas between 16:00 and 20:00 this frequency drops to 42%. In the morning (08-12) 90% of observations show that the total convective area is less than 500 km^2. These results indicate that, in the easterly regime, the convection peaks in size and occurrence in the

late afternoon and early evening hours evening (12-16) and is least frequent and smallest in the morning (08-12). The westerly regime diurnal variability (Figure 3.2b) shows that the smallest total convective area intervals are least frequent in the afternoon hours (12-16) and most frequent at night (20-00). During the late night and early morning hours (00-08) total convective area observations between 700 and 1100 km^2 are less frequent than at other times of the day. Thus, there are two groups of total convective area observations between 00:00 and 08:00: one group of small convective areas (less than 400 km^2) and another group of large convective areas (greater than 1300 km^2).

In summary, larger total convective areas are observed in the westerly regime. During the easterly regime, the convection peaks, in size and occurrence, later in the day than in the westerly regime. The largest convective areas are observed to occur in the late afternoon and early evening (afternoon) hours during the easterly (westerly) regime. In the westerly regime, there is also a secondary maximum in total convective area that occurs between 00:00 and 08:00. Observations of small convective areas (i.e. less than 100 km^2) are most frequent in the late night (night) hours during the easterly (westerly) regime.

3.2.2 Convective Fraction

Figure 3.3a shows the convective fraction variability associated with the easterly and westerly regimes. It can be seen that the majority of the observations indicate fractions varying between 0.2 and 0.5. Another important feature of this plot is that the easterly curve is slightly displaced to the right, indicating a higher frequency of larger convective fractions in the easterly regime. Since the convective area is greater in the

westerly regime (as discussed in section 3.2.1), then the smaller convective fractions observed in the westerly regime can only be explained by significantly larger stratiform areas of precipitation.

Figure 3.3b shows the convective fraction variability associated with the diurnal cycle using all observations regardless of wind regime. It can be seen that most right-shifted curve is the late afternoon and early evening (16-20) curve. This curve is associated with higher frequencies in the intermediate fraction intervals. Hence, the convection is more dominant in the late afternoon and early evening hours, with approximately 30% of observations between 16:00 and 19:59 showing convective fractions greater than 0.5. The largest convective fractions are least frequent near sunrise (04-08), when 15% of observations indicate fractions greater than 0.5.

Figure 3.4a shows the convective fraction variability associated with the diurnal cycle during the easterly regime. Figure 3.4b shows the same variability during the westerly regime. One striking difference between these two figures is that there is a much higher frequency of lower convective fractions in the westerly regime, especially at the late night hours (00-04). The easterly regime diurnal variability (Figure 3.4a) does not show a very clear diurnal cycle pattern. The curves appear to be shifted to the right with respect to the overall TRMM/LBA diurnal cycle plot (Figure 3.3b). During the night and early morning hours (00-08), 18% of convective fractions are observed to be greater than 0.5, whereas in the late afternoon and early evening hours (16-20) 36% of the convective fractions exceed 0.5. In the westerly regime, convective fractions greater than 0.5 are most infrequent in the late night period (00-04), when 13% of all observations in the westerly regime exceed a convective fraction of 0.5. This same range of convective

fractions is most frequent in the westerly regime during the late afternoon and early evening hours, representing 23% of the observations.

In summary, larger convective fractions are observed in the easterly regime. Larger convective fractions are most frequent in the late afternoon and early evening hours and least frequent overnight. Large convective areas coupled with small convective fractions in the westerly regime indicate that comparatively larger stratiform precipitation areas are found in the westerly regime.

3.3 Convective Vertical Structure

In this section, the vertical characteristics of convection are examined. The first product, the reflectivity distribution, shows the absolute frequency of reflectivities with height occurring in a time period or wind regime. The absolute frequency was calculated for a total of 16 1-km vertical levels, between 2.5 and 17.5 km. Reflectivities were grouped into eight 5-dBZ bins starting at 20 dBZ. The reflectivity distribution is affected by the number and the size of convective features, and also by the intensity of individual convective features. Therefore, a smaller number of observations should indicate that convection is less frequent and less intense at a certain time and/or wind regime. Vigorous convection should appear as an increase in the frequency in the higher reflectivity intervals. The reflectivity (or dBZ) height represents the maximum height in a convective column where that particular reflectivity interval was observed. Thus, the 30-dBZ height indicates the maximum height in a convective column where a 30-dBZ (± 2.5) reflectivity was observed. Ten reflectivity heights, between 45 and 0 dBZ, were calculated for each regime and averaged every hour. The reflectivity heights show an

averaged vertical profile of the convective cloud, similar to what one would see in a vertical cross-section.

3.3.1 Reflectivity Distribution

Figure 3.5 shows the absolute frequency of reflectivities versus height during the easterly regime (Figure 3.5a) and westerly regime (Figure 3.5b) respectively. The most important and striking differences between the two regimes are the higher frequency of reflectivities greater than 45 dBZ in the lowest levels in the easterly regime and also a higher frequency of lower reflectivities in the westerly regime. During the westerly regime periods, there were 17204 observations of reflectivities greater than 45 dBZ at 2.5 km, representing less than 3% of all the observations. On the other hand, during the easterly regime periods there were 32456 observations of reflectivities greater than 45 dBZ, representing approximately 7.5% of all observations. Therefore, easterly regime convective clouds usually have more intense cores than westerly regime convective clouds, consistent with previous studies such as Cifelli *et al.* (2002) and Petersen *et al.* (2002).

Figure 3.6 show the reflectivity distribution variability associated with the diurnal cycle during the easterly regime periods, and Figure 3.7 shows the same variability for westerly regime periods. The easterly regime shows a minimum number of observations in the morning (Figure 3.6c). The maximum number of observations occurs in the afternoon (Figure 3.6d) and early evening (Figure 3.6e) hours. In the 4-hour period of the afternoon (i.e. 12:00 to 15:59) there were 14460 observations at 2.5 km showing reflectivities greater than 45 dBZ, representing approximately 10% of all observations at

that height. The morning hours (i.e. 08:00 to 11:59) had 747 observations greater than 45 dBZ at the same height (2%). The westerly regime also shows a minimum number of observations in the morning hours (Figure 3.7c), whereas the maximum occurs in the afternoon hours (Figure 3.7d). In the morning hours, there were 1657 observations greater than 45 dBZ at 2.5 km (less than 1% of observations), and in the afternoon hours there were 7436 observations greater than 45 dBZ at that same height (3%). In both regimes, the higher (lower) number of observations is associated with the higher (lower) frequency of high reflectivities.

In summary, easterly regime convection has a greater frequency of intense cores. Convection is most frequent and most intense in the afternoon hours and least frequent and least intense in the morning hours. Distribution variability associated with the diurnal cycle is greater in the easterly regime.

3.3.2 Reflectivity Heights

Figure 3.8 shows the hourly-averaged reflectivity heights during the easterly regime (Figure 3.8a) and westerly regime (Figure 3.8b) periods. The easterly regime has greater variability over the diurnal cycle, where the maximum 0-dBZ heights occur between 16:00 and 17:00 and the minimum occurs between 08:00 and 10:00. This is in agreement with previous results discussed in this chapter. The westerly regime shows that the maximum heights occur between 20:00 and 21:00 and the minimum occurs between 10:00 and 11:00. Therefore, it appears that there is a lag between the easterly and westerly convective life cycles. Average reflectivity heights are always higher by at least 500 m in the easterly regime. Another important difference between the easterly and

westerly vertical profiles is the height of the 45-dBZ contour. In the easterly regime, the 45-dBZ level peaks near 4 km, whereas in the westerly regime the peak height for this reflectivity value is 1 km lower. The difference in reflectivity heights between the two wind regimes is as much as 1.5 km for the 0 and 5 dBZ heights. The standard deviation of heights increases for lower dBZ values. In the easterly regime, the standard deviation of heights varies between 2.1 km (for the 30-dBZ height) and 4.1 km (for the 0-dBZ height). In the westerly regime, the standard deviation varies between 1.6 km (30-dBZ height) and 3.3 km (0-dBZ height). Therefore, the standard deviation is significantly larger in the easterly regime, indicating a larger variability of reflectivity heights, and thus vertical cloud structure, associated with the diurnal cycle.

3.4 Convective Precipitation

The evaluation of the characteristics of convective precipitation is accomplished by: 1) investigating the intensity of the precipitation through the frequency and variability of rain rates; and 2) investigating the type of precipitation through the frequency and variability of the fraction of precipitation areas and rainfall volume associated with warm rain. The rain rate is a loose proxy for convective intensity. The rain rate was calculated using the Z-R relationships described in Chapter Two. Different Z-R relationships are used for each wind regime. The warm- rain-producing area analysis is the percentage of the raining area owed to warm rain processes. The warm rain volume analysis is the fraction of the total convective rainfall associated with warm rain processes.

3.4.1 Precipitation Intensity

Figure 3.9 shows the rain rate variability associated with the easterly and westerly regimes. It can be seen that the westerly curve is always above the easterly curve, indicating that light precipitation is slightly more frequent in the westerly regime. In the easterly regime 65% of observations indicated rain rates less than 1.0 mm/h, whereas in the westerly regime this same range of rain rates represents 68% of all observations in this regime. Overall there is little variation in the distance between the curves. This indicates that the rain rate frequency is nearly the same in both wind regimes for the intervals shown in Figure 3.9. Figure 3.9 also shows that rain rates greater than 29 mm/h represent less than 2% of occurrences in the westerly regime, but in the easterly regime they represent 5% of occurrences.

Figure 3.10a (b) shows the rain rate variability associated with the diurnal cycle during the easterly (westerly) regime. The easterly regime diurnal variability (Figure 3.10a) shows that light precipitation (less than 1.0 mm/h) is more predominant near sunrise (04-08) and during the morning hours (08-12), with as much as 98% of the rain rates in this category between 08:00 and 09:00. Light precipitation is least frequent in the afternoon period (12-16), when rain rates less than 1.0 mm/h can account for as low as 47% of observations between 16:00 and 17:00. Rain rates greater than 25 mm/h correspond to less than 12% of observations at all times of the day. Rain rates greater than 35 mm/h, 50 mm/h and 70 mm/h correspond, respectively, to 9%, 6% and 4% of the observations in the easterly regime. The westerly regime diurnal variability (Figure 3.10b) shows minimum and maximum frequency of light precipitation before the easterly extremes. Light precipitation is most frequent in the late night and morning hours (00-12), with as much as 84% of the rain rates being less than 1.0 mm/h at 10:00. Light

precipitation is least predominant in the afternoon and evening (12-00), with 55% of rain rates observed to be less than 1.0 mm/h at 14:00. Rain rates greater than 25 mm/h correspond to 8% of all observations in the westerly regime. Rain rates greater than 35 mm/h, 50 mm/h and 70 mm/h correspond, respectively, to as much as 5%, 3% and 2% of observations.

In summary, lighter precipitation is slightly more frequent in the westerly regime, but heavier precipitation (i.e. rain rates greater than 35 mm/h) in the easterly regime is twice as frequent as in the westerly regime. Lighter rain rates are least frequent in the afternoon and evening hours and most frequent in the late night and morning hours.

3.4.2 Precipitation Type

Figure 3.11a (b) shows the diurnal variability, for each wind regime, of the fraction of rain-producing areas (rainfall volume) that is associated only with warm rain processes (e.g. condensation, collision and coalescence). Hence, Figure 3.11a represents the fraction of the convective areas that are deemed to be raining via warm rain processes (refer to Chapter Two for warm rain definition). Figure 3.11b represents the fraction of the total convective rainfall that was produced by warm rain processes. It can be seen in Figure 3.11a that the westerly curve is 92% of the time (or 22 out of the 24 hours) above or leveled with the easterly curve, indicating a higher fraction of warm-rain-producing areas in the westerly regime. The minimum and maximum fractions of warm-rain-producing areas are higher in the westerly regime, which vary between 8% and 40% in the easterly regime, and between 15% and 43% in the westerly regime. Moreover, the easterly and westerly curves are nearly synchronized during most of the day. The

maximum fraction of warm-rain-producing areas occurs between 10:00 and 11:00 during both regimes, near the time of convective initiation via surface heating. The minimum fractions of warm-rain-producing areas occur at 03:00 in the easterly regime and between at 01:00 in the westerly regime. Figure 3.11b shows that the fraction of the rainfall volume associated with warm rain processes is less than 15% at all times of the day in the westerly regime. The easterly regime shows greater fluctuations during the day, with a minimum fraction of 1% in the late night hours and a maximum of 33% at 09:00. At all times, except the peak value at 09:00, the fraction of total rain volume (produced by convective features) associated with warm rain processes is 16% or less.

In summary, warm-rain-producing areas are more frequent in the westerly regime. The diurnal cycle variability is the almost equal in both regimes, with warm rain areas least frequent in the afternoon and early evening hours and most frequent in the morning hours. The fraction of rain volume that is associated with warm rain processes is significantly smaller than the fraction associated with mixed rain processes. The variability of such fractions is greater in the easterly regime, but is generally no greater than 16%. Warm rain is most frequent in the morning hours, and mixed rain is most frequent around midnight.

3.5 Convective Upper Core Characteristics

The upper core region is the part of the cloud where high reflectivities are often associated with ice-based precipitation at sub-freezing temperatures. Visual inspection of radiosonde data showed that the 0-°C-isotherm is located near 5 km. In this part of the cloud, solid phase hydrometeors are formed and grow. Investigating this part of the cloud

is important to give insight into the microphysical processes dominating hydrometeor growth and type. These processes influence the precipitation and electrification characteristics of the cloud (Takahashi, 1978; Williams, 1989; Williams *et al.*, 1994). The upper core characteristics of the convective clouds are evaluated by looking into the frequency of droplet sizes and hydrometeor phase (i.e. liquid or solid). The droplet size is investigated using the mean drop diameter (D_0), described in Chapter Two. Drop size is calculated using two different ZDR-D_0 relationships. The upper core ice fraction shows what fractions of the upper core hydrometeor mass is in the solid phase, or the ratio of ice to total mass (ice plus water) in the upper core region of the cloud.

3.5.1 Upper Core Mean Drop Diameter

Figure 3.12 shows the upper core mean drop diameter variability associated with the easterly and westerly regimes using the a) Bringi and Chandra Z_{dr}-D_0 relationship and b) Tokay Z_{dr}-D_0 relationship. Regardless of the relationship used the easterly curve is always above the westerly curve, indicating a higher frequency of smaller drops in the easterly regime. Using the Bringi and Chandra relationship, in the easterly regime 76% of observations indicated upper core drops to have mean diameters less than 1.0 mm, whereas in the westerly regime this same range of rain rates represents 64% of all observations in this regime. Using Tokay's relationship, in the easterly regime 67% of observations indicated upper core mean drop diameters to be less than 1.0 mm, whereas in the westerly regime this same range of drop diameters represents 54% of all observations in this regime. Using Bringi and Chandra's (Tokay's) relationship, the majority of mean drop diameters are observed to be greater than 0.25 (0.50) mm and less

than 1.50 (1.25) mm. Thus, Bringi and Chandra's relationship yield a greater spread of mean drop diameters than Tokay's relationship. Despite the qualitative similarities between Figures 3.12a and 3.12b, there are large quantitative differences in the frequency of certain mean drop diameters. The frequency difference is greatest for drops between 0.25 and 0.50 mm, where this difference is equal to 19% (13%) of observations in the easterly (westerly) regime.

Figure 3.13a shows the upper core mean drop diameter variability associated with the diurnal cycle using the a) Bringi and Chandra relationship and b) Tokay relationship. It can be seen that the late-afternoon and early evening curves (16-20) are above all the others. This indicates that at this time there is a higher frequency of smaller droplets. Hence, the upper core region of convective clouds has smaller mean drop diameters in the late afternoon and early evening hours. The observations at 16:00 show that mean drop diameters less than 1.0 mm represent 85% of observations using Bringi and Chandra's (B&C) relationship and 77% using Tokay's relationship, regardless of wind regime. Near sunrise (04-08) and in the morning hours (08-12) we observe the lowest frequency of small drops (i.e. less than 1.0 mm), with only 44% (33%) of observations at 06:00 being less than 1.0 mm using B&C (Tokay's) relationship. As in Figure 3.12, we observe a greater spread of diameters using Bringi and Chandra's relationship. The diurnal variations in drop size are as much as 10% higher in Figure 3.13a.

Figure 3.14a shows the upper core mean drop diameter variability associated with the easterly regime using Bringi and Chandra's relationship, and Figure 3.14b shows the same variability using Tokay's relationship. The easterly regime diurnal variability shows the same periods of smallest and largest mean drop diameter identified in Figure 3.13. In

the easterly regime, the smallest droplets are observed in the late afternoon and early evening hours with 88% (82%) of them being less than 1 mm at 17:00 using B&C (Tokay). The largest mean drop diameters occur near sunrise and in the morning hours where only 27% (18%) of the drops were less than 1 mm using B&C (Tokay). The westerly regime diurnal variability (Figure 3.14b) also shows the same times for largest and smallest drop sizes. However, in the westerly curve there are two groups of times with similar characteristics: one from midnight to noon, associated with the smallest frequency of small drops (i.e. less than 1 mm) and another group from noon to midnight associated with the largest frequency of small droplets. At 03:00, 46% (35%) of drops are less than 1 mm using Bringi and Chandra's (Tokay's) relationship. At 16:00, 81% (71%) of drops are less than 1 mm.

In summary, smaller mean drop diameters are more frequent in the easterly regime. The diurnal cycle variability is more pronounced in the easterly regime, with smaller droplets most frequent in the late afternoon and evening hours and least frequent near sunrise and in the early morning hours. The spread of mean drop diameters is greater when Bringi and Chandra's relationship is used.

3.5.2 Upper Core Ice Fraction

Figure 3.16a shows the ice fraction variability associated with the easterly and westerly regimes. Figure 3.16 represents the hourly-averaged ice fraction, or in other words, the fraction of ice mass to total mass (water plus ice masses) occurring within the upper core region of a convective cloud at any given time. It can be seen that the easterly curve is right-shifted with respect to the westerly curve, indicating a higher frequency of

large ice fractions in the easterly regime. In the easterly regime 52% of observations indicated ice fractions less than 0.5, whereas in the westerly regime this same range of ice fractions represents 72% of all observations in this regime. The modal ice fraction interval for the easterly curve is the 0.5-0.6 interval, and in the westerly curve the mode of observations occurs in the 0.4-0.5 ice fraction interval. In the ice fraction intervals where most observations are concentrated (0.3 to 0.7), the difference between the curves varies between 4% and 9%. Therefore, the westerly regime is associated with smaller ice fractions in the upper core region. Figure 3.16b shows the ice fraction variability associated with the diurnal cycle. It can be seen that the most right-shifted curves are the afternoon (12-16) and late afternoon and early evening (16-20) curves. These curves are associated with higher frequencies in the largest ice fraction intervals. Hence, the upper core region of convective clouds have greater ice fractions in the afternoon, with 55% to 56% of observations between noon and 19:59 being less than 0.5, regardless of wind regime. The most left-shifted curves are the early morning (04-08) and morning (08-12) curves. Thus, the smallest ice fractions occur in the morning hours, with as much as 82% of observations at 07:00 being less than 0.5. At all times the modal ice fraction intervals are either 0.4 to 0.5 or 0.5 to 0.6.

Figure 3.17a shows the upper core ice fraction variability associated with the diurnal cycle during the easterly regime, and Figure 3.17b shows the same variability during the westerly regime. The easterly regime diurnal variability (Figure 3.17a) shows that large ice fractions (greater than 0.5) are more predominant in the afternoon and early evening hours, with as much as 53% of the ice fractions greater than 0.5 at 16:00. Small ice fractions are most frequent in the morning hours, when ice fractions greater than 0.5

can account for as low as 22% of observations at 07:00. The westerly regime diurnal variability (Figure 3.17b) shows maximum frequency of large ice fractions occurring at the same time as in the easterly regime. Large ice fractions are most frequent in the afternoon and early evening hours, with as much as 37% of the ice fractions being greater than 0.5 at 16:00. Small ice fractions are most predominant in the late night and early morning hours, with 13% of ice fractions observed to be greater than 0.5 mm/h at 04:00.

In summary, larger upper core ice fractions are more frequent in the easterly regime. Smaller ice fractions are most frequent near sunrise and in the morning hours and larger ice fractions are more frequent in the afternoon and evening hours.

a)

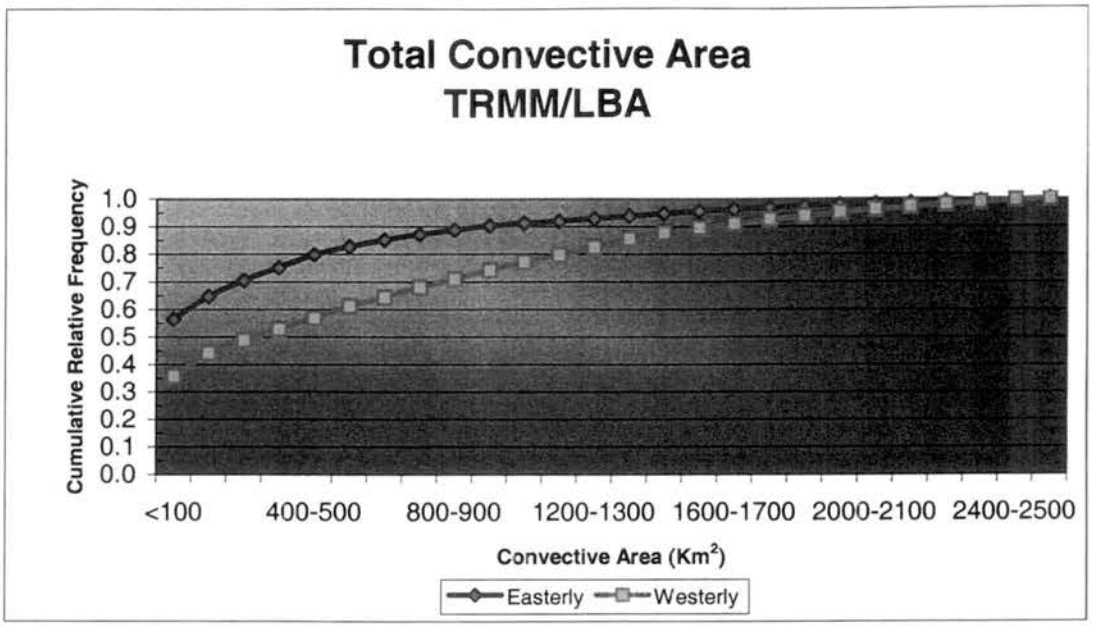

b)

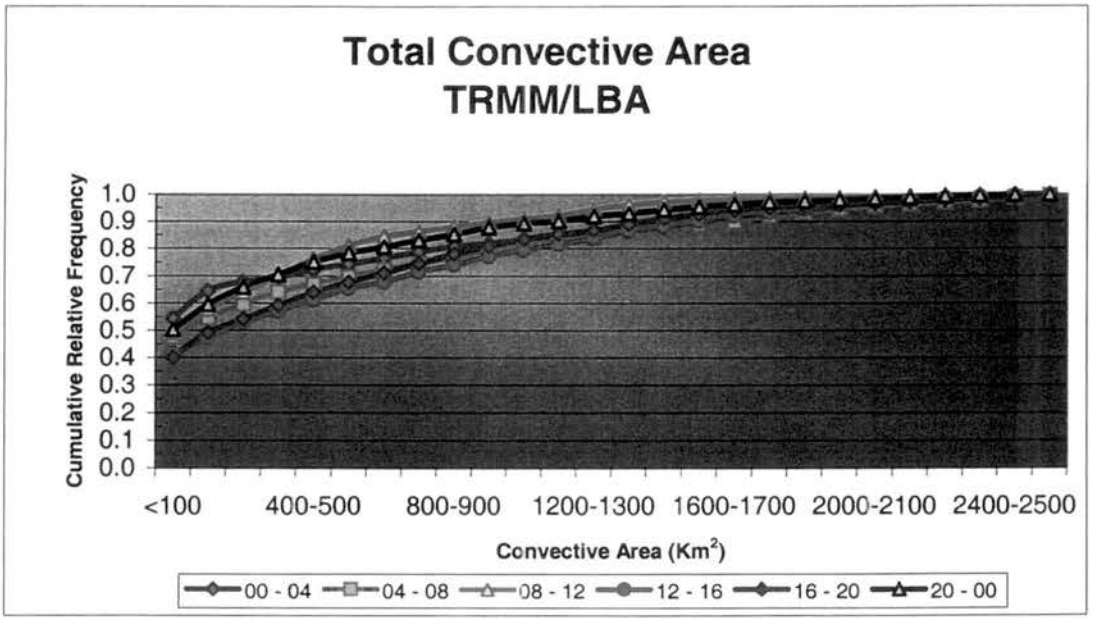

Figure 3.1: Intra-regional variability of the convective area in the TRMM/LBA region associated with a) the wind regimes, and b) the diurnal cycle.

a)

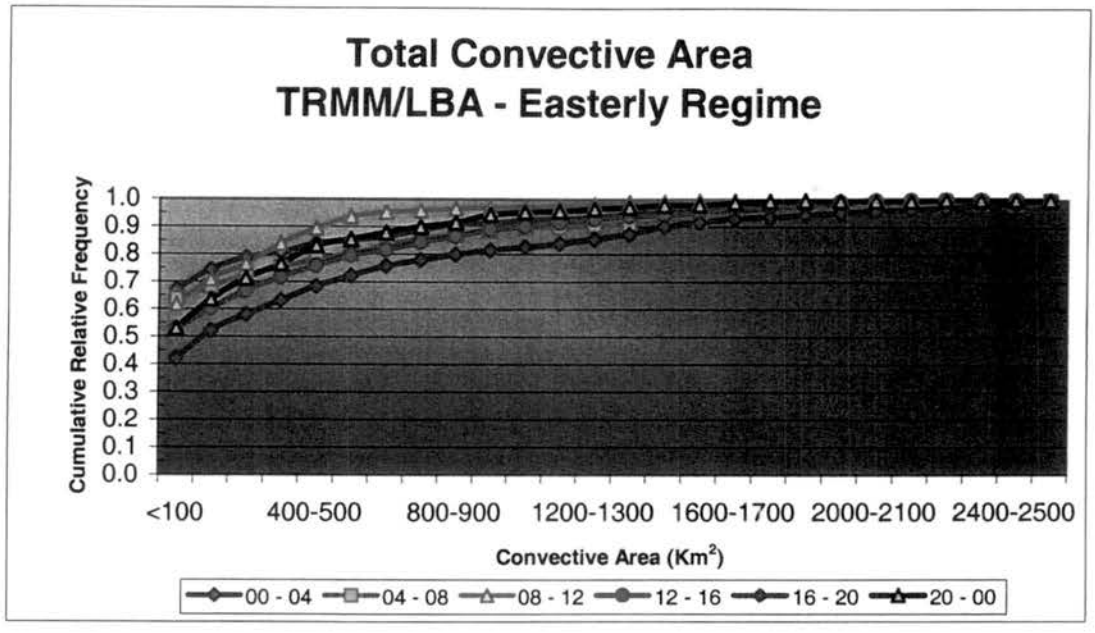

b)

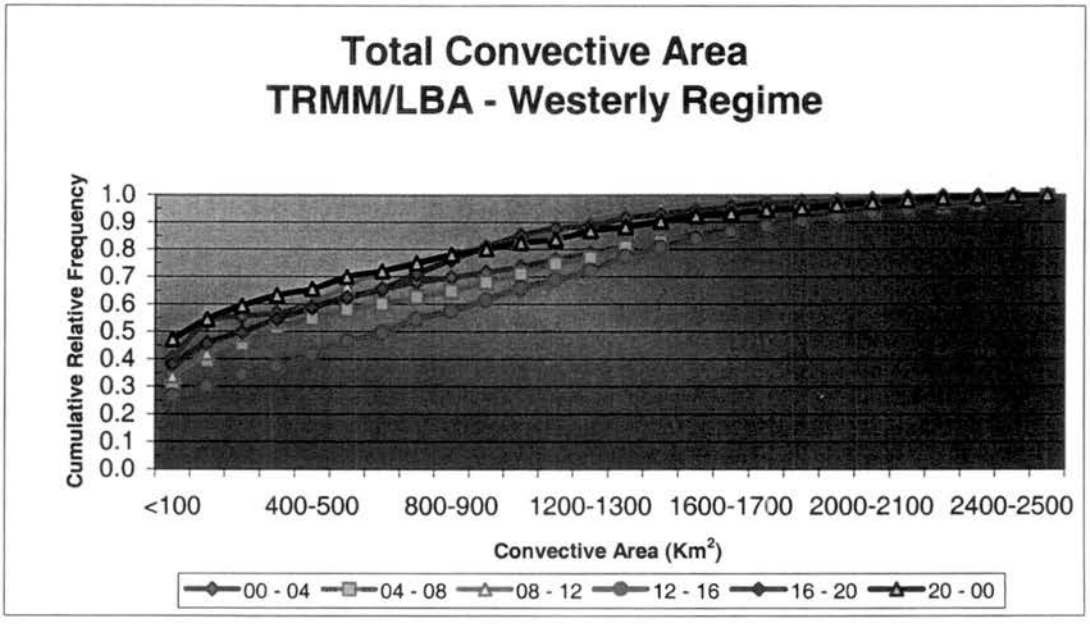

Figure 3.2: Intra-regional variability of the convective area in the TRMM/LBA region associated with the diurnal cycle during the a) easterly regime and b) westerly regime.

a)

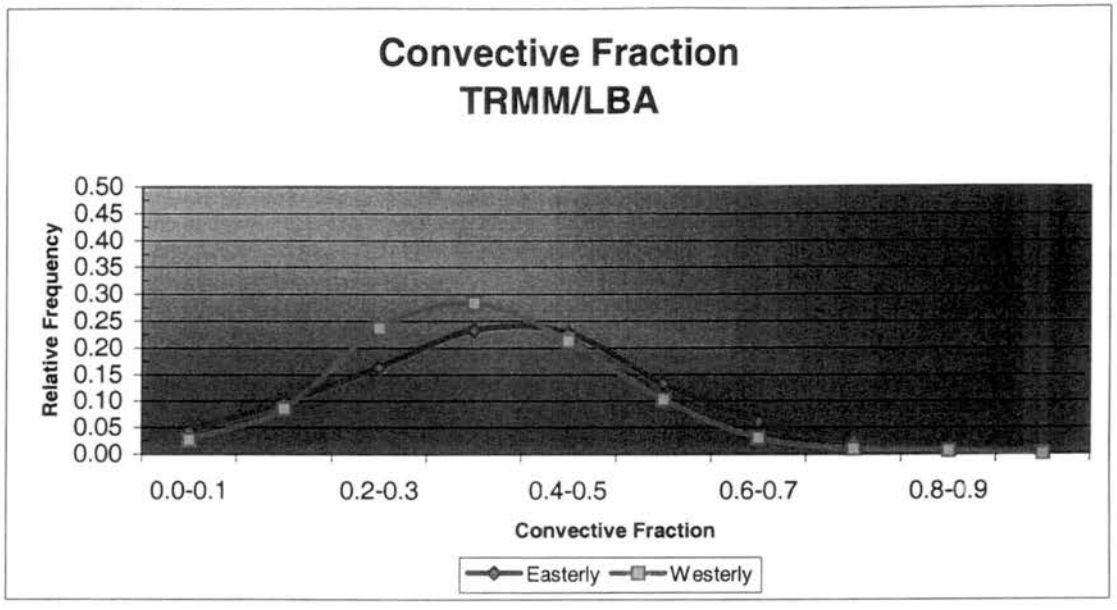

b)

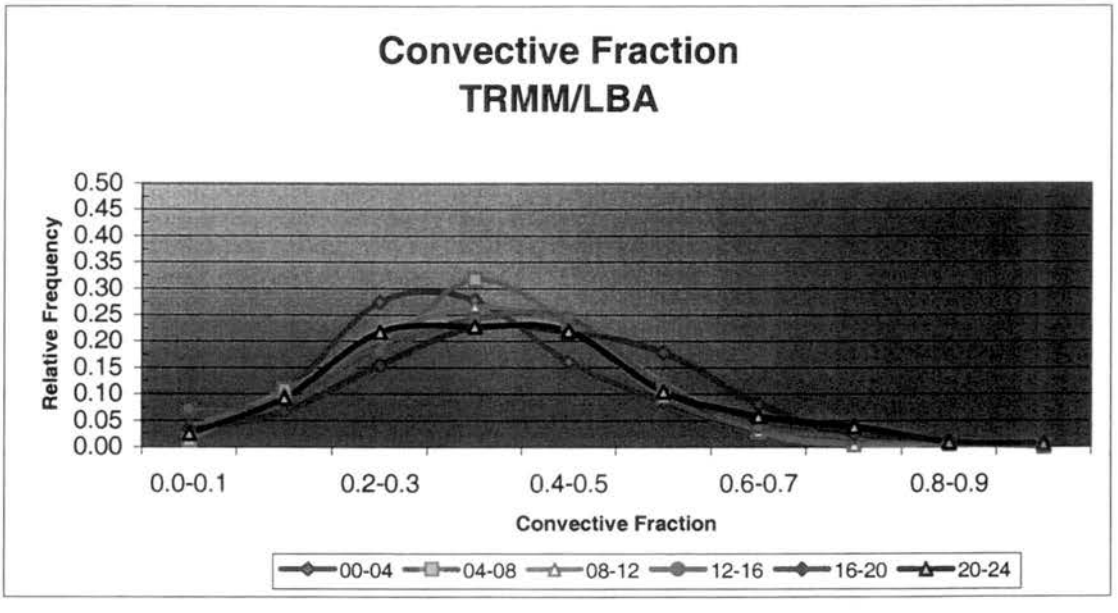

Figure 3.3: Intra-regional variability of the convective fraction in the TRMM/LBA region associated with a) the wind regimes, and b) the diurnal cycle.

a)

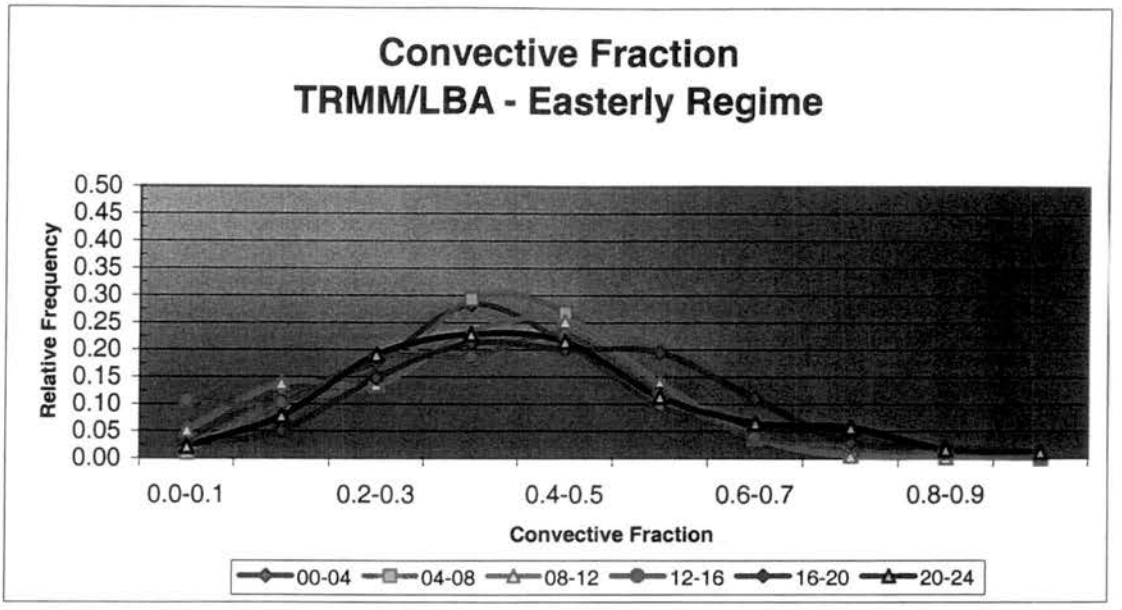

b)

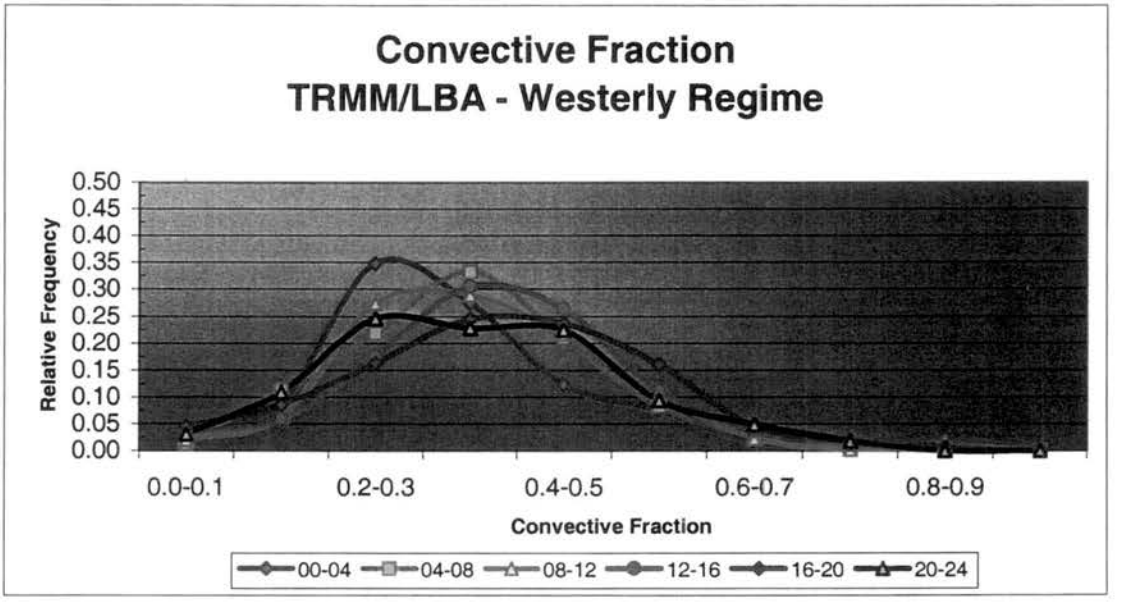

Figure 3.4: Intra-regional variability of the convective fraction in the TRMM/LBA region associated with the diurnal cycle during the a) easterly regime and b) westerly regime.

a)

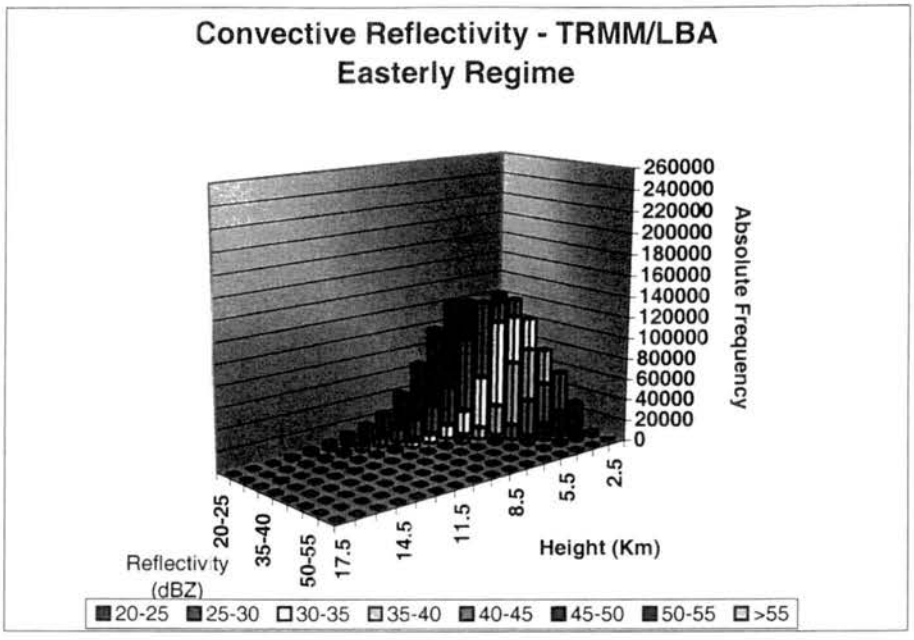

b)

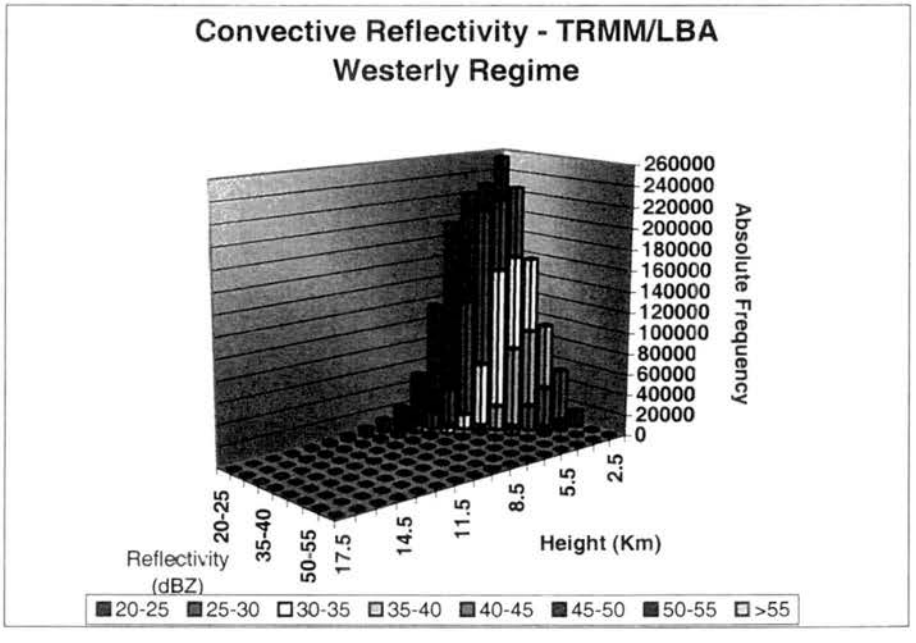

Figure 3.5: TRMM/LBA vertical reflectivity distribution during the a) easterly regime, and b) westerly regime.

a)

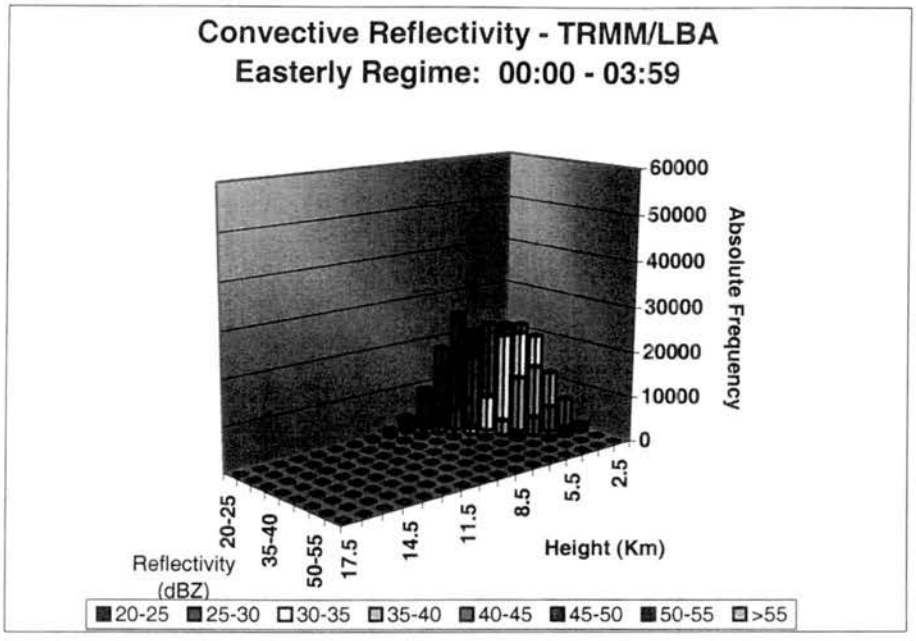

b)

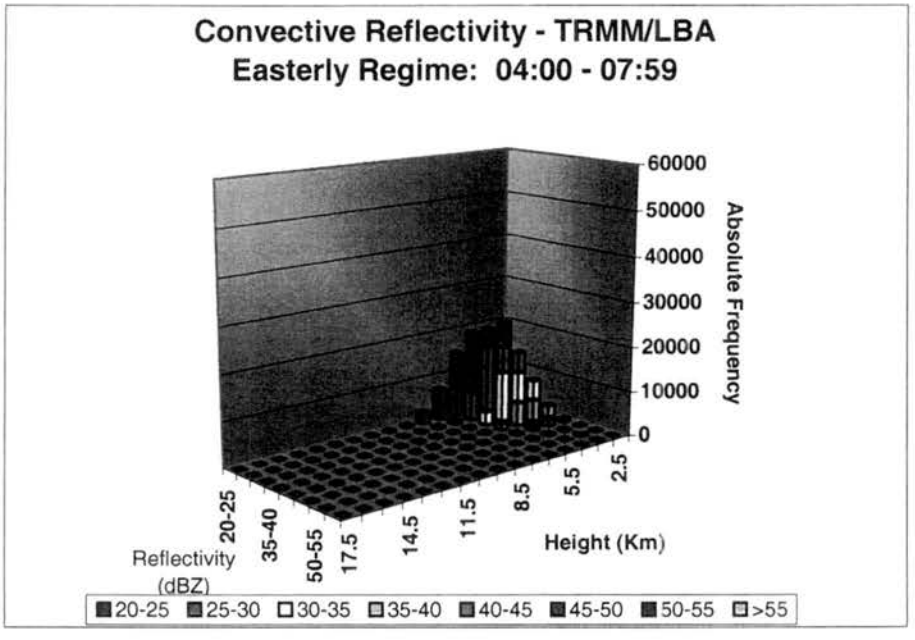

Figure 3.6: TRMM/LBA vertical reflectivity distribution during the easterly regime for observations between a) 00:00 and 03:59, b) 04:00 and 07:59, c) 08:00 and 11:59, d) 12:00 and 15:59, e) 16:00 and 19:59, and f) 20:00 and 23:59.

c)

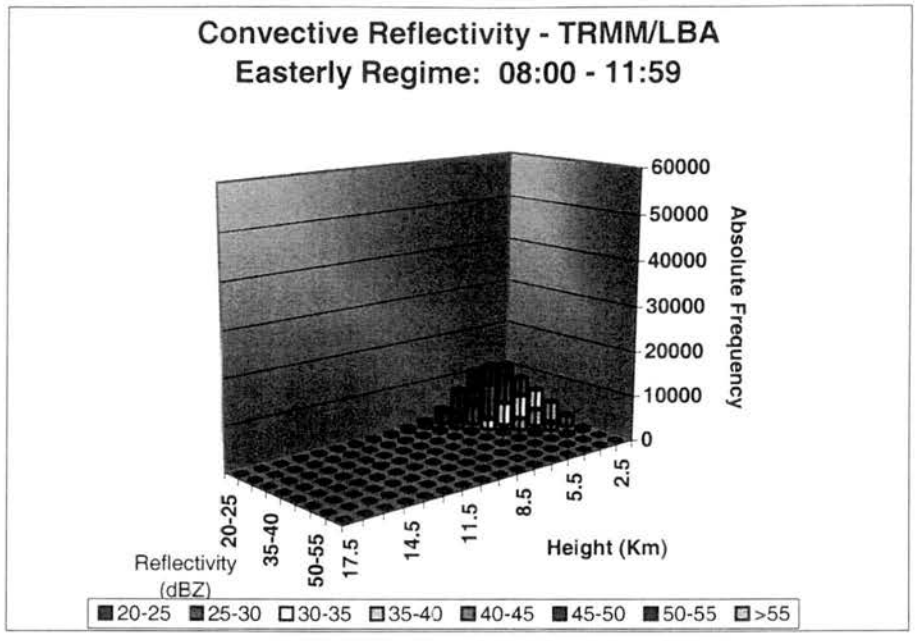

d)

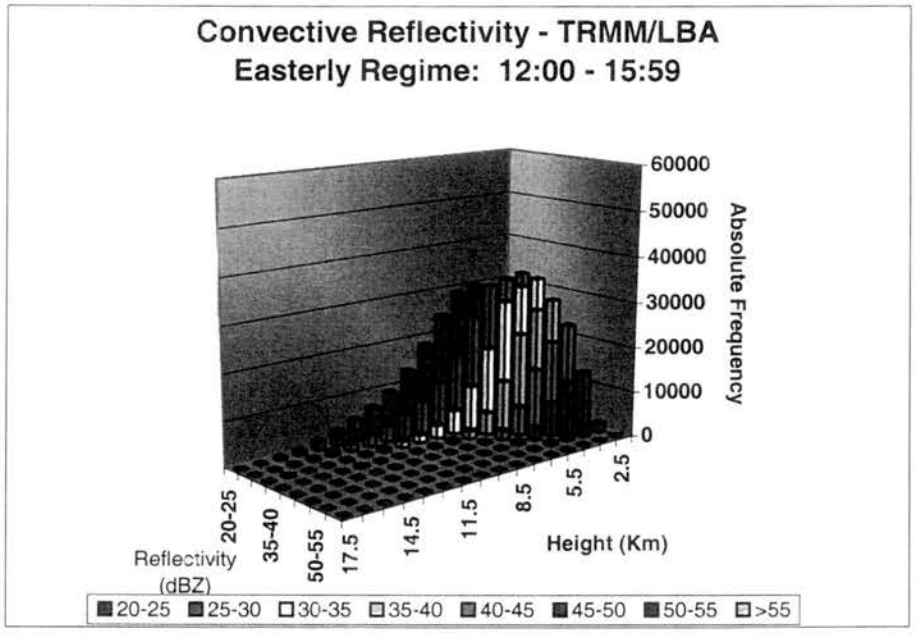

Figure 3.6: (Cont.)

e)

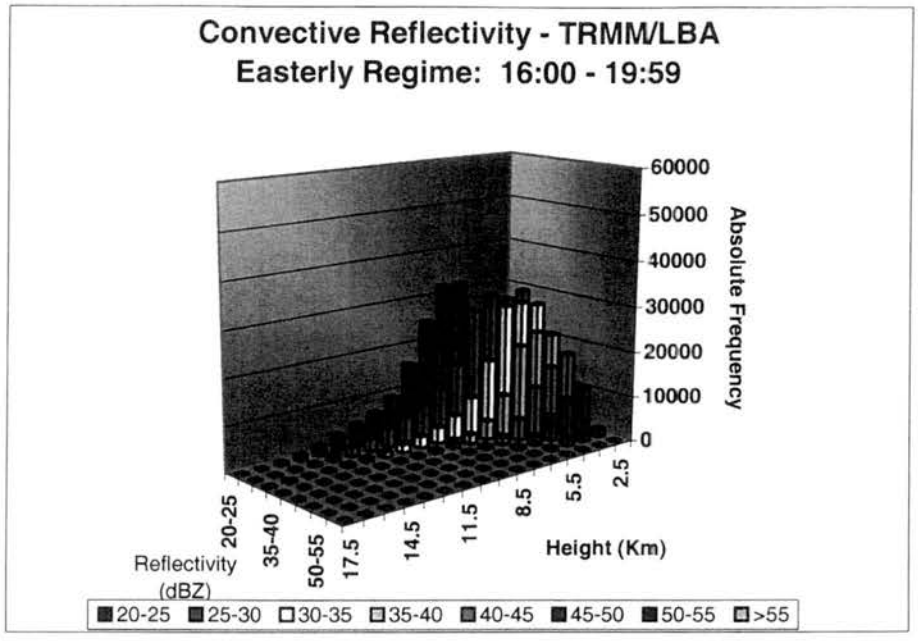

f)

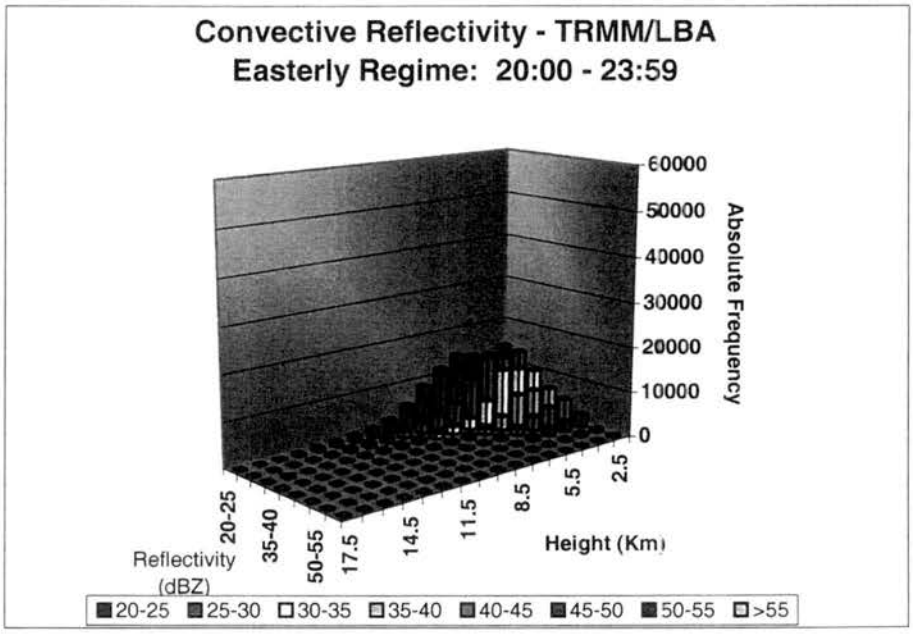

Figure 3.6: (Cont.)

a)

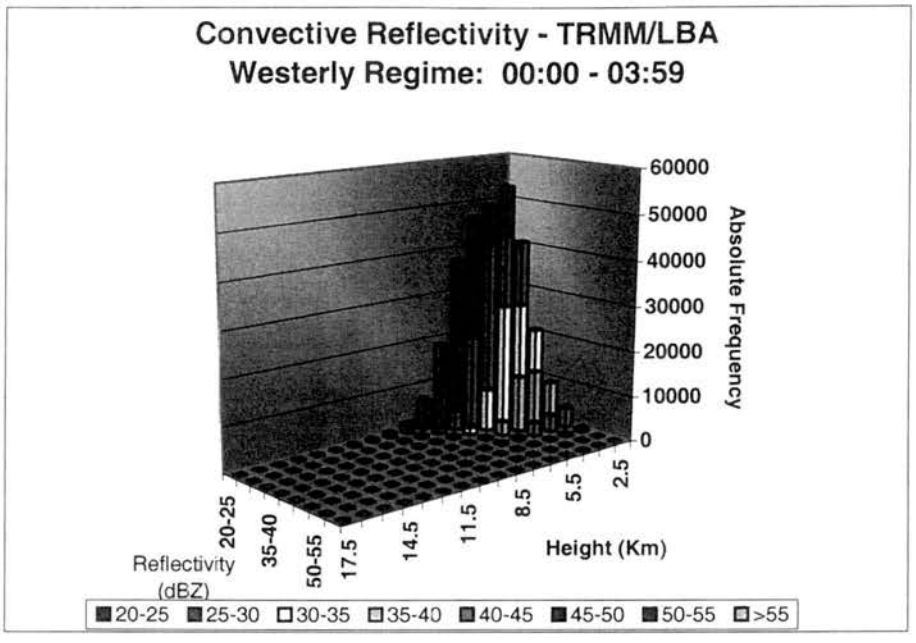

b)

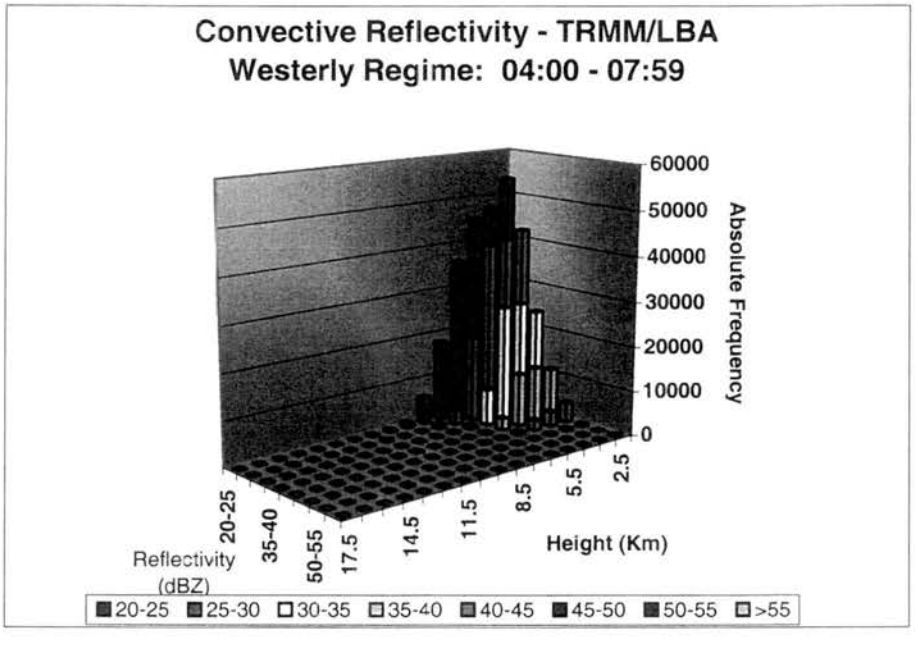

Figure 3.7: TRMM/LBA vertical reflectivity distribution during the westerly regime for observations between a) 00:00 and 03:59, b) 04:00 and 07:59, c) 08:00 and 11:59, d) 12:00 and 15:59, e) 16:00 and 19:59, and f) 20:00 and 23:59.

c)

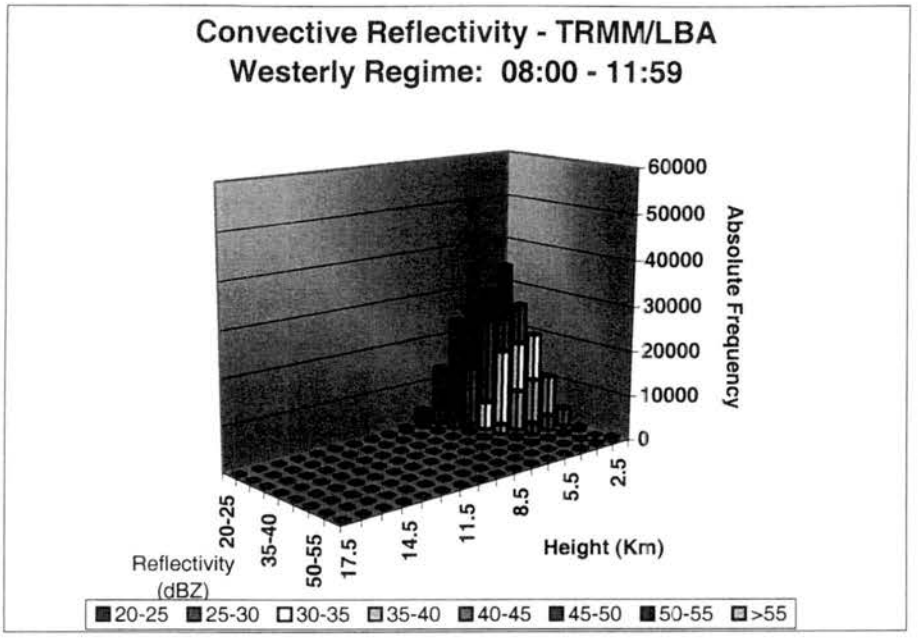

d)

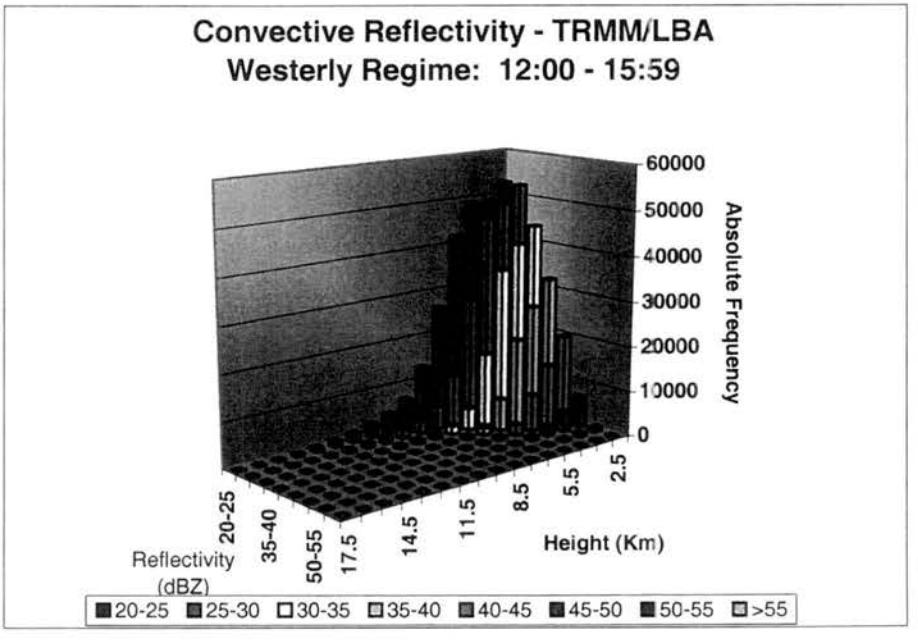

Figure 3.7: (Cont.)

e)

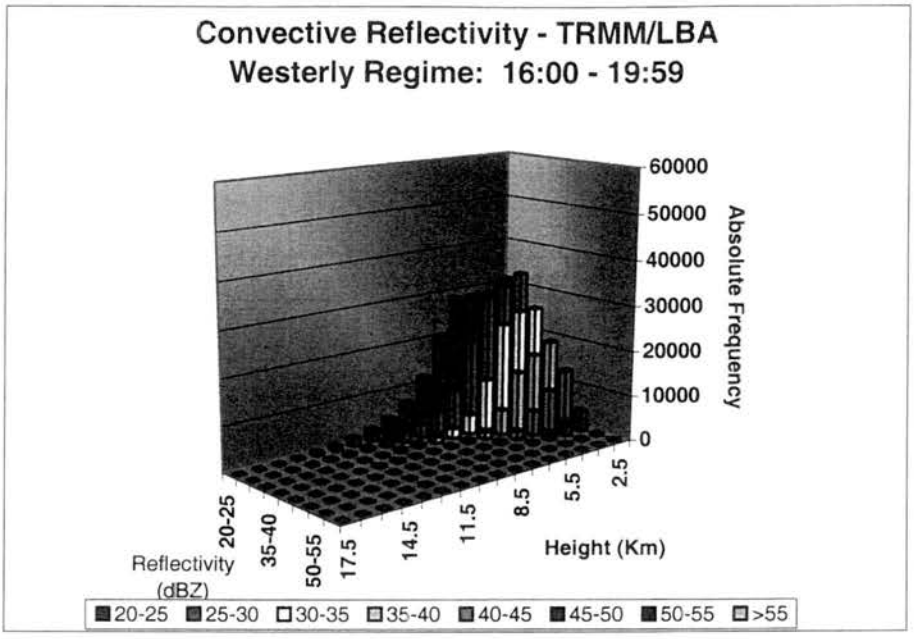

f)

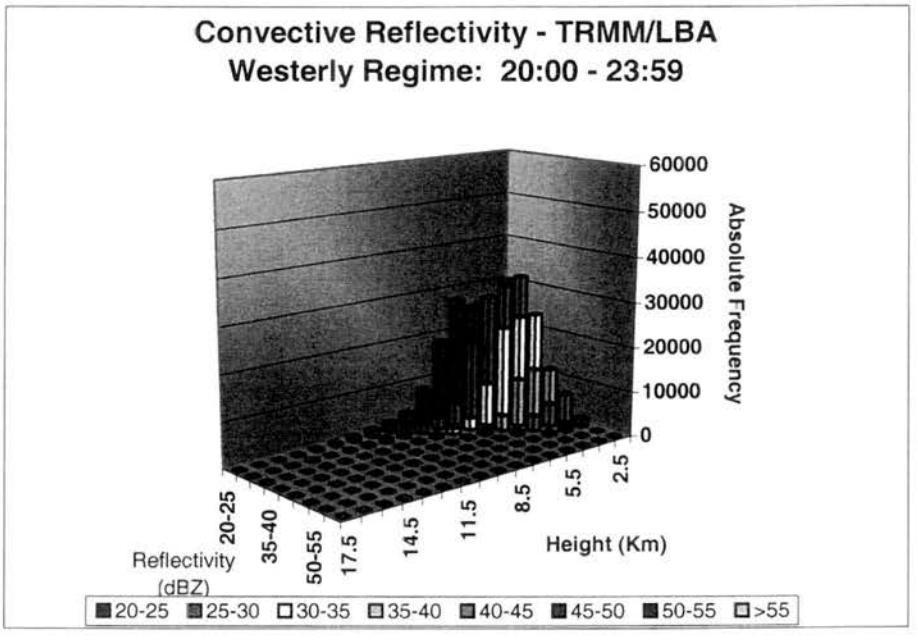

Figure 3.7: (Cont.)

a)

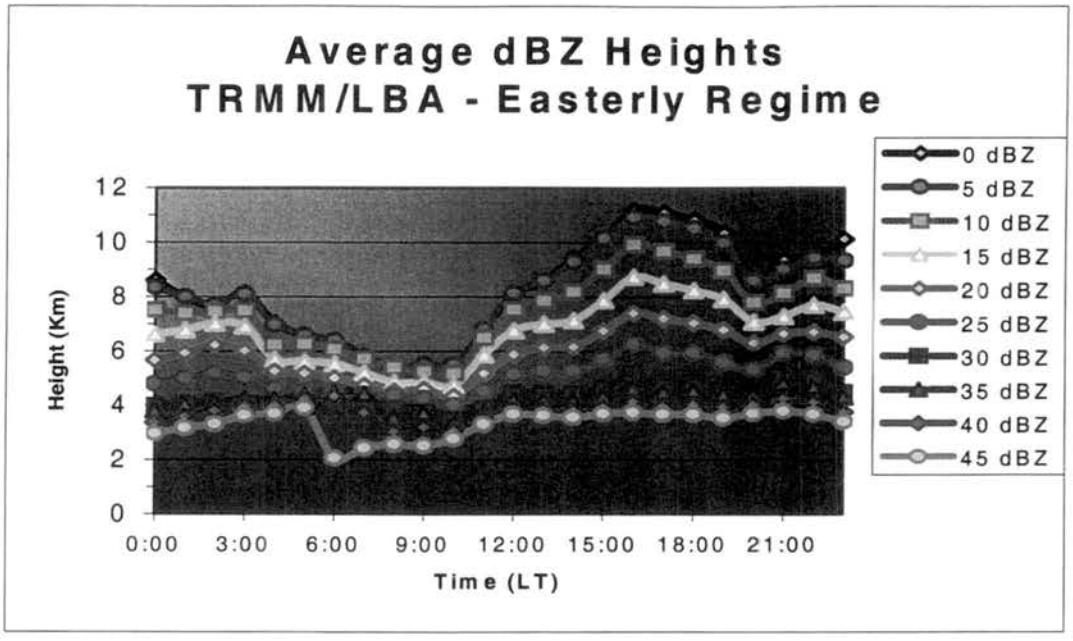

b)

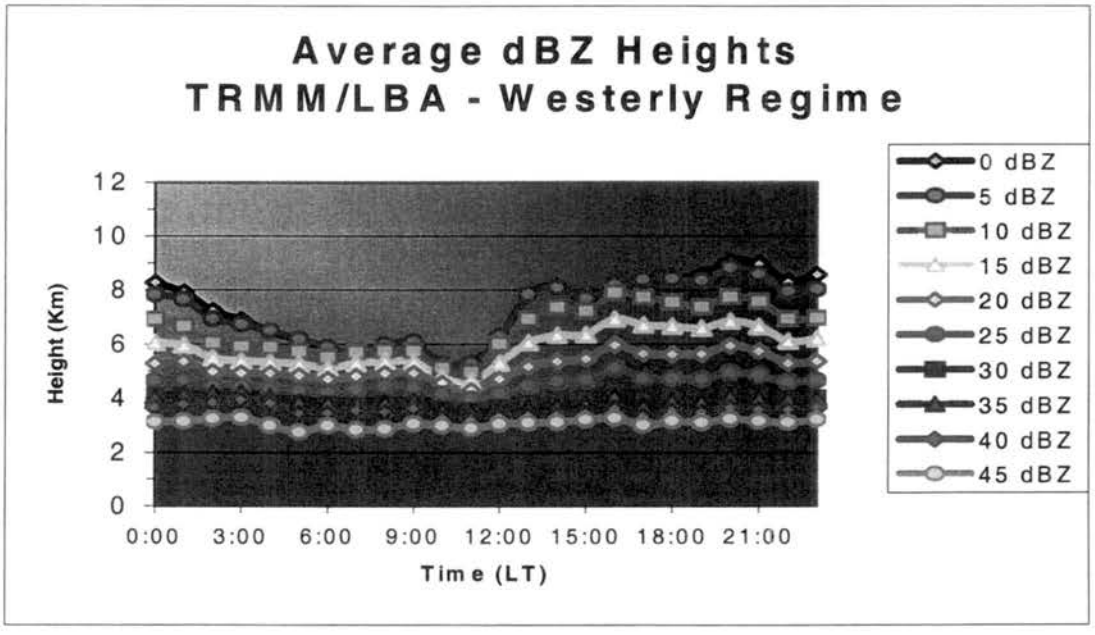

Figure 3.8: TRMM/LBA hourly-averaged reflectivity heights during the a) easterly regime, and b) westerly regime.

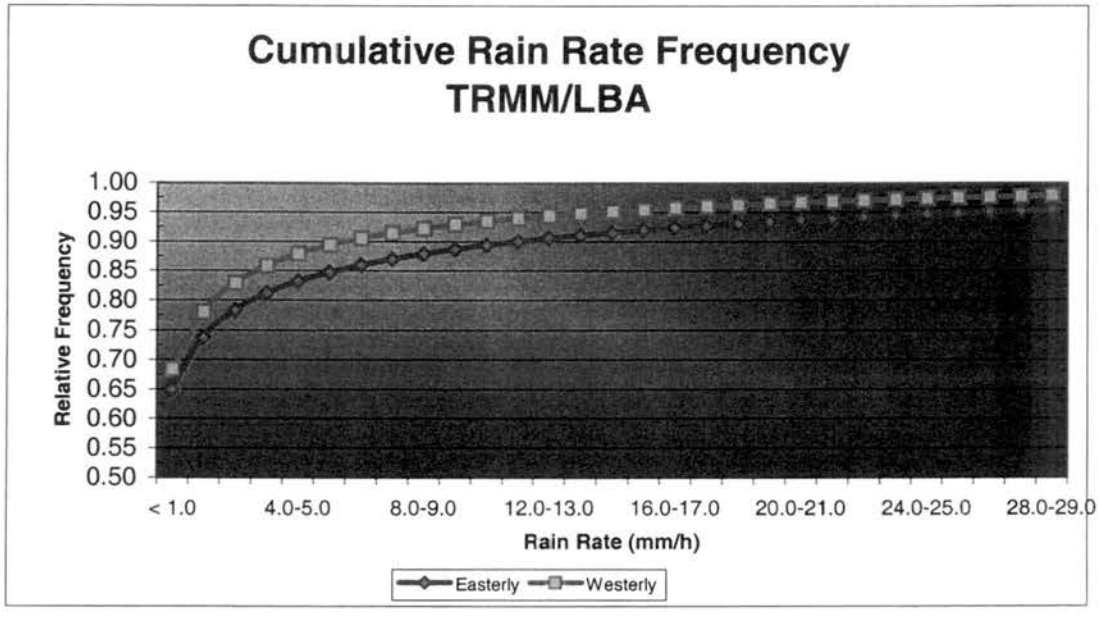

Figure 3.9: Intra-regional variability of the rain rate in the TRMM/LBA region associated with the wind regimes.

a)

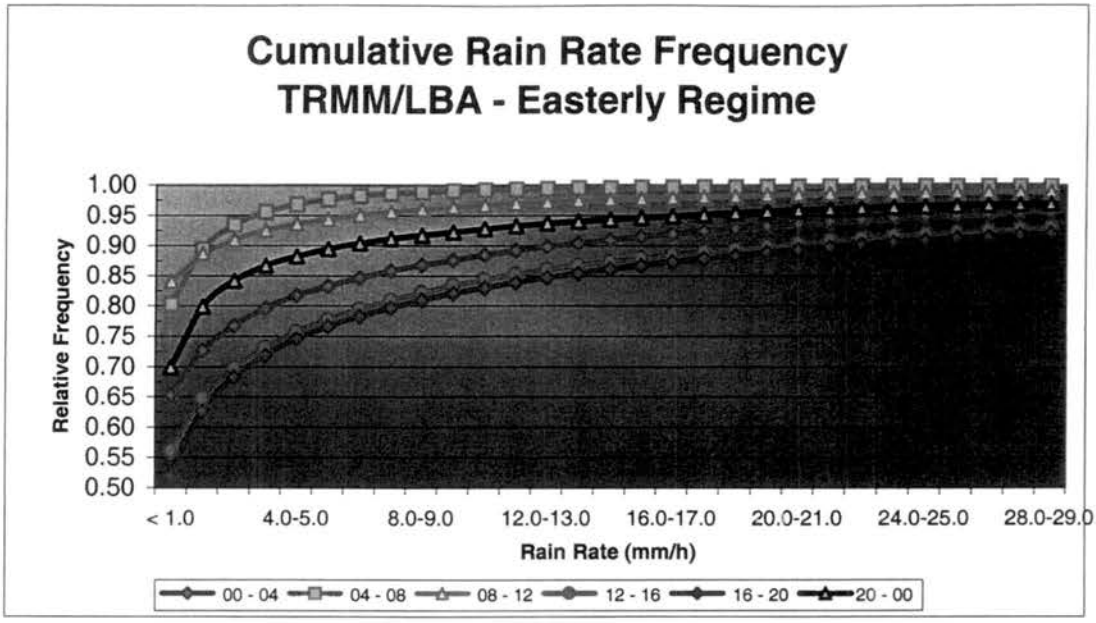

b)

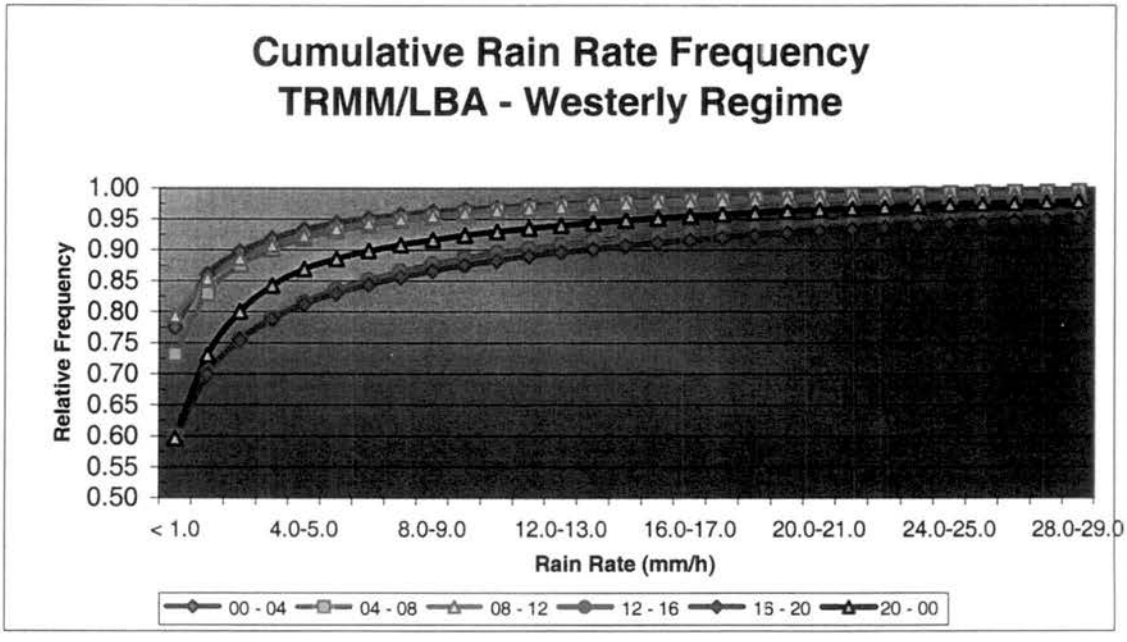

Figure 3.10: Intra-regional variability of the rain rate in the TRMM/LBA region associated with the diurnal cycle during the a) easterly regime and b) westerly regime.

a)

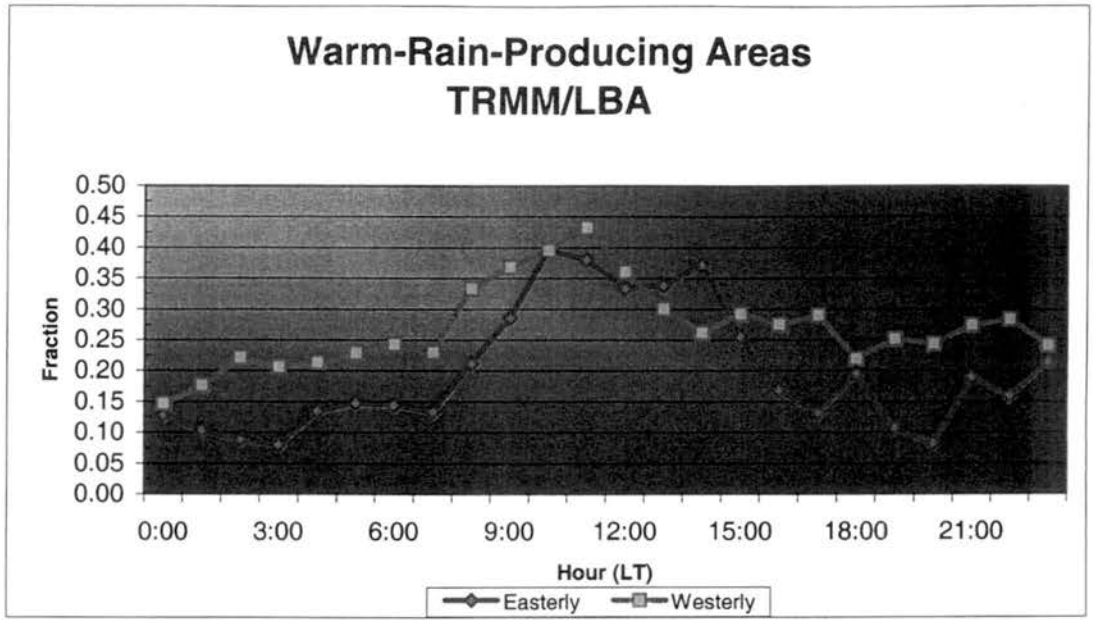

b)

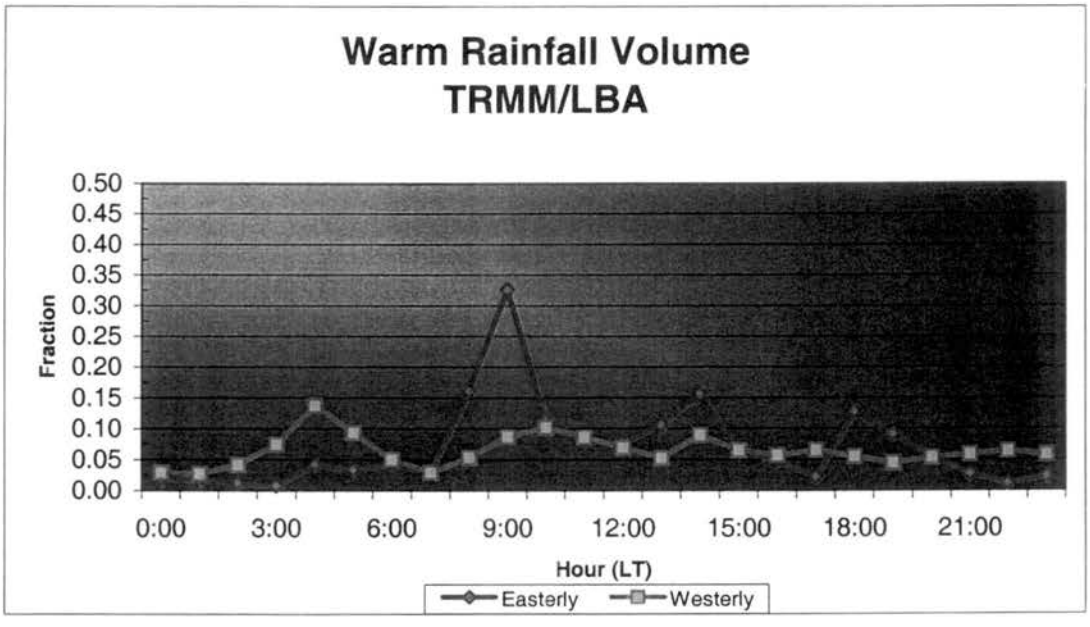

Figure 3.11: Hourly-averaged fraction of a) rain-producing areas and b) rainfall volume, associated with warm rain processes during TRMM/LBA in the easterly and westerly regimes.

a)

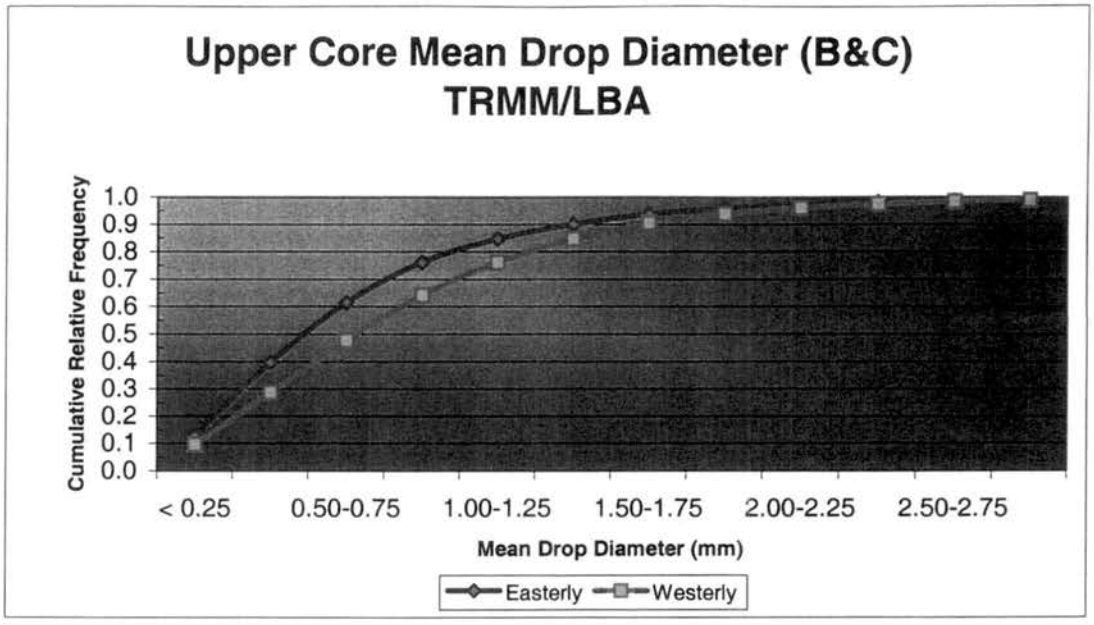

b)

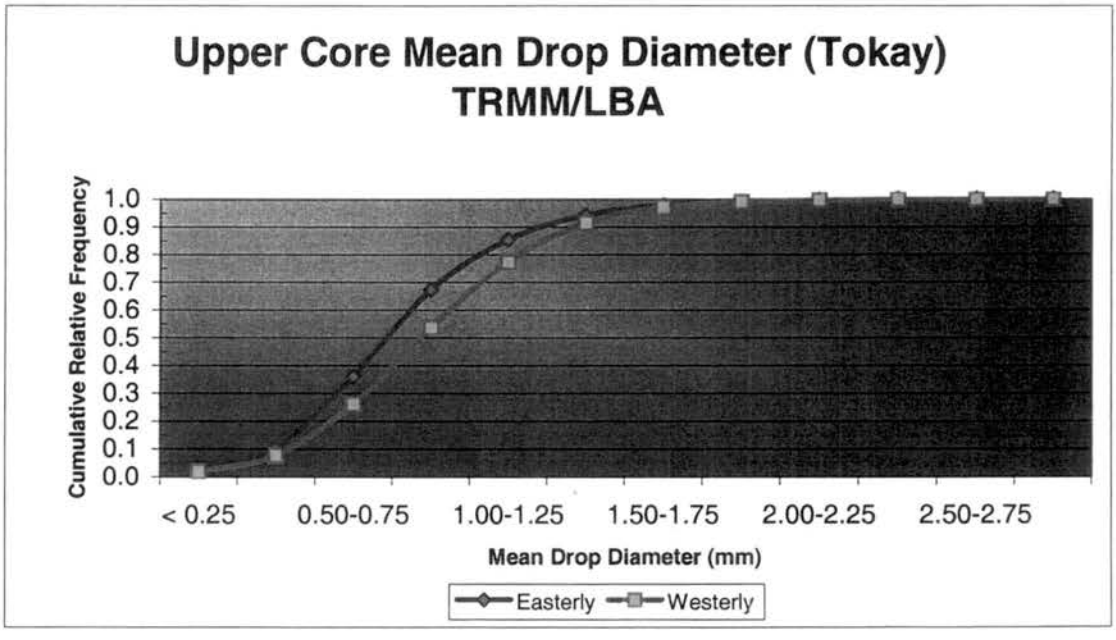

Figure 3.12: Intra-regional variability of the upper core mean drop diameter in the TRMM/LBA region associated with the wind regimes using the Z_{dr}-D_0 relationship from a) Bringi and Chandra b) Tokay.

a)

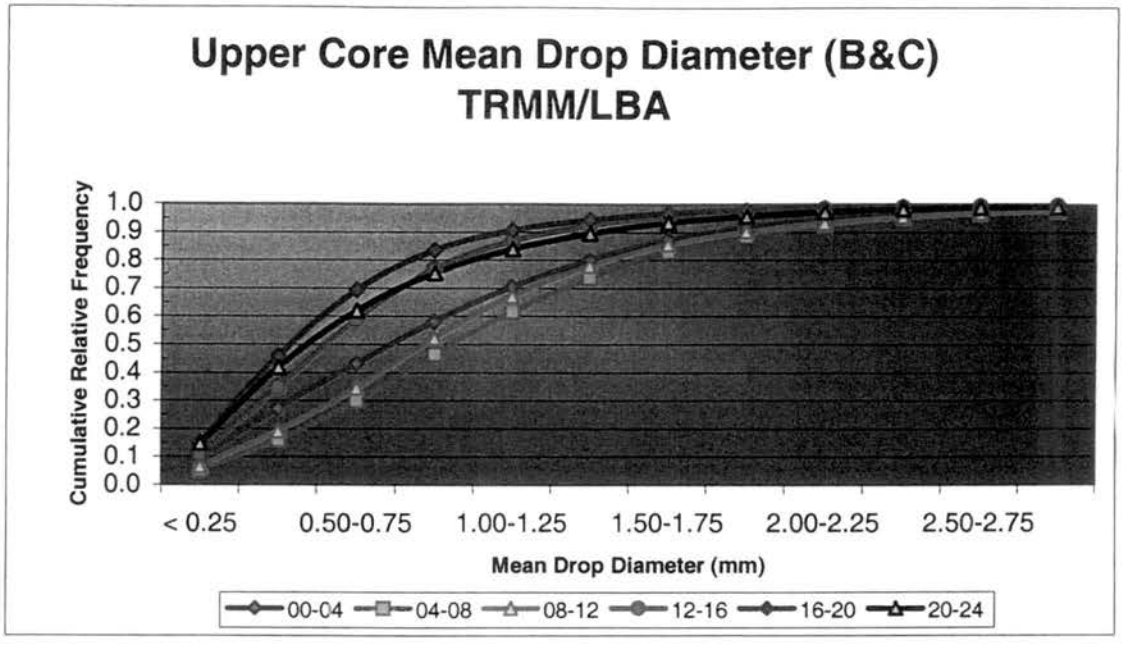

b)

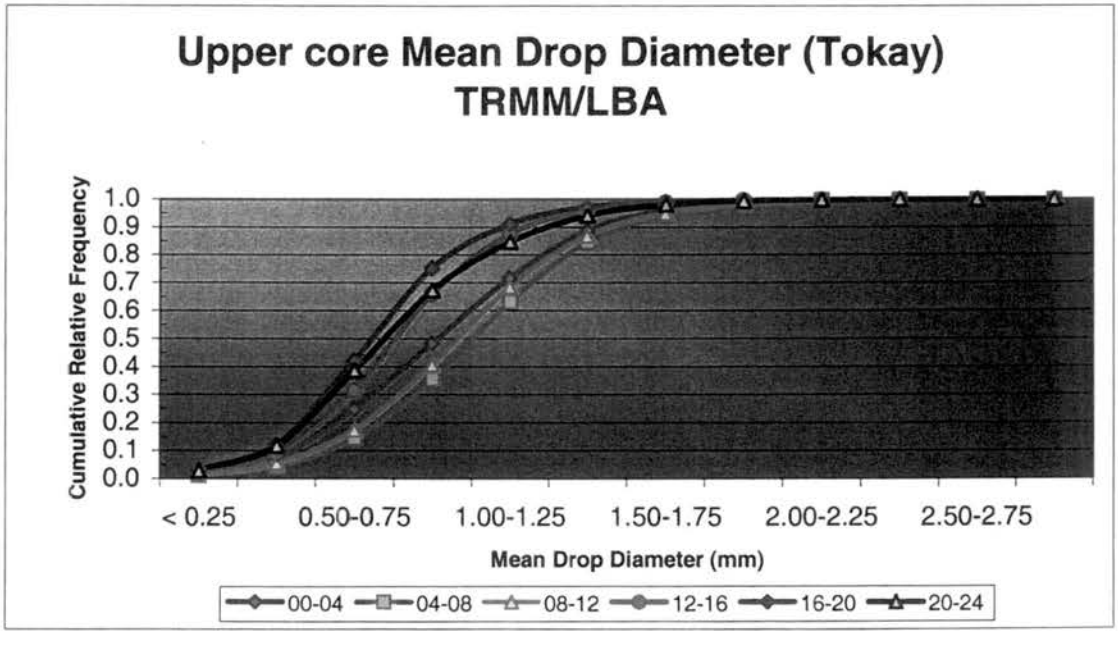

Figure 3.13: Intra-regional variability of the upper core mean drop diameter in the TRMM/LBA region associated with the diurnal cycle using the Z_{dr}-D_0 relationship from a) Bringi and Chandra b) Tokay.

a)

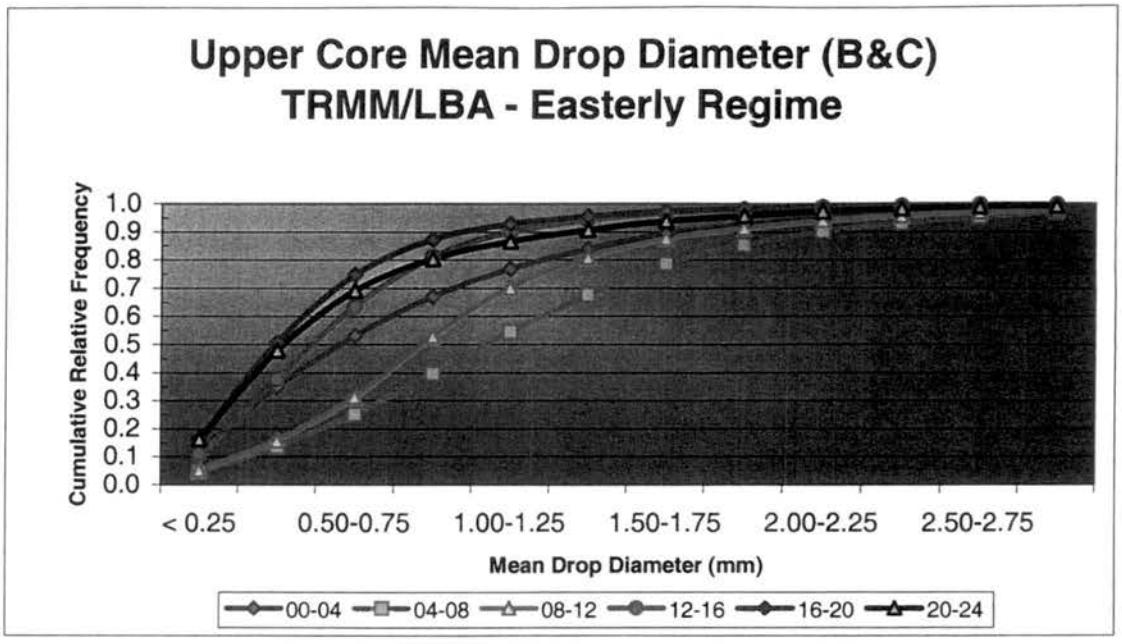

b)

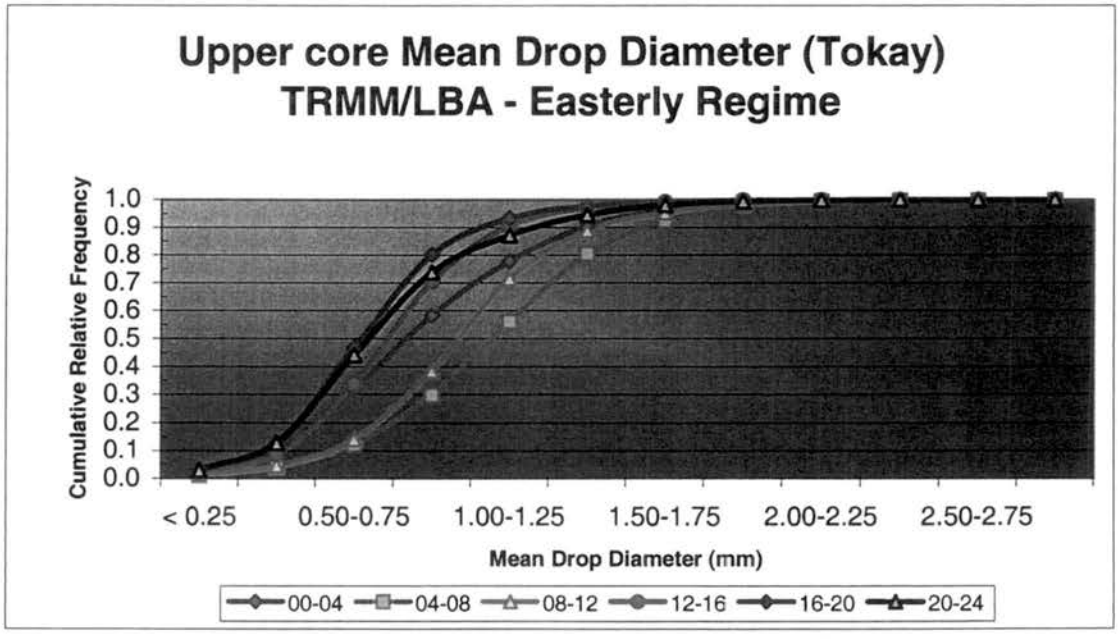

Figure 3.14: Intra-regional variability of the mean drop diameter in the TRMM/LBA region associated with the diurnal cycle during the easterly regime using the Zdr-D_0 relationship from a) Bringi and Chandra and b) Tokay.

a)

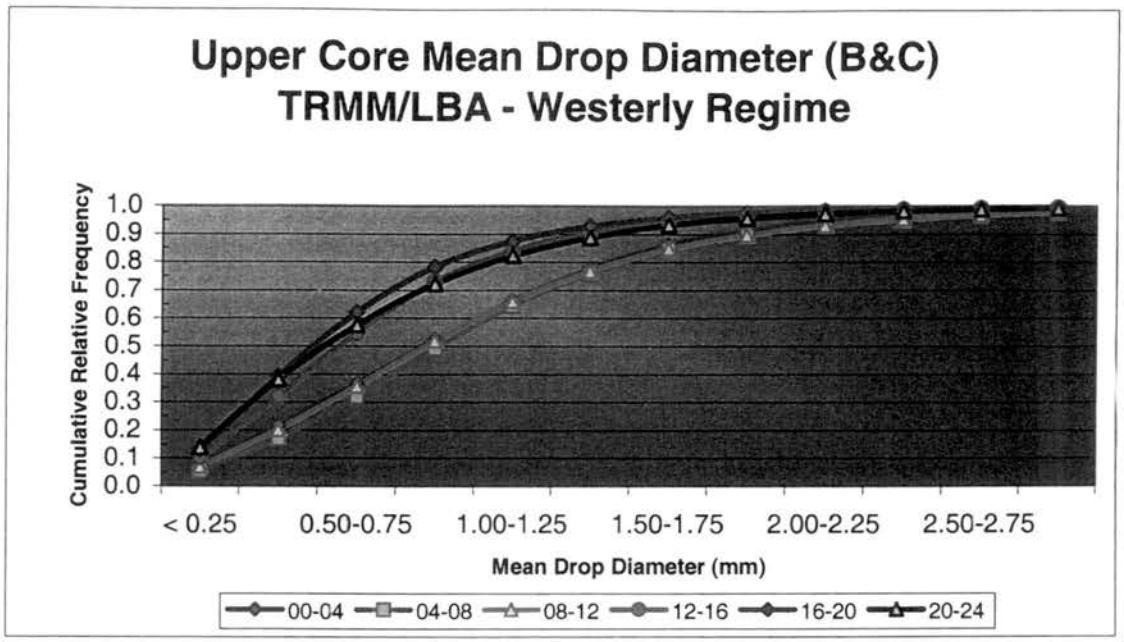

b)

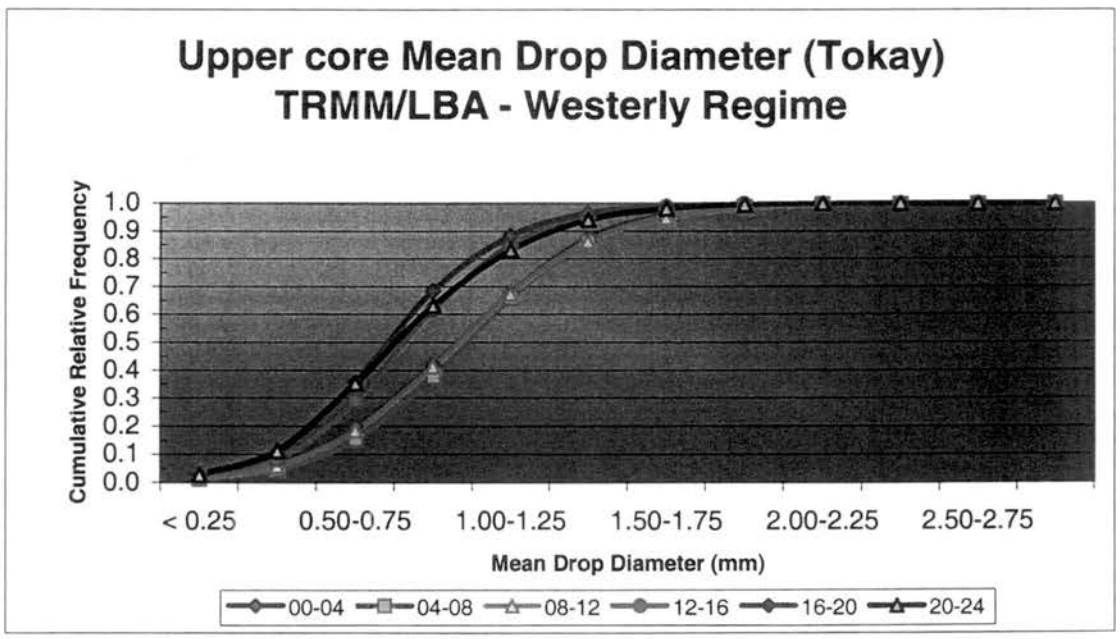

Figure 3.15: Intra-regional variability of the mean drop diameter in the TRMM/LBA region associated with the diurnal cycle during the westerly regime using the Zdr-D_0 relationship from a) Bringi and Chandra and b) Tokay.

a)

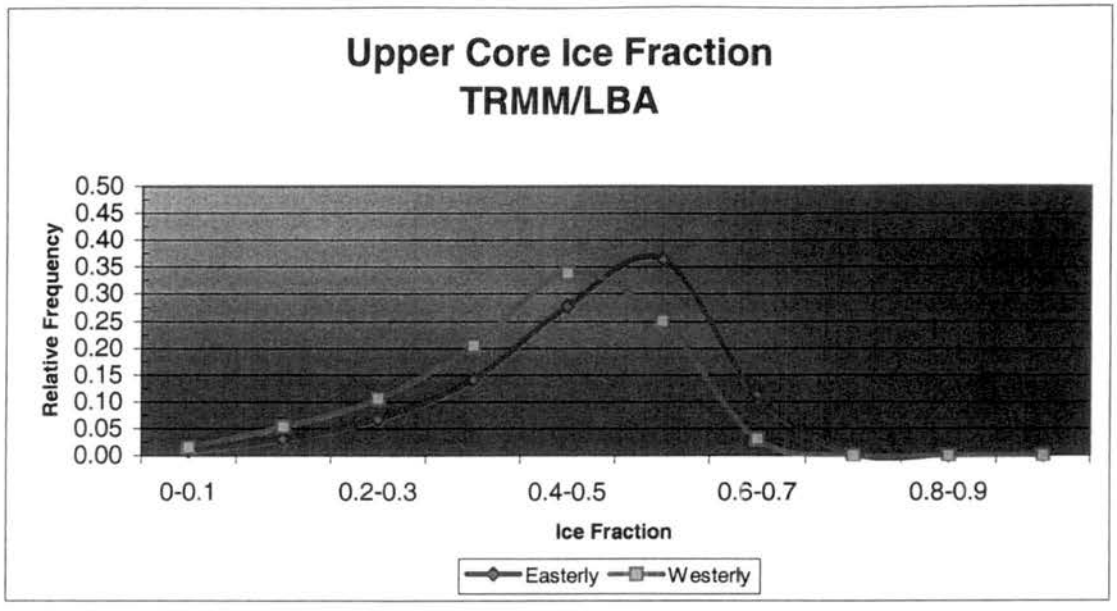

b)

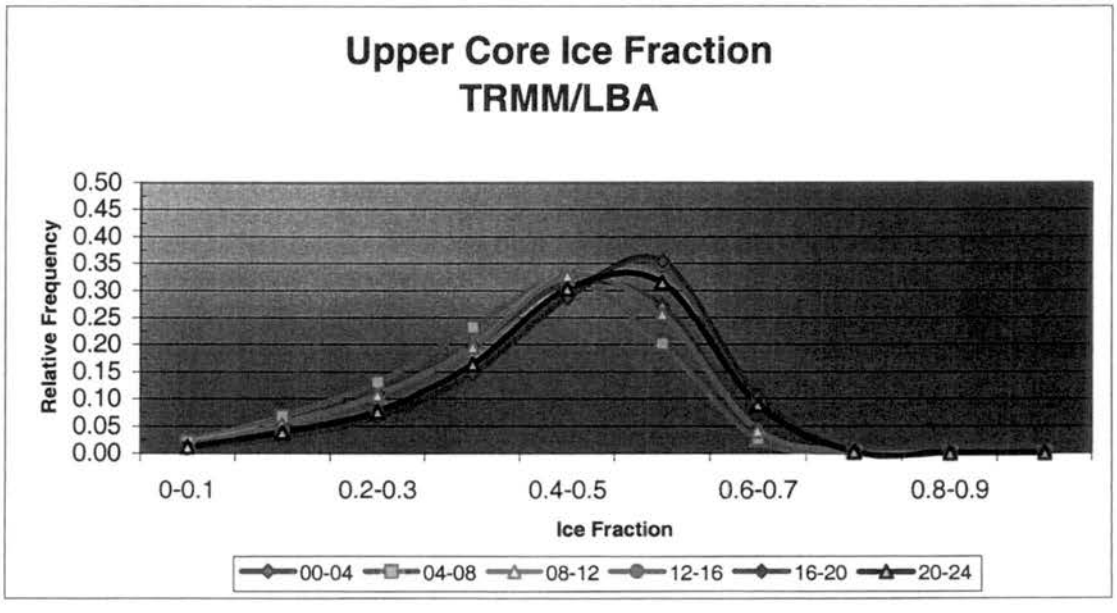

Figure 3.16: Intra-regional variability of the upper core ice fraction in the TRMM/LBA region associated with a) the wind regimes, and b) the diurnal cycle.

a)

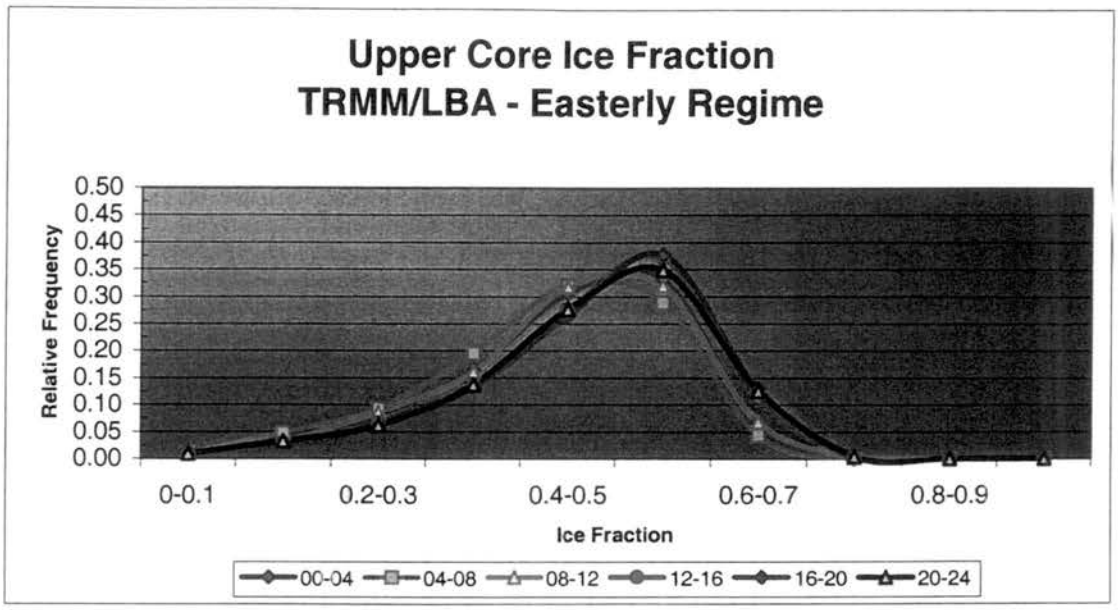

b)

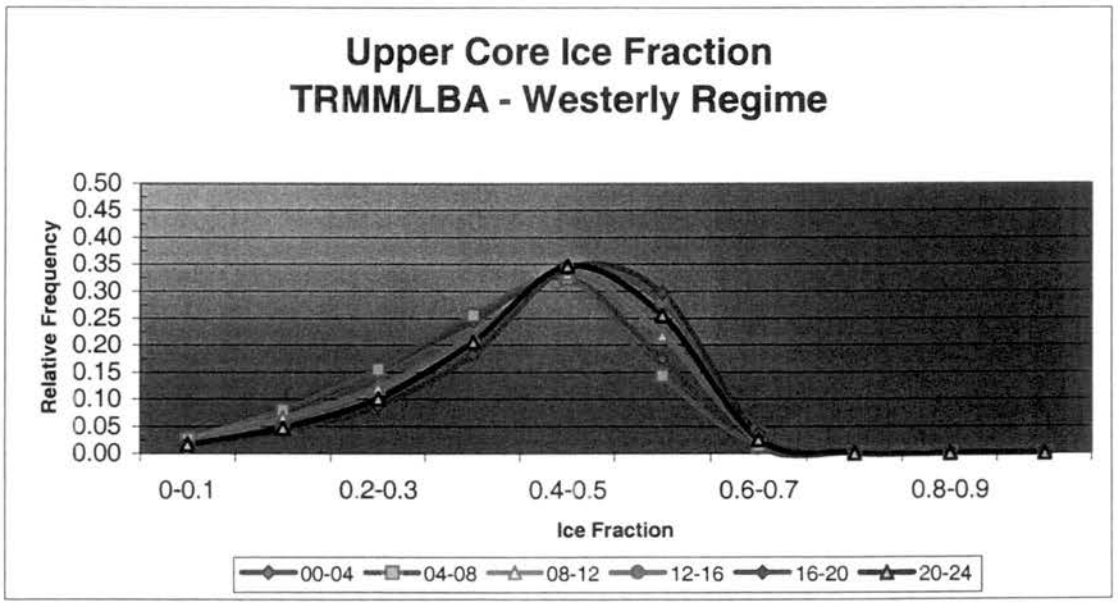

Figure 3.17: Intra-regional variability of the upper core ice fraction in the TRMM/LBA region associated with the diurnal cycle during the a) easterly regime and b) westerly regime.

CHAPTER FOUR

EPIC Intra-regional Variability

4.1 Overview

The characteristics of convection in the Eastern Pacific portion of the ITCZ complex are described in this chapter. Radar data used in this chapter was collected by the C-band radar onboard NOAA Research Vessel Ronald H. Brown. The EPIC campaign was briefly described in Chapter One. The methodology used in this chapter is described in Chapter Two. For the EPIC dataset, convection is characterized by evaluating three main features: horizontal structure, vertical structure and precipitation characteristics. These three components of convection are analyzed within the EPIC region by examining the variability associated with the diurnal cycle and the wind regime.

The variability associated with the diurnal cycle is investigated by dividing the day into six periods of four hours. The first of these six periods begins at 00:00 and ends at 03:59 while the last period begins at 20:00 and ends at 23:59. The variability associated with wind regime is investigated by dividing the observations into northerly and southerly regimes depending on the phase of the easterly wave at the time and date of the observation. The time and date periods used in this study have been previously described in Chapter One. More information about the easterly wave regimes and the EPIC campaign in general may be found in Petersen *et al.* (2003).

4.2 Convective Horizontal Structure

The horizontal characteristics of convection are evaluated by examining two products: the convective area and the convective fraction. The convective area represents the total area covered by radar echoes tagged as convective at any given time. The instantaneous convective area was calculated in the 100-km by 100-km domain of this study, and the total number of observations for each time period and wind regime was divided into twenty-five convective area intervals ranging from 0 to 2500 km^2. The convective area plots are shown in terms of cumulative relative frequency. The convective area may be affected in two ways: 1) the number of convective features, and 2) the size of individual convective features. Therefore, larger convective areas are associated with either a larger number of individual convective systems or the occurrence of larger (in the context of areal coverage) convective systems. The convective fraction uses the convective area information, but also takes into account identified regions of stratiform precipitation. The convective fraction indicates the instantaneous ratio of the area occupied by convective features to the area covered by all features (i.e. convective and stratiform). The relative frequency of the convective fraction is calculated for ten fraction intervals ranging from 0 to 1.

4.2.1 Convective Area

Figure 4.1a shows the convective area variability associated with the northerly and southerly regimes. It can be seen that the southerly curve is always below the northerly curve, indicating a higher frequency of larger convective areas in the southerly

regime. In the northerly regime 25% of observations indicated convective areas less than 100 km^2, whereas in the southerly regime this same range of areas represents only 10% of all observations in this regime. The occurrence of areas between the 700 and 2000 km^2 was observed to be slightly higher in the southerly regime. Therefore, the southerly regime is associated with either a higher number of individual convective systems or larger convective features. Figure 4.1a also indicates that approximately 10% of the convective features are greater than 2000 km^2 in both regimes. Figure 4.1b shows the convective area variability associated with the diurnal cycle. It can be seen that most sloped curves are the late night (00-04) and early morning (04-08) ones. These curves are associated with lower frequencies in the lowest intervals and higher frequencies in the intermediate intervals. Hence, the convection is more widespread in the late night and early morning hours, with only 12% of observations between midnight and 03:59 being less than 100 km^2, regardless of wind regime. The smallest convective features and/or least number of convective features occur in the afternoon (12-16), with as much as 24% of all instantaneous convective areas between noon and 15:59 being less than 100 km^2.

Figure 4.2a shows the convective area variability associated with the diurnal cycle during the northerly regime, and Figure 4.2b shows the same variability during the southerly regime. These two plots are a combination of the effects of diurnal cycle and wind regime and should show a mixture of the characteristics observed in Figure 4.1. The northerly regime diurnal variability (Figure 4.2a) shows a very similar pattern to the overall EPIC diurnal cycle variability, with the largest and smallest convective areas occurring at the same periods of the day observed in Figure 4.1b. However, the small area (less than 100 km^2) frequencies are very small during the night hours (00-04) of the

southern regime. During the afternoon hours of the northerly regime, 31% of convective areas are observed to be less than 100 km^2, whereas near sunrise (04-08) this frequency drops to 18%. The southerly regime diurnal variability (Figure 4.2b) shows that the maximum frequency of small areas (i.e. less than 100 km^2) occurs near sunset (16-20), when it totals 16% of observations (less than the minimum frequency in the northerly regime). The minimum occurs in the late night hours (00-04), when it represents only 1% of observations.

In summary, larger convective areas are observed in the southerly regime. Small total convective areas (i.e. less than 100 km^2) are significantly more frequent in the northerly regime. Smaller convective areas are more frequent in the afternoon and near sunset, and least frequent at night and near sunrise.

4.2.2 Convective Fraction

Figure 4.3a shows the convective fraction variability associated with the northerly and southerly regimes. It can be seen that the majority of the observations indicate fractions varying between 0.3 and 0.6. Another important feature of this plot is that the northerly curve is slightly displaced to the right, indicating a higher frequency of larger convective fractions in the northerly regime. These results are in agreement with Petersen *et al.* (2003). Since the convective area is greater in the southerly regime (as discussed in section 4.2.1), then this smaller convective fraction can only be explained by significantly larger stratiform areas in the southerly regime.

Figure 4.3b shows the convective fraction variability associated with the diurnal cycle. It can be seen that the most right-shifted curves are the late night (00-04) and early

morning (04-08) ones. These curves are associated with higher frequencies in the intermediate fraction intervals. Hence, the convection is more dominant in the late night and early morning hours, with nearly 42% of observations between midnight and 03:59 showing convective fractions greater than 0.5 regardless of wind regime. The smallest convective fractions occur in the afternoon (12-16), with only 29% of observations indicating fractions greater than 0.5.

Figure 4.4a (b) shows the convective fraction variability associated with the diurnal cycle during the northerly (southerly) regime. The northerly regime diurnal variability (Figure 4.4a) shows a very similar pattern to the overall EPIC diurnal cycle variability, with the largest and smallest convective areas occurring at the same periods of the day observed in Figure 4.3b. However, the large convective fractions (greater than 0.5) frequencies are higher than those observed in Figure 4.3b. This observation agrees with Figure 4.3a, which indicates higher frequencies of large convective fractions in the northerly regime. During the afternoon hours, 34% of convective fractions are observed to be greater than 0.5, whereas in the night hours this frequency increases to 55%. The southerly regime diurnal variability (Figure 4.4b) also shows the same periods of minimum convective fractions, but the largest convective fractions appear to occur in the early morning hours rather than in the late night hours. One striking difference is that there is a much higher frequency of lower convective fractions in the afternoon hours during the southerly regime. Convective fractions greater than 0.5 are least frequent in the afternoon hours, representing 20% of the total number of occurrences. This same range of convective fractions is most frequent in the early morning hours, representing 39% of the observations.

In summary, larger convective fractions are observed in the northerly regime. The diurnal cycle variability is approximately the same in both regimes, with larger fractions most frequent in the late night and early morning hours and least frequent in the afternoon. Large convective areas coupled with small convective fractions in the southerly regime suggest that larger stratiform areas are a characteristic of the southerly regime (consistent with Petersen *et al.*, 2003).

4.3 Convective Vertical Structure

The vertical characteristics of convection are evaluated by examining two products: the reflectivity distribution and the reflectivity heights. The reflectivity distribution simply shows the absolute frequency of reflectivities with height occurring in a time period or wind regime. The absolute frequency was calculated for a total of 16 vertical levels, between 2.5 and 17.5 km. Reflectivities were grouped into eight 5-dBZ bins starting at 20 dBZ. The reflectivity distributions are affected in two ways: 1) by the number or size of convective cells, and 2) by the intensity of convective systems. Therefore, a larger number of observations should indicate that convection is more frequent at a certain time and/or wind regime. Vigorous convection should appear as an increase in the frequency of occurrence in the higher reflectivity intervals. The reflectivity (or dBZ) height represents the maximum height in a convective column where that reflectivity value was observed. Thus, the 30-dBZ height indicates the maximum height in a convective column where a 30-dBZ ($\pm$ 2.5) reflectivity was observed. Ten reflectivity heights, between 45 and 0 dBZ, were calculated for each regime and averaged every hour. The reflectivity heights show an averaged vertical profile of the convective

cloud, similar to what one would see in a vertical cross-section or in a range height indicator (RHI) radar scan.

4.3.1 Reflectivity Distribution

Figure 4.5 shows the absolute frequency of reflectivities occurring at each vertical level during the northerly regime (Figure 4.5a) and southerly regime (Figure 4.5b) periods. These plots show a quite impressive similarity in most of the lower reflectivity intervals. The most important and striking difference between the two regimes is the higher frequency of reflectivities greater than 45 dBZ in the lowest levels. During the southerly regime periods, there were only 2879 observations of reflectivities above 45 dBZ at 2.5 km, representing less than 1% of all the observations. On the other hand, during the northerly regime periods there were 12051 observations of reflectivities above 45 dBZ, representing approximately 3.5% of all observations. Therefore, it is suggested that the northerly regime convective clouds have more intense cores than southerly regime convective clouds.

Figure 4.6 (4.7) shows the reflectivity distribution variability associated with the diurnal cycle during the northerly (southerly) regime periods. The northerly regime shows a minimum number of observations between the afternoon (Figure 4.6d) and early evening (Figure 4.6e). The maximum number of observations occurs in the late night (Figure 4.6a) and early morning (Figure 4.6b) hours. In the 4-hour period of the afternoon (i.e. 12:00 to 15:59) there were 37235 observations at 2.5 km, representing approximately only 10% of all observations at that height. The late night hours (i.e. 00:00 to 03:59) had 93556 observations at the same height (26% of all observations) at that height. The

southerly regime shows a minimum number of observations in the afternoon hours (Figure 4.7d), whereas the maximum occurs in the early morning hours (Figure 4.7b). In the afternoon hours, there were 37460 observations at 2.5 km (also 10% of observations), and in the early morning hours there were 72384 observations at that same height (20%). In both regimes, the higher (lower) number of observations is associated with the higher (lower) frequency of high reflectivities.

In summary, northerly regime convection has a higher frequency of occurrence for intense cores. Convection is most frequent and most intense in the late night and early morning hours and least frequent and least intense in the afternoon and early evening hours.

4.3.2 Reflectivity Heights

Figure 4.8 shows the hourly-averaged reflectivity heights during the northerly regime (Figure 4.8a) and southerly regime (Figure 4.8b) periods. The northerly regime shows a much steadier change during the diurnal cycle. The maximum heights occur between 05:00 and 07:00 and the minimum occurs near 16:00. This is in agreement with the previous results discussed in this chapter. The southerly regime shows that the maximum heights occur between 07:00 and 09:00 and the minimum occurs near 18:00. Therefore, it appears that there is a 2-hour lag between the northerly and southerly convective life cycles. Averages are slightly higher (approximately 200 m) in the northerly regime. The other interesting feature that can be seen in the southerly reflectivity heights is the presence of a secondary minimum just before the maximum time. This minimum is observed for all reflectivity heights to occur between 03:00 and

04:00, a few hours before the convection peaks. The hourly absolute frequencies (not shown) indicate that a smaller number of reflectivity observations occur at this time. This may be indicative of a destructive meteorological interaction in the regional scale at this time of the day.

4.4 Precipitation Characteristics

The evaluation of the characteristics of convective precipitation is twofold: 1) to investigate the intensity of the precipitation by examining the frequency and variability of rain rates; and 2) to investigate the type of precipitation by also examining the frequency and variability of the warm-rain-producing areas and warm rain volume. The rain rate was calculated using the Z-R relationships described in Chapter Two. The same Z-R relationship is used for both, the northerly and southerly regimes. The warm-rain-producing area fraction indicates the percentage of the raining areas that is generated by warm rain processes. The warm rain volume fraction indicates the percentage of the total convective rainfall that is associated with warm rain processes.

4.4.1 Precipitation Intensity

Figure 4.9 shows the rain rate variability associated with the northerly and southerly regimes. It can be seen that the southerly curve is always above the northerly curve, indicating a higher frequency of light precipitation in the southerly regime. The difference between the curves is no greater than 5% at all times. In the northerly regime 47% of observations indicated rain rates less than 1.0 mm/h, whereas in the southerly regime this same range of rain rates represents 49% of all observations in this regime.

Rain rates greater than 20 mm/h represent less than 3% (1%) of occurrences in the northerly (southerly) regime. All these results indicate that the southerly regime is associated with lighter precipitation. This is consistent with larger the stratiform areas that were observed to occur in the southerly regime (as discussed previously).

Figure 4.10a (b) shows the rain rate variability associated with the diurnal cycle during the northerly (southerly) regime. The northerly regime diurnal variability (Figure 4.10a) shows that light precipitation (less than 1.0 mm/h) is more predominant near sunset (16-20), with as much as 66% of the rain rates in this category at 16:00. Light precipitation is less frequent near sunrise (04-08), when rain rates less than 1.0 mm/h can account for as low as 37% of all observations. Rain rates greater than 25 mm/h correspond to less than 2% of observations at all times of the day. Rain rates greater than 30 mm/h correspond to less than 1% of observations. The southerly regime diurnal variability (Figure 4.10b) shows maximum frequency of light precipitation a few hours later. Light precipitation is most frequent at night (20-00), with as much as 70% of the rain rates being less than 1.0 mm/h at this time of the day. Light precipitation is least predominant near sunrise (04-08), with only 40% of rain rates observed to be less than 1.0 mm/h at this time of the day. Rain rates greater than 25 mm/h correspond to less than 1% of all observations in the southerly regime.

In summary, lighter precipitation (characteristics of extensive areas of stratiform precipitation discussed earlier) is more frequent in the southerly regime. Lighter rain rates are least frequent near sunrise in both wind regimes. Lighter rain rates are most frequent near sunset in the northerly regime, and at night in the southerly regime.

4.4.2 Precipitation Type

Figure 4.11a (b) shows the diurnal variability, for each wind regime, of the fraction of rain-producing areas (rainfall volume) that is associated with warm rain processes. Figure 4.11a shows that rain-producing areas associated with warm rain processes represent 24% or more of all observations at all times of the day in both regimes. It can be seen that the southerly curve is mostly above or coincident with the northerly curve, indicating a higher frequency of warm-rain-producing areas in the southerly regime. This is consistent with the results shown in the previous sections indicating higher frequency of stratiform areas and lighter precipitation in the southerly regime. The minimum and maximum relative frequencies of warm rain are approximately the same in both regimes, with warm type echoes varying between 24% and 67% of the rain-producing areas. Moreover, there is a lag of 2 hours between the northerly and southerly curves, a difference that was also identified in the vertical structure of each wind regime. The maximum frequency of warm-rain-producing areas occurs between 17:00 and 21:00 during the northerly regime, and between 19:00 and 23:00 in the southerly regime. The period of minimum frequencies is much longer, ranging form 02:00 to 12:00 in the northerly regime, and from 07:00 to 14:00 in the southerly regime. Figure 4.11b shows that the fraction of the rainfall volume associated with warm rain processes is less than 12% at all times between midnight and noon in both regimes. Between noon and midnight, the peaks in warm rainfall volume are observed. The maximum fraction of rainfall volume associated with warm rain processes in the northerly (southerly) regime occurs in the afternoon (at night), peaking at 31% (27%) of occurrences at that hour.

In summary, warm rain is more frequent in the southerly regime. The diurnal cycle indicates a 2-hour lag, between northerly and southerly regimes, in the peak of warm-rain-producing areas. This lag is equal to 4 hours in the warm rain volume analysis. Warm-rain-producing areas are least frequent near sunrise in both regimes (when deeper convection is most prevalent – Figure 4.8) and most frequent near sunset (at night) during the northerly (southerly) regime.

a)

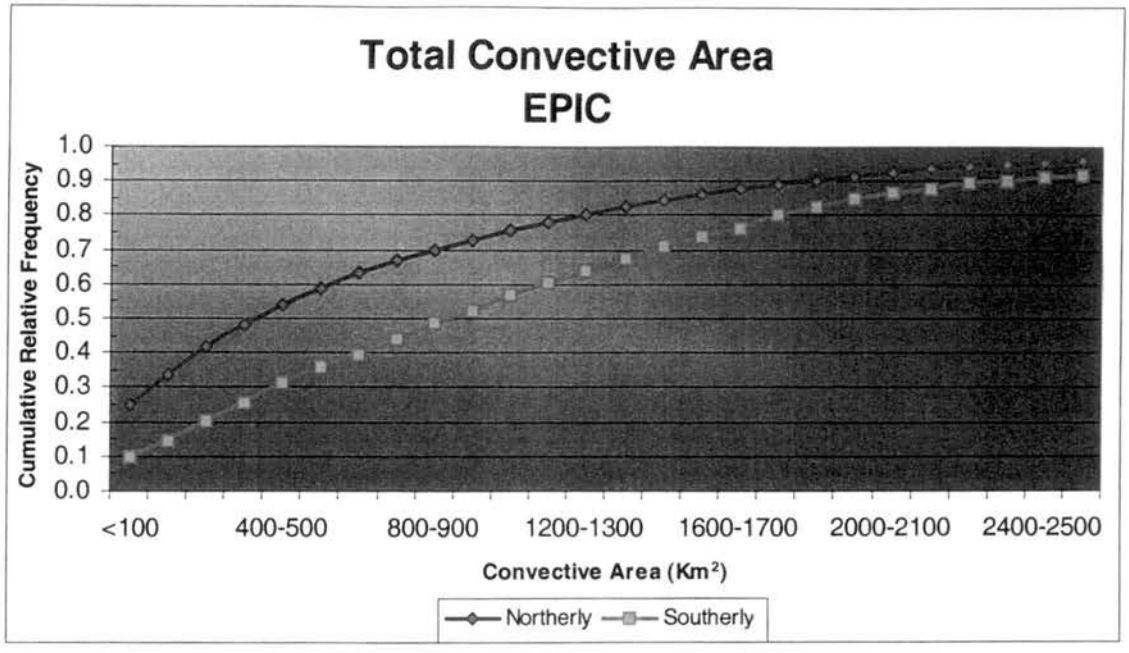

b)

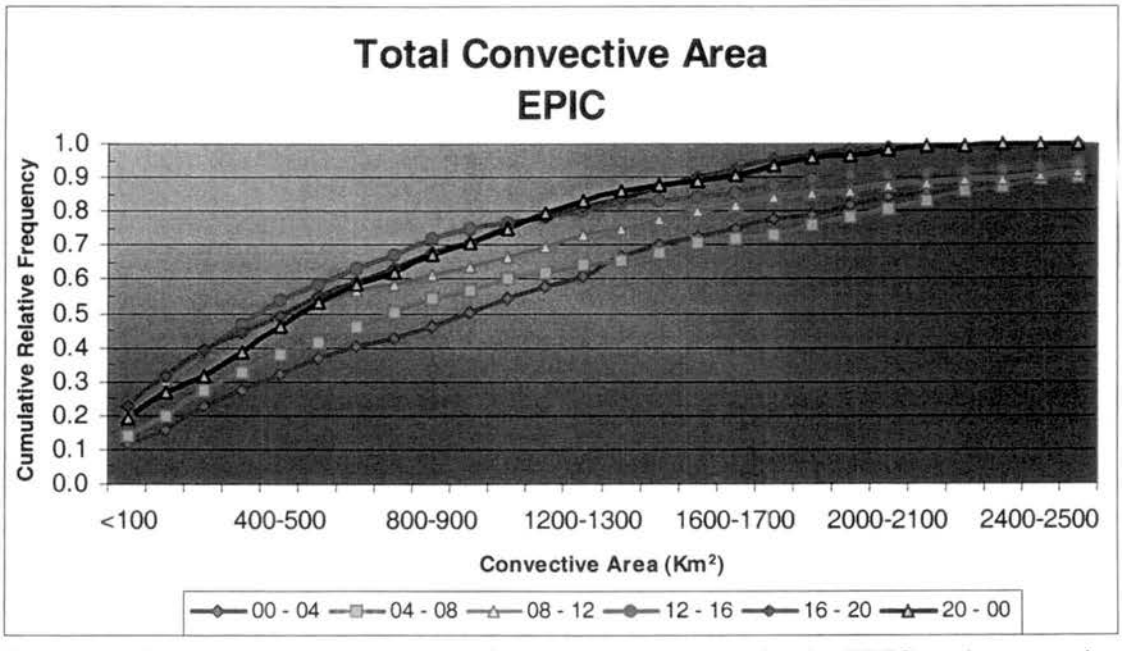

Figure 4.1: Intra-regional variability of the convective area in the EPIC region associated with a) the wind regimes, and b) the diurnal cycle.

a)

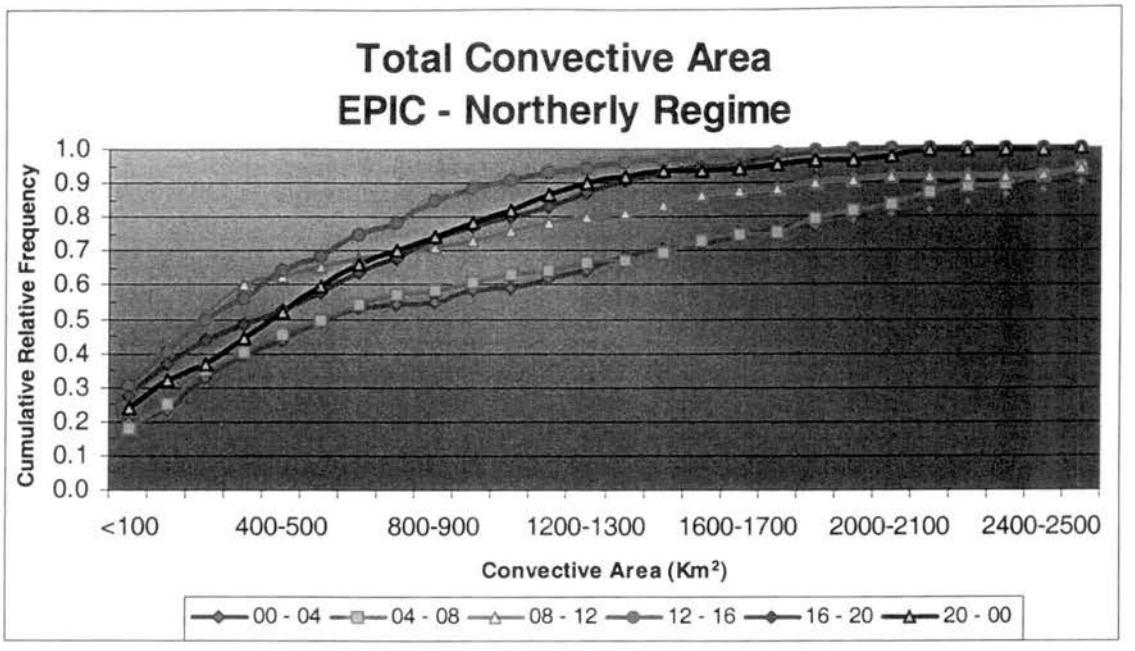

b)

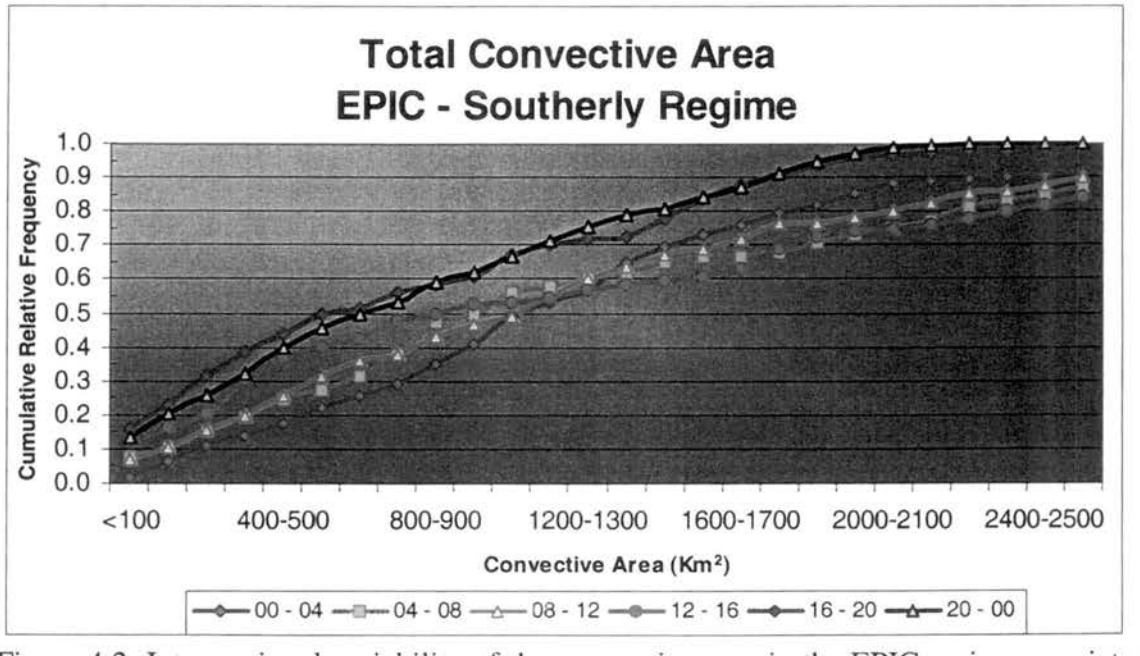

Figure 4.2: Intra-regional variability of the convective area in the EPIC region associated with the diurnal cycle during the a) northerly regime and b) southerly regime.

a)

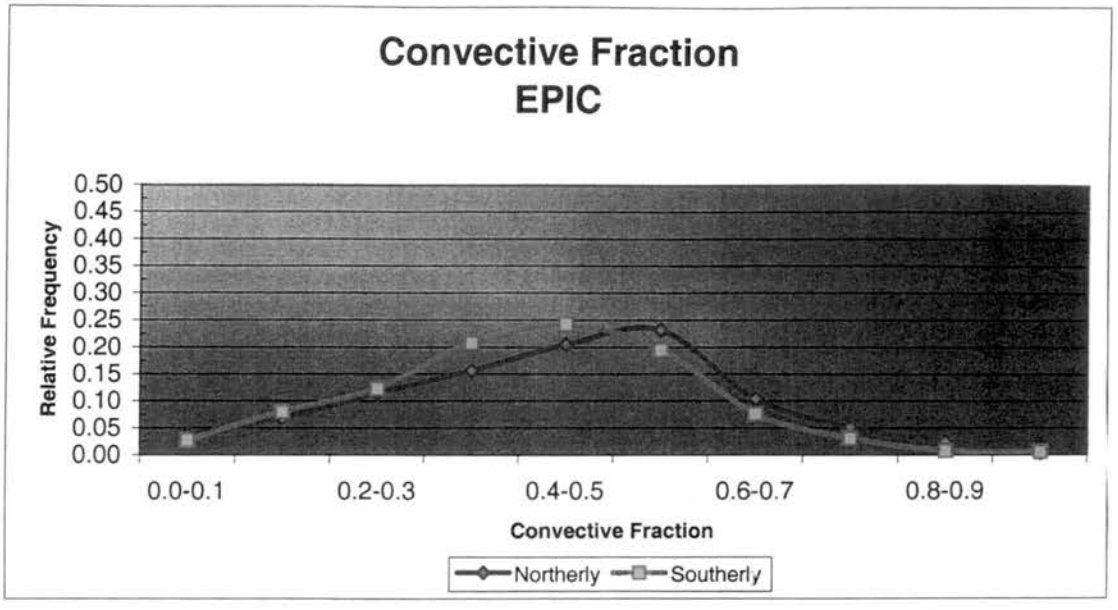

b)

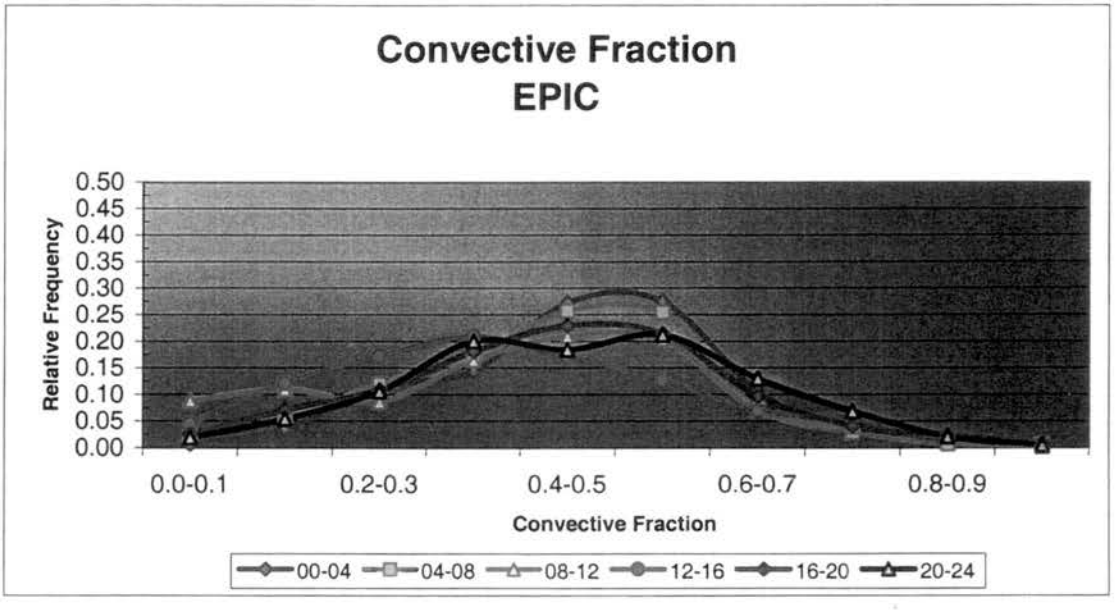

Figure 4.3: Intra-regional variability of the convective fraction in the EPIC region associated with a) the wind regimes, and b) the diurnal cycle.

a)

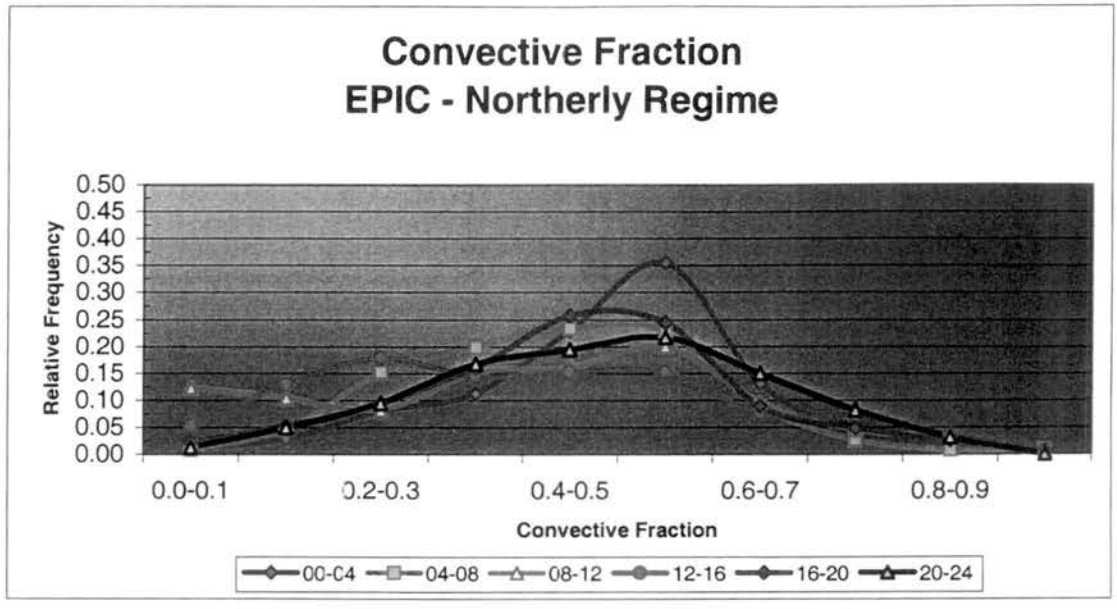

b)

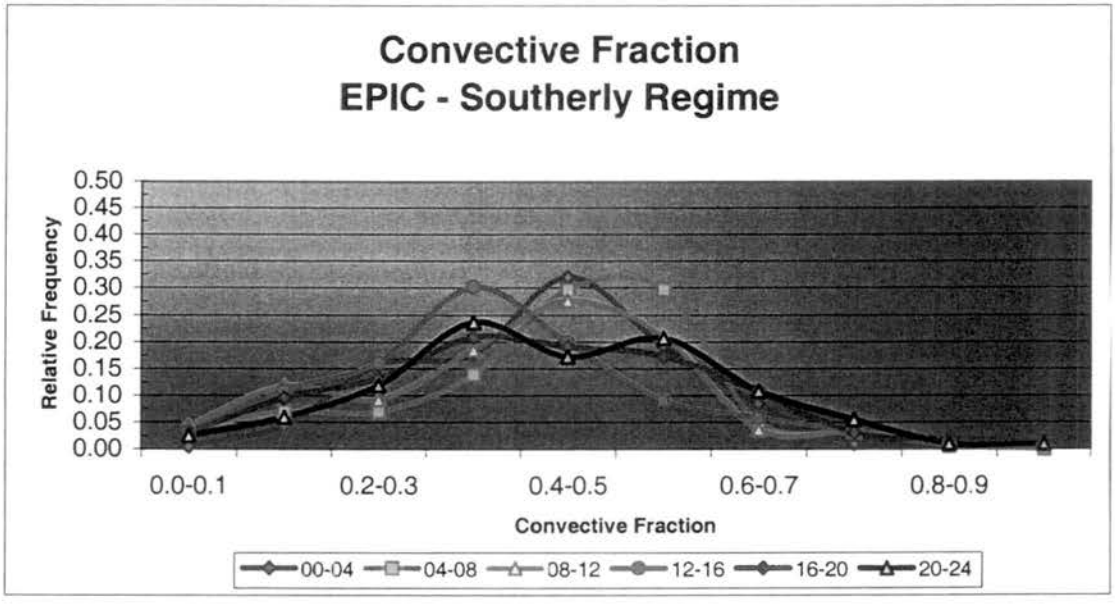

Figure 4.4: Intra-regional variability of the convective fraction in the EPIC region associated with the diurnal cycle during the a) northerly regime and b) southerly regime.

a)

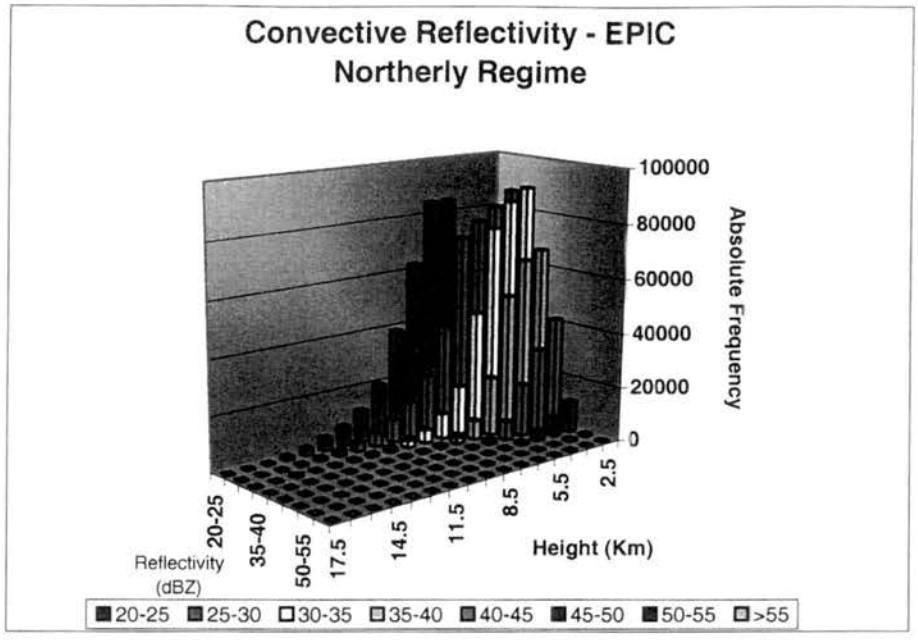

b)

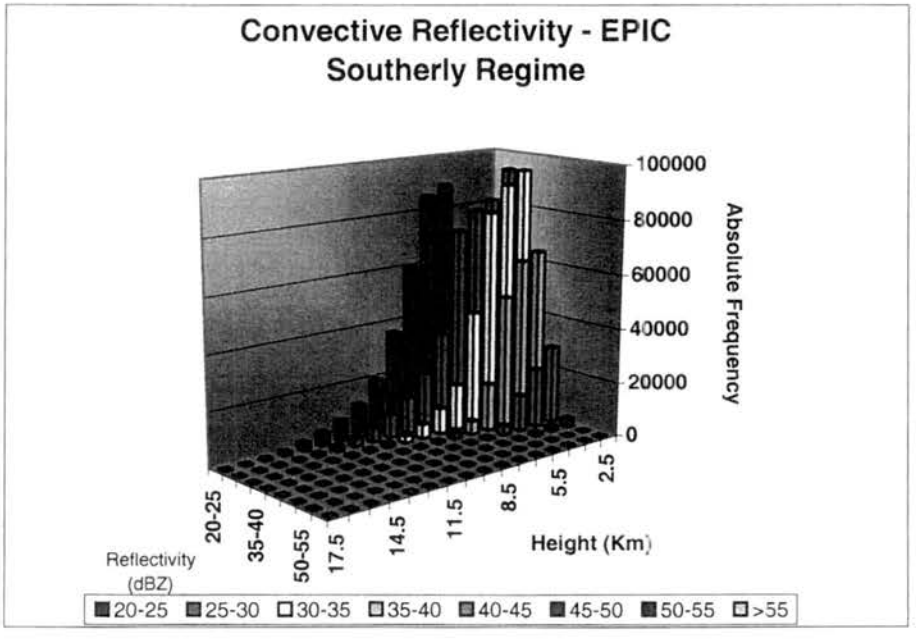

Figure 4.5: EPIC vertical reflectivity distribution during a) northerly regime, and b) southerly regime.

a)

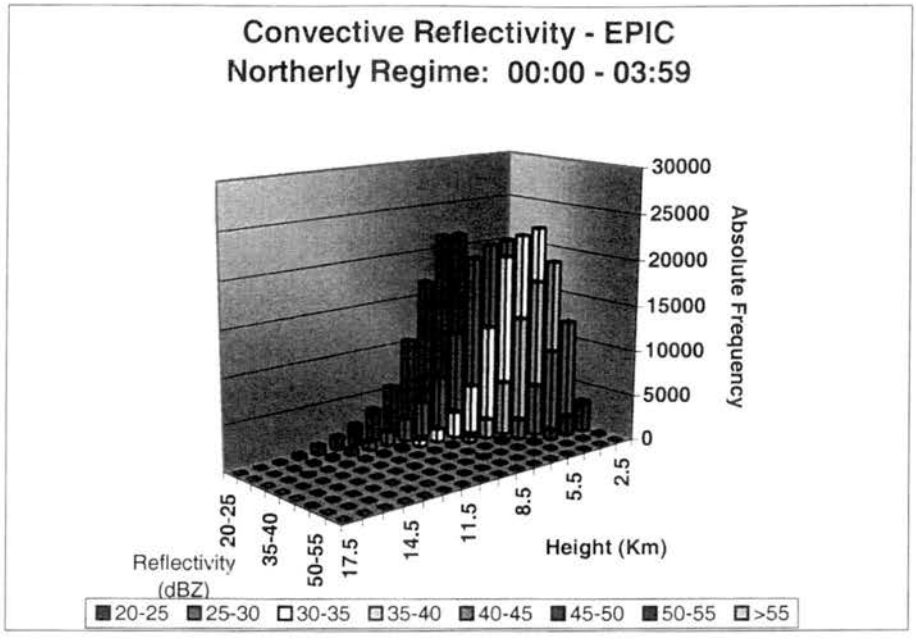

b)

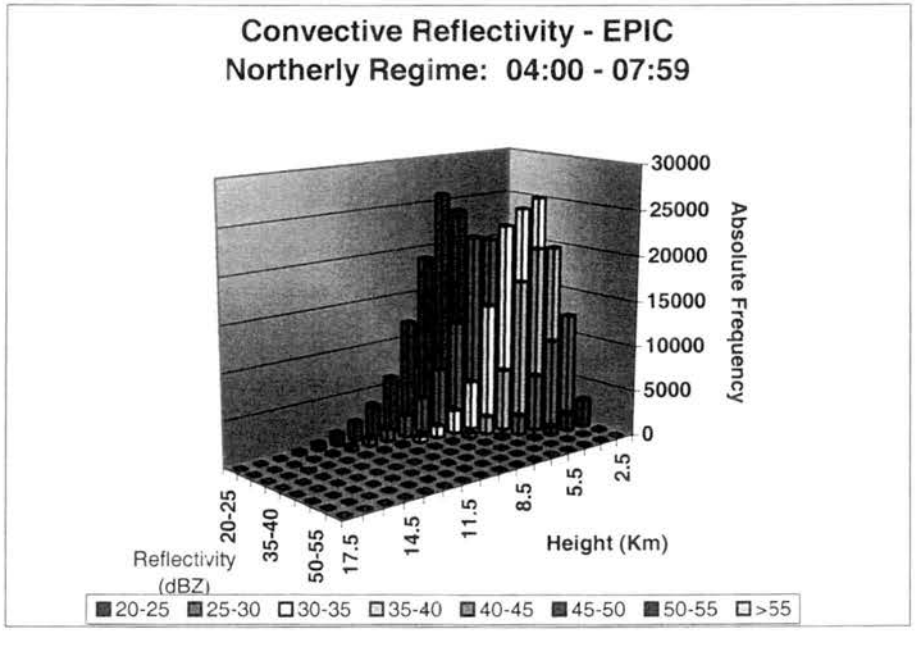

Figure 4.6: EPIC vertical reflectivity distribution during the northerly regime for observations between a) 00:00 and 03:59, b) 04:00 and 07:59, c) 08:00 and 11:59, d) 12:00 and 15:59, e) 16:00 and 19:59, and f) 20:00 and 23:59.

c)

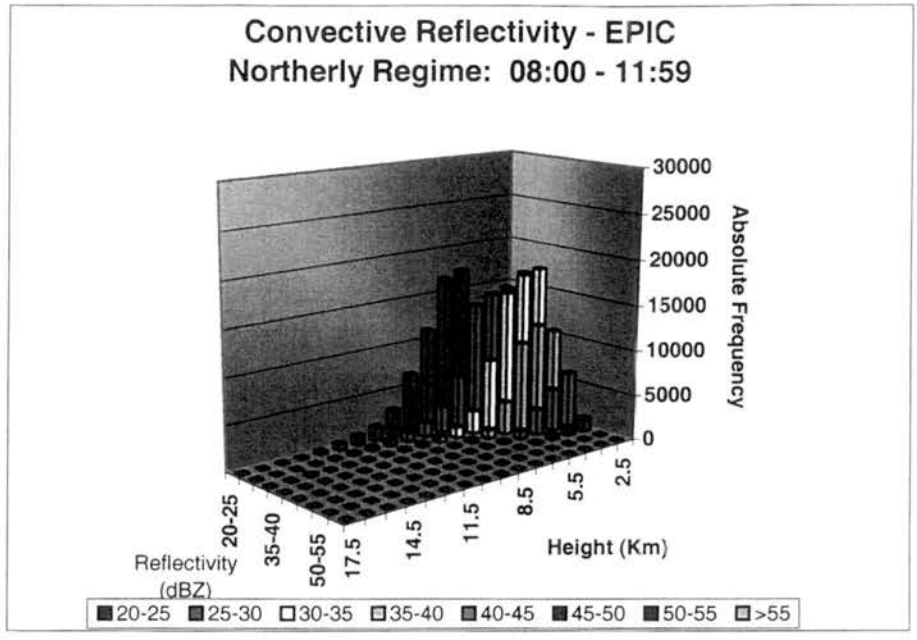

d)

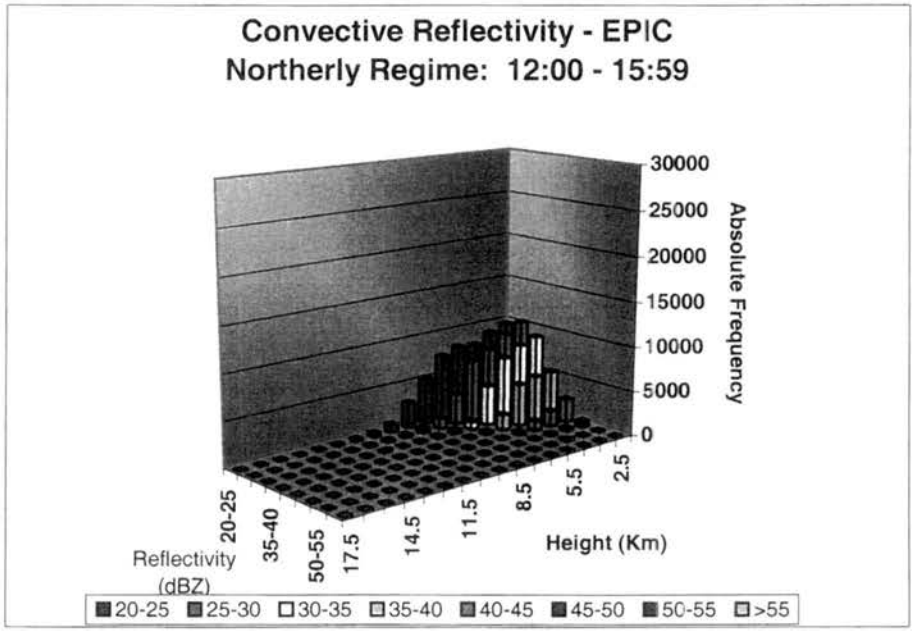

Figure 4.6: (Cont.)

e)

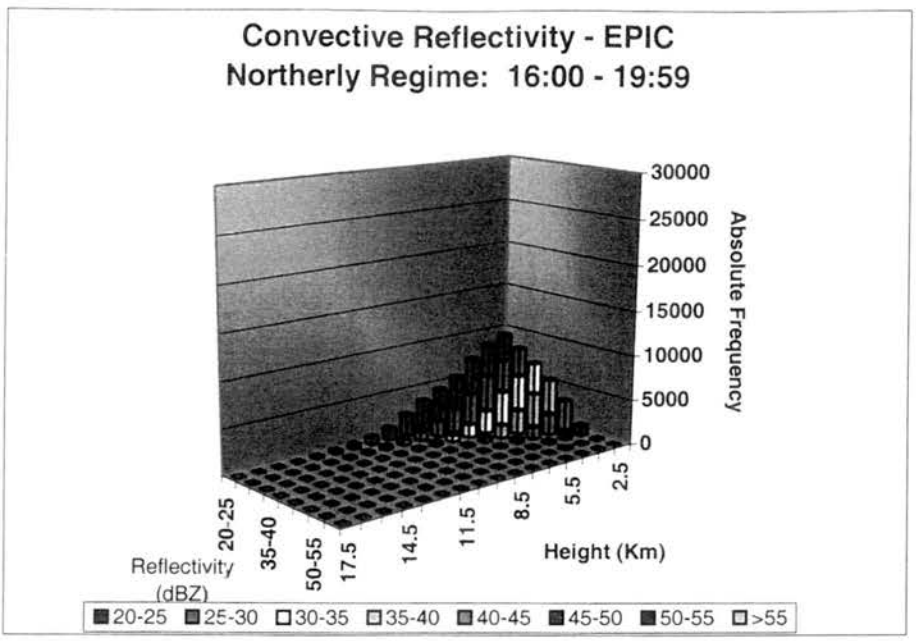

f)

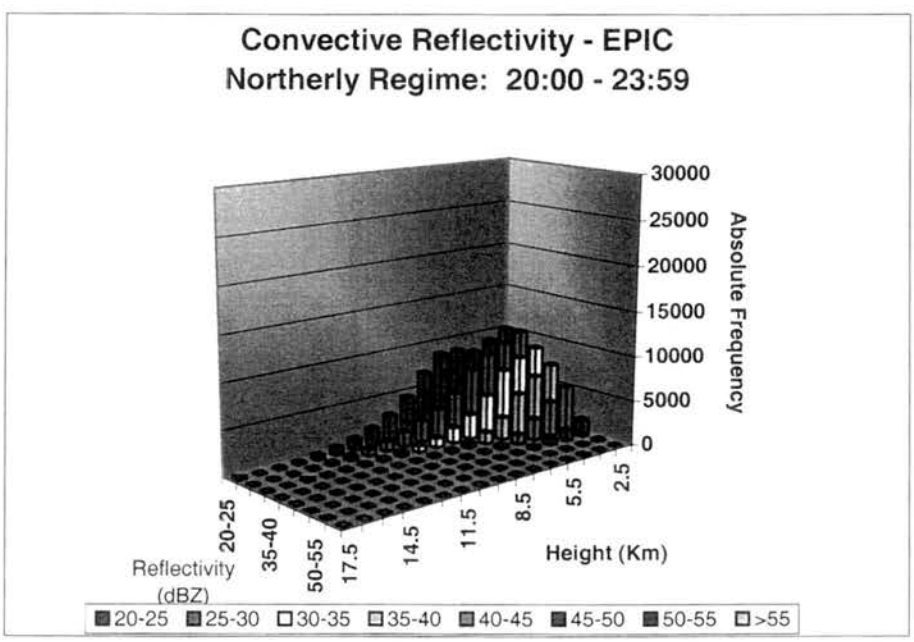

Figure 4.6: (Cont.)

a)

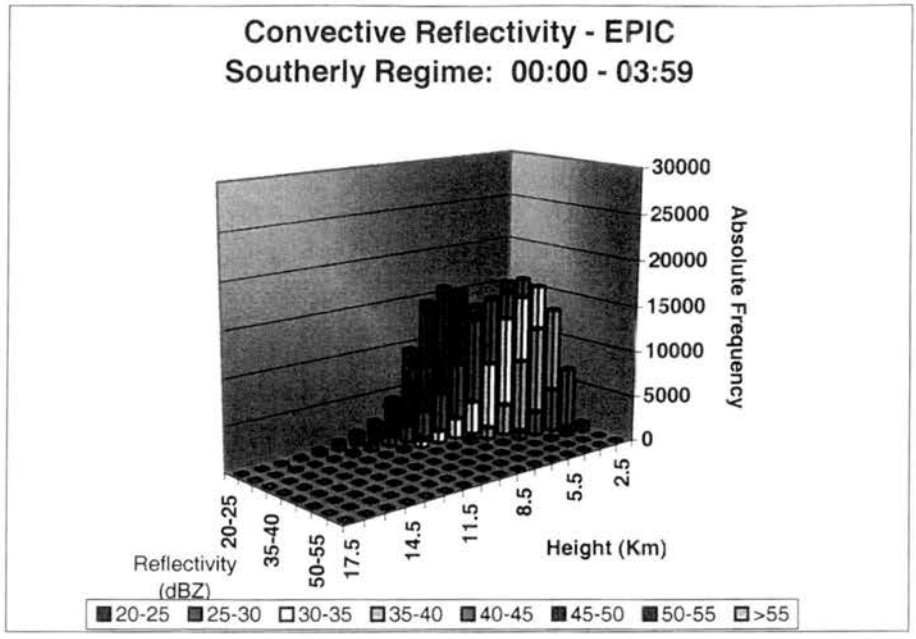

b)

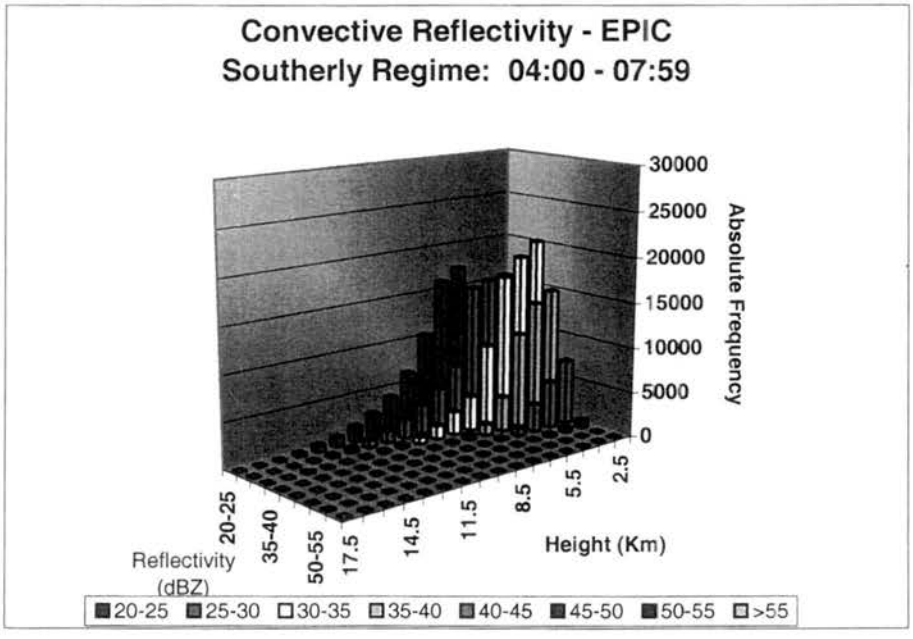

Figure 4.7: EPIC vertical reflectivity distribution during the southerly regime for observations between a) 00:00 and 03:59, b) 04:00 and 07:59, c) 08:00 and 11:59, d) 12:00 and 15:59, e) 16:00 and 19:59, and f) 20:00 and 23:59.

c)

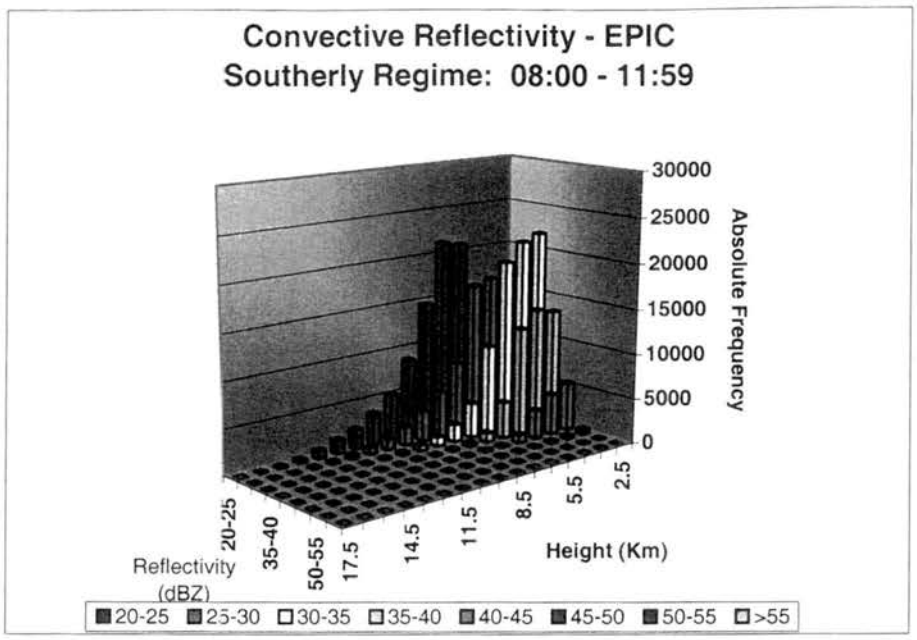

d)

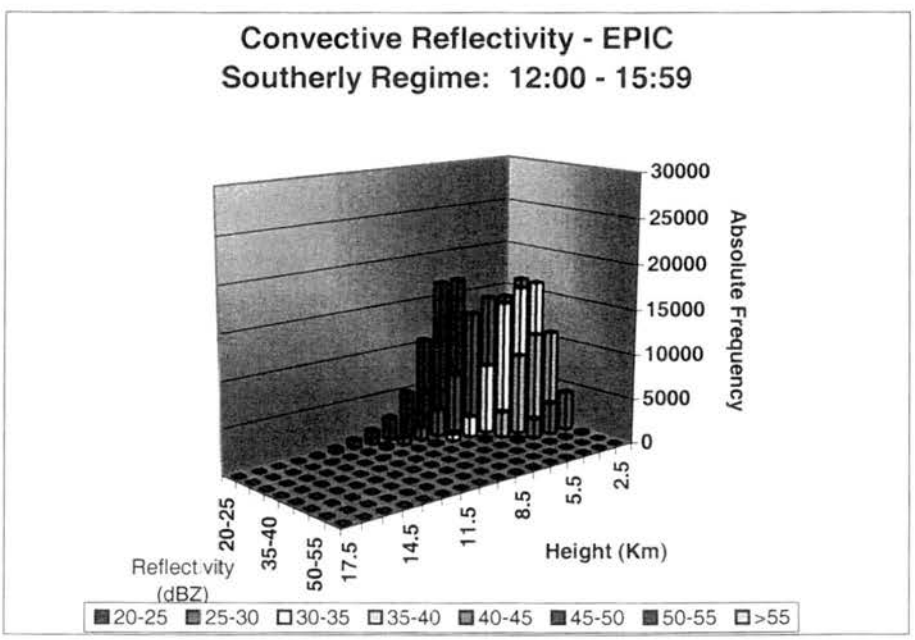

Figure 4.7: (Cont.)

e)

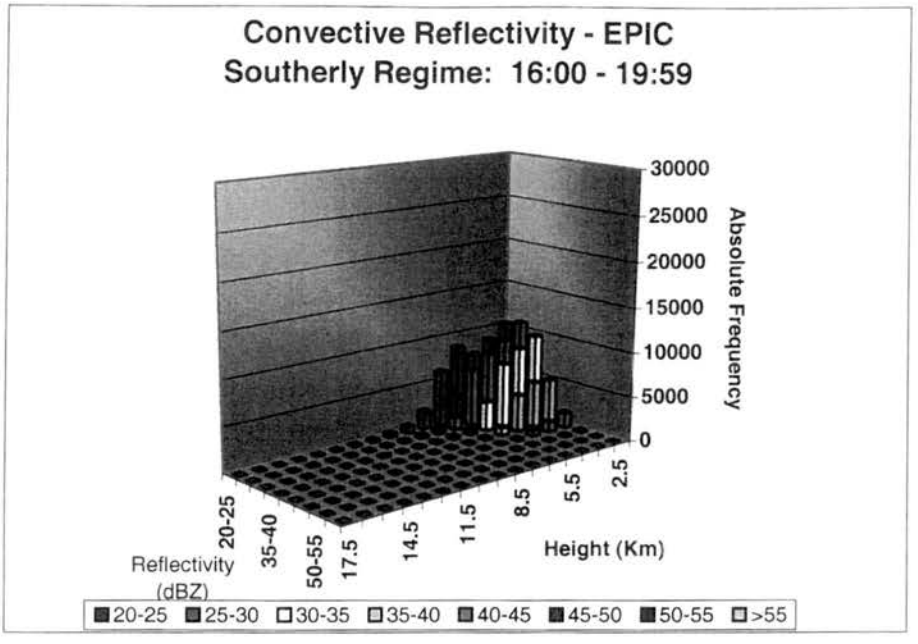

f)

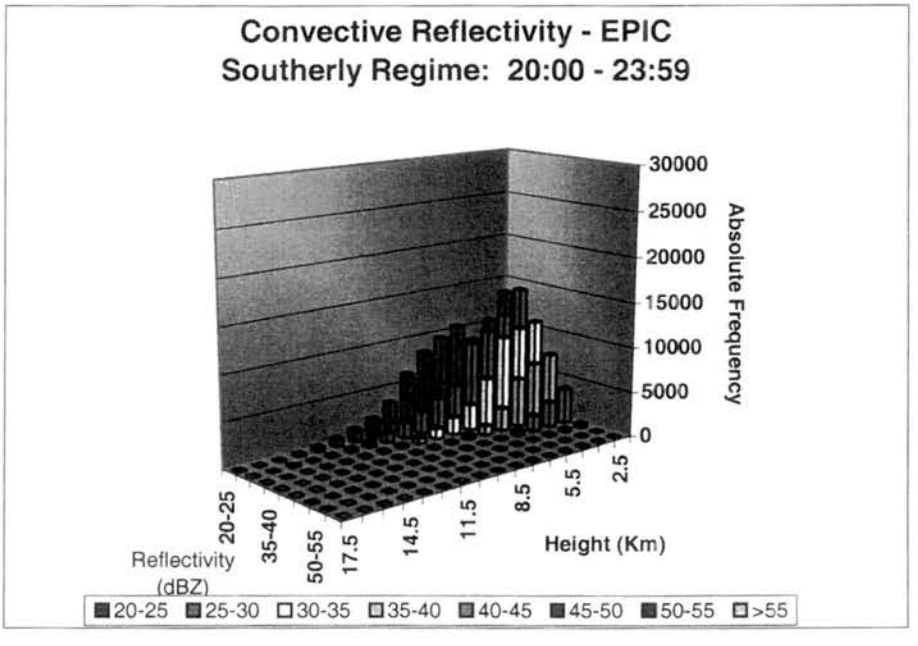

Figure 4.7: (Cont.)

a)

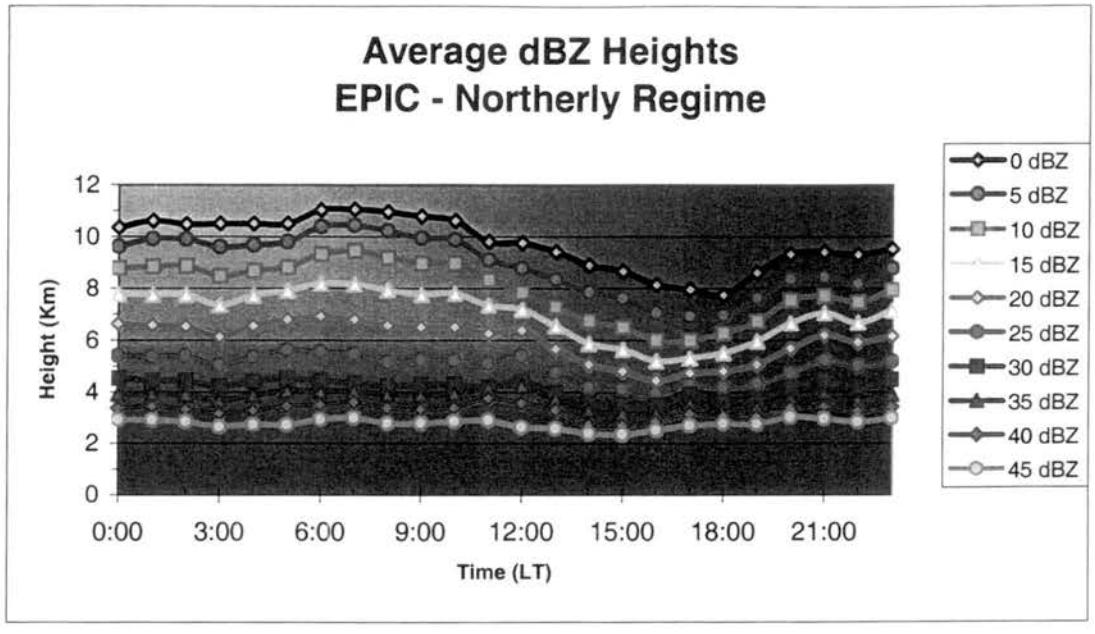

b)

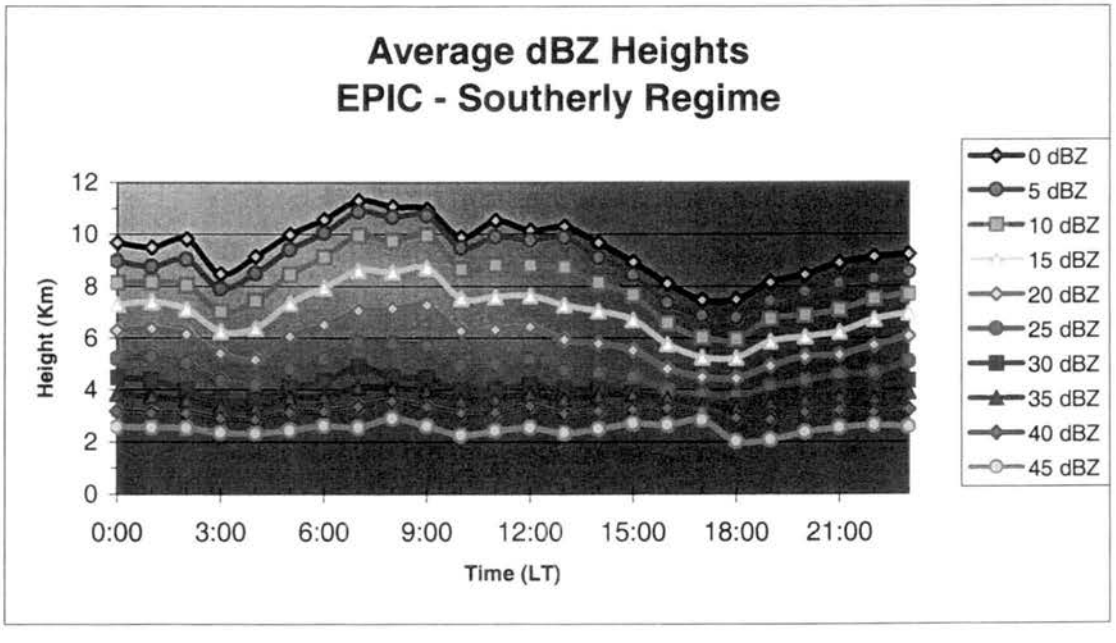

Figure 4.8: EPIC hourly-averaged reflectivity heights during the a) northerly regime, and b) southerly regime.

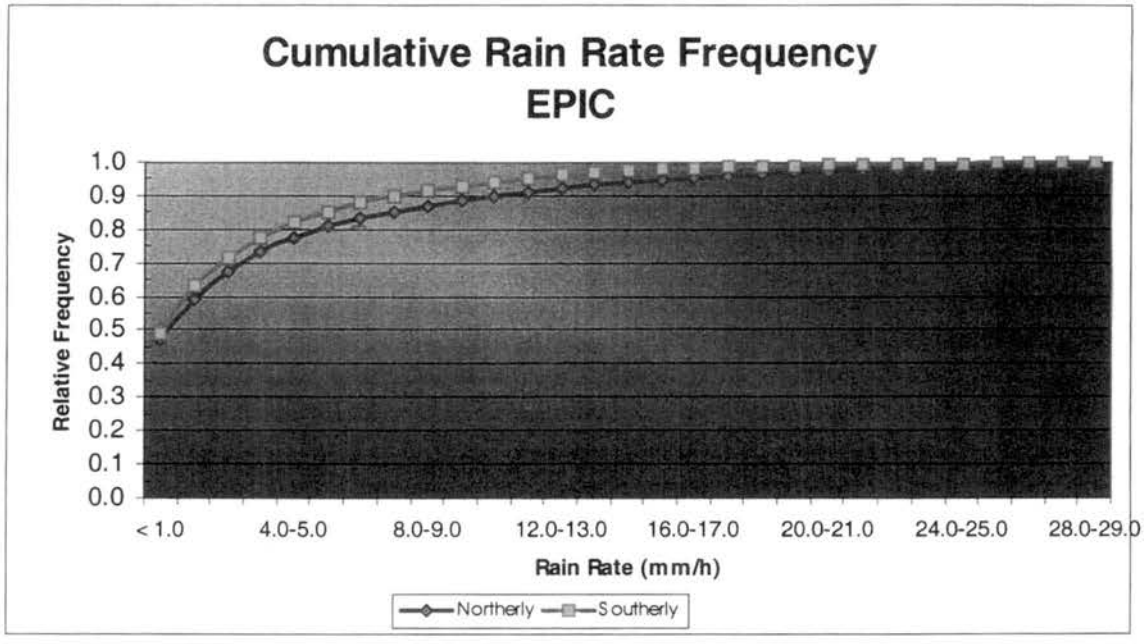

Figure 4.9: Intra-regional variability of the rain rate in the EPIC region associated with the wind regimes.

a)

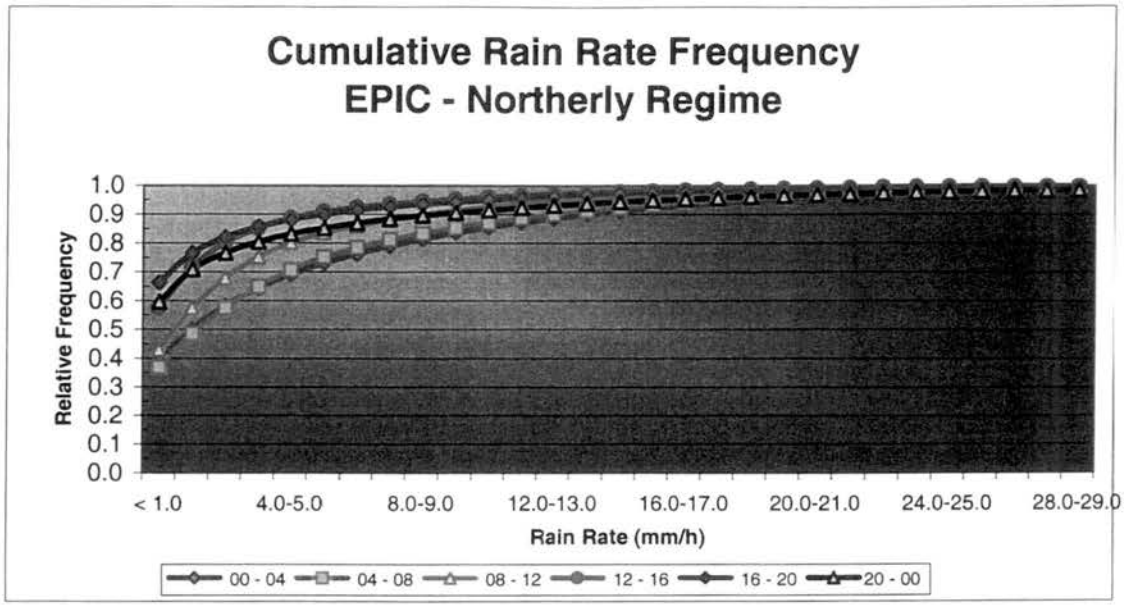

b)

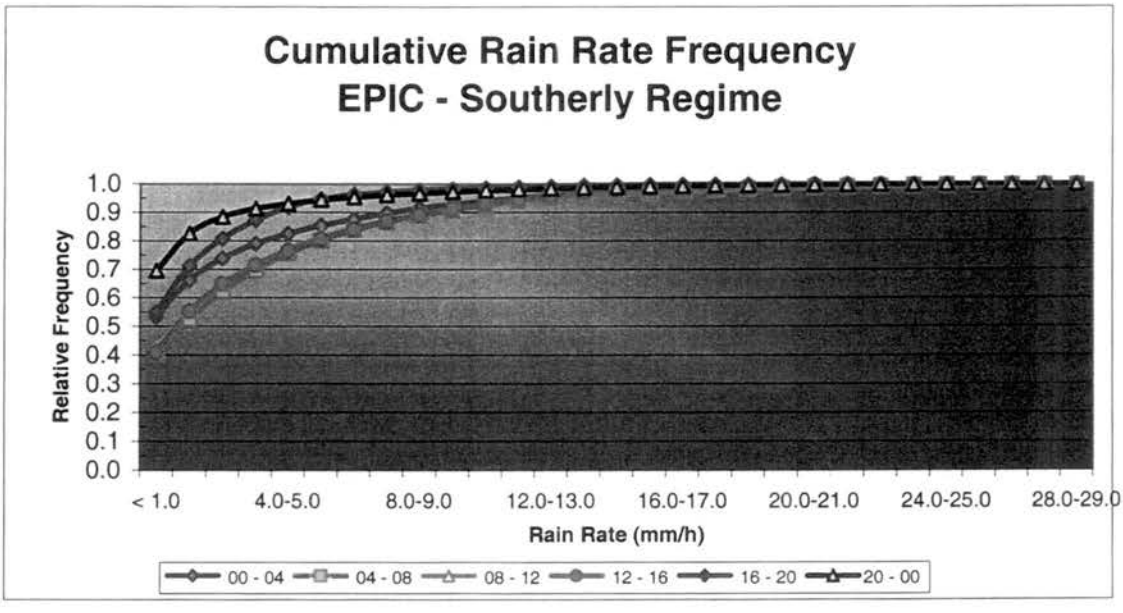

Figure 4.10: Intra-regional variability of the rain rate in the EPIC region associated with the diurnal cycle during the a) northerly regime and b) southerly regime.

a)

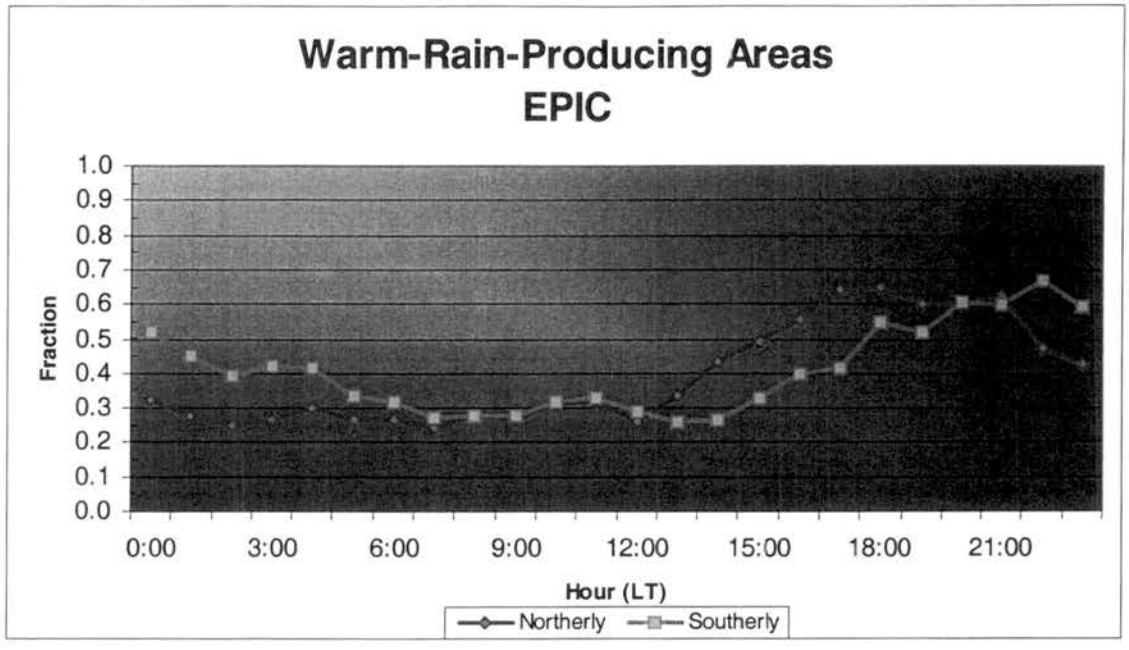

b)

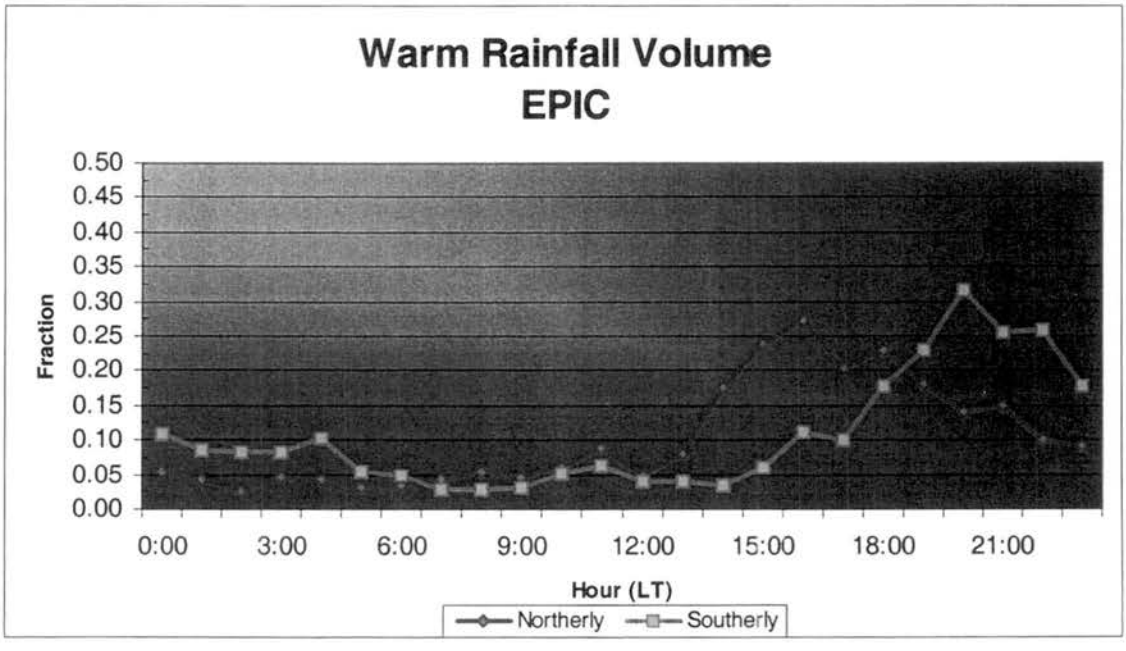

Figure 4.11: Hourly-averaged fraction of a) rain-producing areas and b) rainfall volume, associated with warm rain processes during EPIC in the northerly and southerly regimes.

CHAPTER FIVE

TRMM/LBA-EPIC Inter-regional Variability

5.1 Overview

In this chapter, we evaluate the differences between the characteristics of convection in the TRMM/LBA and EPIC regions using the same type of analyses shown in the previous two chapters. The methodology for each analyses used in this chapter is described in Chapter Two. For the inter-regional comparison between the TRMM/LBA and EPIC regions, convection was also examined using the same three main features used in the previous two chapters: horizontal structure, vertical structure and precipitation characteristics. These three components of convection are analyzed in this chapter using all information available from each of the datasets regardless of time of the day or wind regime. The upper core region of convective clouds is not evaluated in this chapter, since polarimetric data were not available in EPIC.

5.2 Convective Horizontal Structure

In this section, two reflectivity-derived products are used to evaluate the horizontal characteristics of convection: the convective area and the convective fraction. The convective area analysis shows the total area covered by radar echoes tagged as convective at any given time. The instantaneous convective area was calculated in the 100-km by 100-km domain of this study, and the total number of observations for each

time period and wind regime was divided into twenty-five convective area intervals ranging from 0 to 2500 km^2. The convective area may be affected by the number of convective features and also by the size of individual convective features. Therefore, larger convective areas are associated with either a larger number of individual convective systems or the presence of larger convective systems. The convective fraction uses the total convective and stratiform areas to indicate the instantaneous ratio of the area occupied by convective features to the area covered by all features (i.e. convective and stratiform). The relative frequency of the convective fraction is calculated for ten fraction intervals ranging from 0 to 1.

5.2.1 Convective Area

Figure 5.1 shows the total convective area for the TRMM/LBA and EPIC regions. It can be seen that the TRMM/LBA curve is always above the EPIC curve, indicating a higher frequency of smaller convective areas in the TRMM/LBA region. In the TRMM/LBA region 47% of observations indicated convective areas less than 100 km^2, whereas in the EPIC region this same range of areas represents only 19% of all observations in the region. In the TRMM/LBA region, less than 1% of observations indicated total convective areas greater than 2500 km^2, while in the EPIC region this same range of convective areas represents 5% of observations in the region. The TRMM/LBA curve shows that beyond 1400 km^2, the relative frequency (non-cumulative) of each interval is 1% or less, while in the EPIC region this is observed only beyond 1900 km^2. Total convective areas between 200 and 2000 km^2 are 20% more frequent in the EPIC region, representing 40% (60%) of the observations in the

TRMM/LBA (EPIC) region. Therefore, the TRMM/LBA region is associated with either a lower number of individual convective systems or smaller convective features.

5.2.2 Convective Fraction

Figure 5.2 shows the convective fraction distribution for the TRMM/LBA and EPIC regions. It can be seen that the majority of the observations indicate fractions varying between 0.2 and 0.6. Another important feature of this plot is that the EPIC curve is right-shifted with respect to the TRMM/LBA curve, indicating a higher frequency of larger convective fractions in the EPIC region. The modal convective fraction in the TRMM/LBA (EPIC) region is in the 0.3-to-0.4 (0.4-0.5) interval, representing 26% (22%) of observations in the region. Convective fractions less than 0.1 or greater than 0.8 represent 4% or less of observations in each region.

5.3 Convective Vertical Structure

In this section, we evaluate the vertical characteristics of convection in the TRMM/LBA and EPIC regions. The reflectivity distribution simply shows the absolute frequency of reflectivities with height. The absolute frequency was calculated for a total of 16 vertical levels, between 2.5 and 17.5 km. Reflectivities were grouped into eight 5-dBZ bins starting at 20 dBZ. The reflectivity distributions are affected by the number and size of convective cells, and also by the intensity of convective systems. Therefore, a larger number of observations should indicate that convection is more frequent or more widespread. More vigorous convection should appear as an increase in the frequency of occurrence in the higher reflectivity intervals.

Figure 5.3a (b) shows the absolute frequency of reflectivities occurring at each vertical level in the TRMM/LBA (EPIC) region. Comparing Figures 5.3a and 5.3b, it can be seen that high reflectivities (i.e. greater than 45 dBZ) are more frequent in the TRMM/LBA region. At the lowest four vertical levels (i.e. 2.5-5.5 km) the frequency of intermediate reflectivities (i.e. 30 to 45 dBZ) is higher in the EPIC region. Above 5.5 km, the intermediate reflectivities become relatively more frequent in the TRMM/LBA region. In the TRMM/LBA region, there were 104687 observations of reflectivities above 45 dBZ at all levels, representing over 2% of all the observations. On the other hand, in the EPIC region there were 28000 observations of reflectivities above 45 dBZ, representing approximately 0.8% of all observations in the region. Therefore, it is suggested that, overall, the TRMM/LBA convective clouds have more intense cores than the convective clouds in the EPIC region.

5.4 Precipitation Characteristics

The evaluation of the characteristics of convective precipitation is twofold: 1) to investigate the intensity of the precipitation by examining the variability of rain rates; and 2) to investigate the type of precipitation by also examining the variability of warm rain (previously defined in section 2.10) areas and volume. The rain rate was calculated using the Z-R relationships described in Chapter Two. The warm rain area fraction indicates the percentage of the raining areas that are generating warm rain at any given time. The warm rain volume fraction indicates the percentage of the total convective rainfall that is associated with warm rain processes.

5.4.1 Precipitation Intensity

Figure 5.4 shows the rain rate cumulative frequency in the TRMM/LBA and EPIC regions. It can be seen that the EPIC curve begins below the TRMM/LBA curve, and interception occurs near 10 mm/h. This indicates that light rain rates (i.e. less than 1 mm/h) are more frequent in the TRMM/LBA region. Also, there is a slight tendency for intense rain rates (i.e. greater than 30 mm/h) to occur more frequently in the TRMM/LBA region. In the TRMM/LBA region 67% of observations indicated rain rates less than 1.0 mm/h, whereas in the EPIC region this same range of rain rates represents 48% of all observations in the region. Rain rates greater than 30 mm/h represent 3% of observations in the TRMM/LBA region, while in the EPIC region rain rates greater than 30 mm/h are less than 1% of occurrences in the region. Rain rates between 1 and 15 mm/h, but especially between 1 and 8 mm/h, are more frequent in the EPIC region.

5.4.2 Precipitation Type

Figure 5.6 shows the fraction of rain-producing areas that is associated with warm rain processes in the TRMM/LBA and EPIC regions. Figure 5.6 shows that rain-producing areas associated with warm rain processes are more frequent in the EPIC region. In the TRMM/LBA region, warm-rain-producing areas represent 24% of observations in the region, while in EPIC region this frequency is equal to 38%. Despite the fact that warm-rain areas are more frequent in the EPIC region, Figure 5.7 shows that the fraction of the rainfall volume associated with warm rain processes is nearly the same in both regions. In the TRMM/LBA region the fraction of rainfall associated with warm-processes is equal to 6.5%, whereas in the EPIC region this percentage is slightly higher:

7.2% These values compare well with those found over the western Pacific region obtained by Rickenbach and Rutledge (1998). This apparent contradiction in warm rain areas and volume can probably be explained by the rain rate differences between the two regions. In any case, convective areas associated with mixed-rain processes (i.e. warm and cold processes) dominate in both regions. Rainfall generated by mixed processes is overwhelmingly more frequent in both regions.

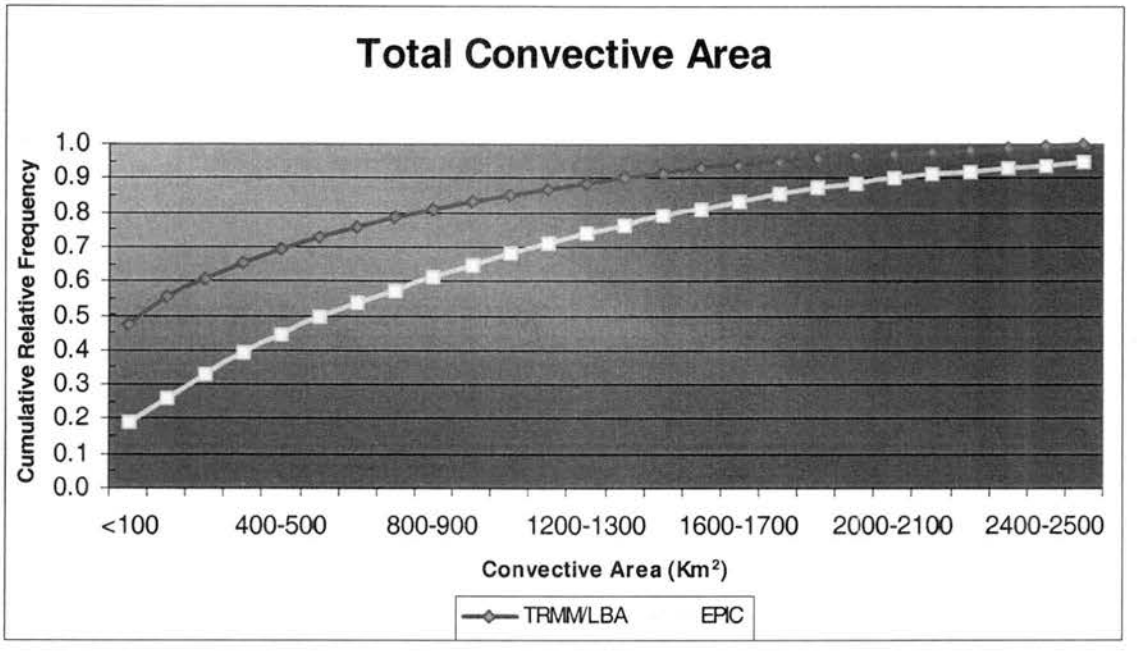

Figure 5.1: Total convective area in the TRMM/LBA and EPIC regions.

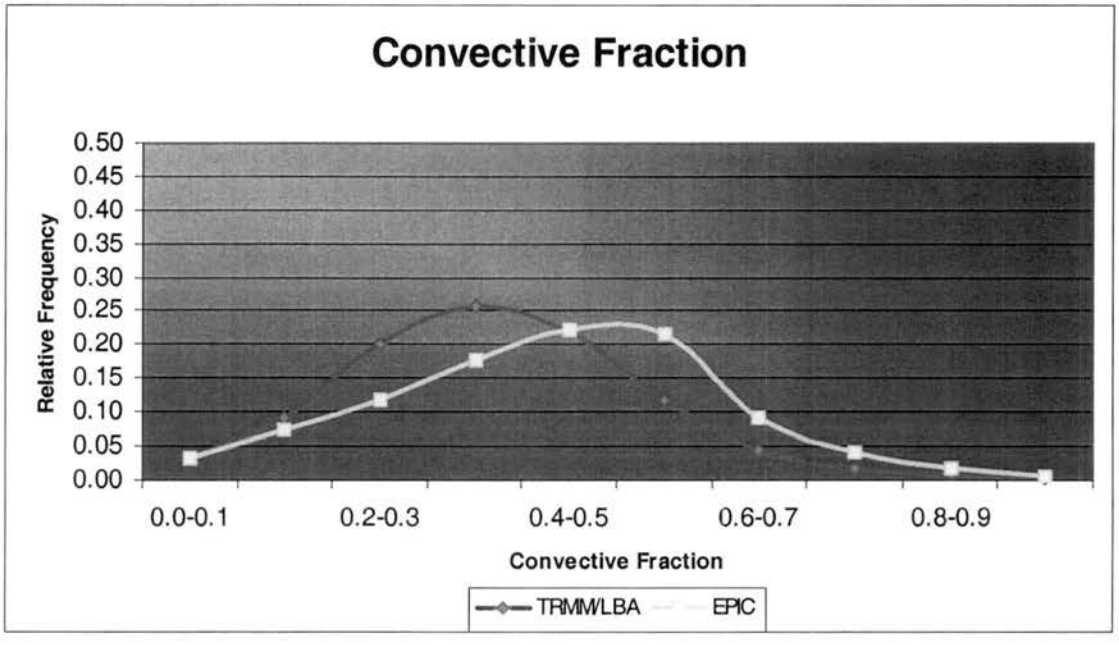

Figure 5.2: Fraction of total echo area associated with convective features in the TRMM/LBA and EPIC regions.

a)

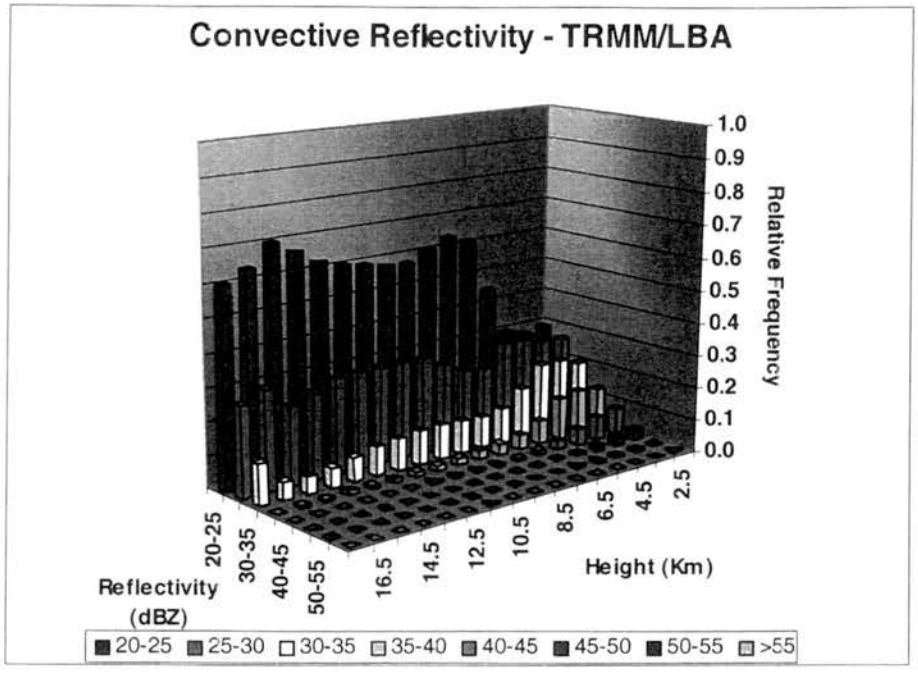

b)

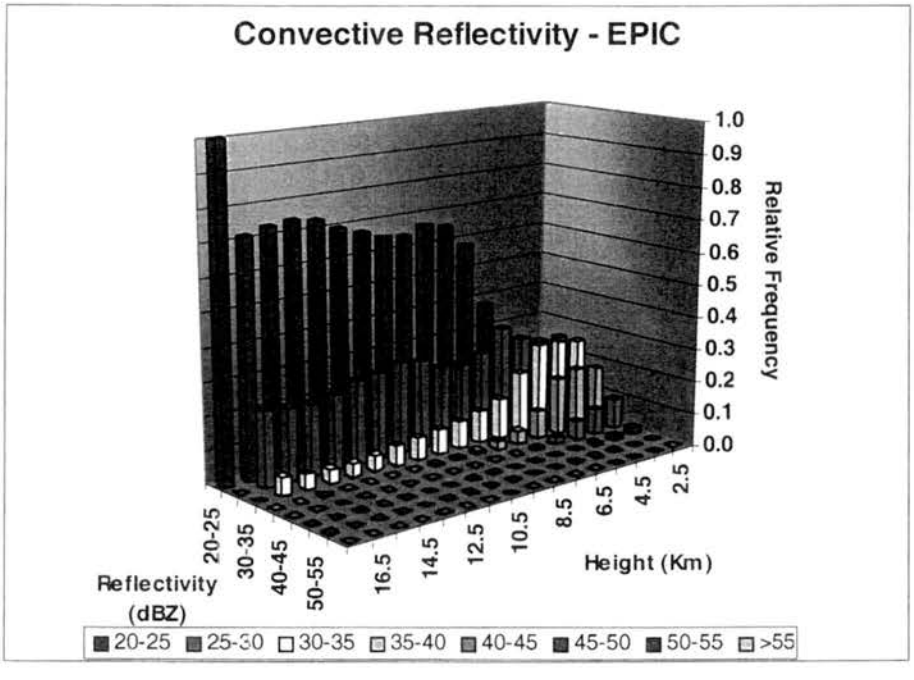

Figure 5.3: Vertical reflectivity distribution in the a) TRMM/LBA, and b) EPIC regions.

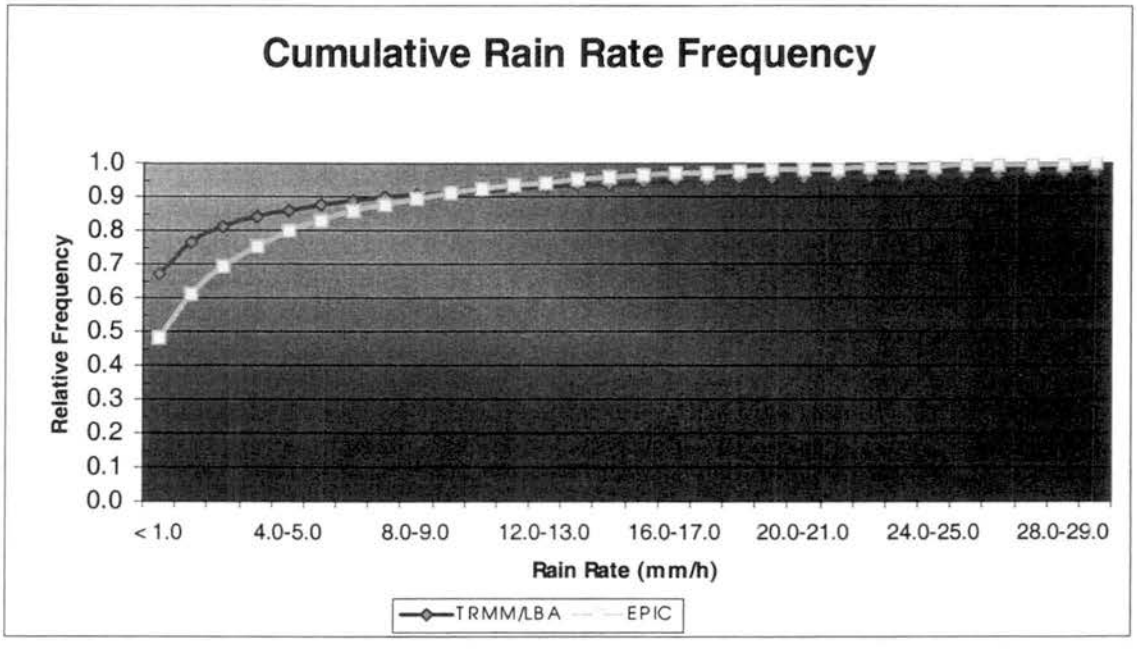

Figure 5.4: Rain rate frequency in the TRMM/LBA and EPIC regions.

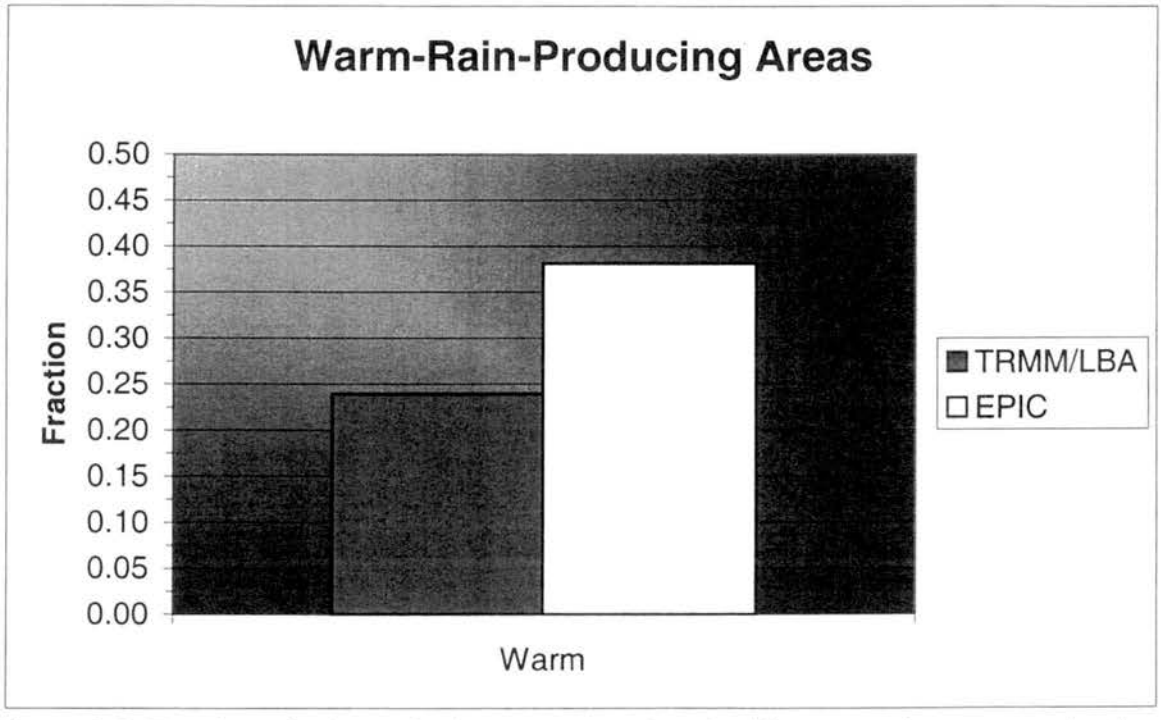

Figure 5.5: Fraction of rain-producing areas associated with warm rain processes in the TRMM/LBA and EPIC regions.

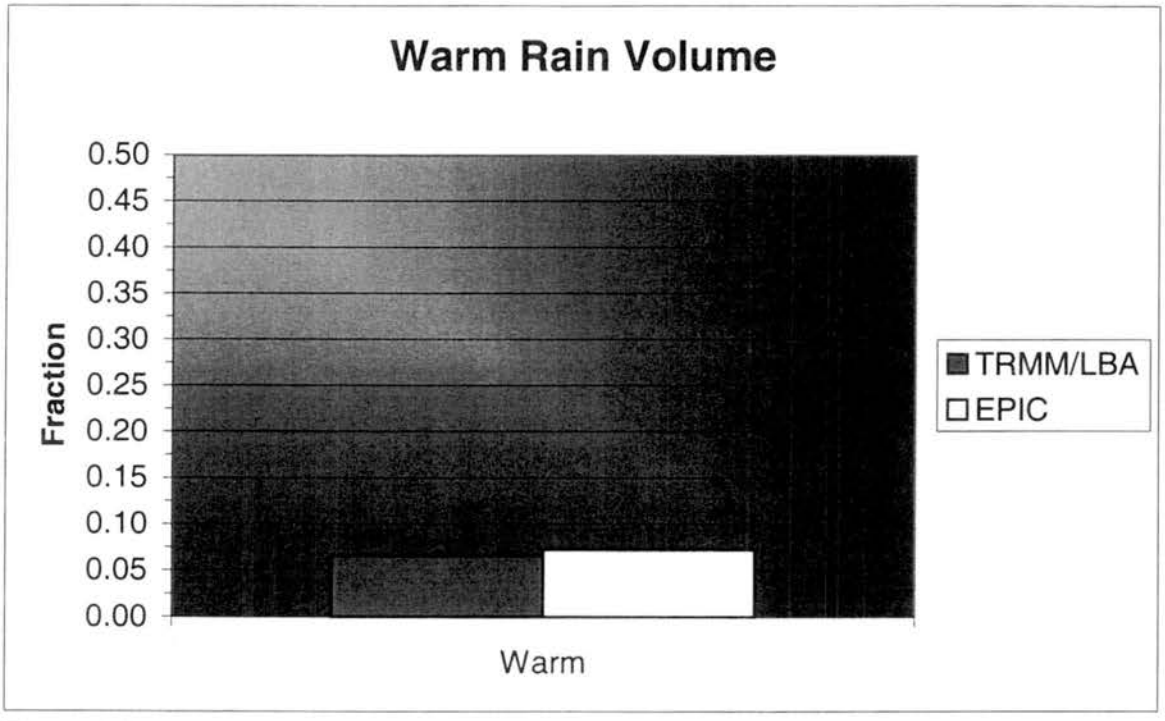

Figure 5.6: Fraction of rainfall volume associated with warm rain processes during the TRMM/LBA and EPIC regions.

CHAPTER SIX

Discussion and Conclusions

6.1 Overview

In this chapter, we discuss the results shown in the previous chapters and offer the conclusions. In the first three sections of this chapter we discuss the results presented in Chapters Three, Four and Five. In the last section, we conclude this study by summarizing the findings of this research. Potential avenues of future research are also discussed in the last section.

6.2 TRMM/LBA Intra-regional Variability Discussion

This section discusses the results shown in Chapter Three, and it is divided into five subsections. The first four subsections will discuss each of the four convection elements studied in the TRMM/LBA region (i.e. horizontal, vertical, precipitation and upper core characteristics). The last subsection summarizes the characteristics and the variability of convection in the southwest Amazon region.

6.2.1 Horizontal Characteristics

Figure 3.1a showed that larger convective areas are more frequent in the westerly regime, and small convective areas (i.e. less than 100 km^2) are 20% more frequent in the easterly regime. This is consistent with previous studies such as Halverson *et al.* (2002)

and Rickenbach *et al.* (2002). Rickenbach *et al.* (2002) discusses the influence of baroclinic waves on the low-level flow over the TRMM/LBA region during the austral summer. In that study, westerly regime events were shown to be a local manifestation of the northwesterly flow along a stationary frontal zone known as the South Atlantic Convergence Zone (SACZ). Liebmann *et al.* (1999) showed that synoptic-scale features, like the SACZ, are responsible for peaks in the outgoing longwave radiation (a proxy for convection strength and size) over the southwestern portion of the Amazon. This corroborates our results showing that larger convective areas are more frequent in the westerly regime. Isolated, small convective features have also been shown in previous studies to be more common in the easterly regime, which supports our findings indicating higher frequency of small convective areas during the same regime (Rickenbach *et al.*, 2002). Figure 3.1b showed that the small convective areas (i.e. less than 100 km^2) are least frequent in the afternoon hours and near sunset. Figure 3.2 showed that there is a lag in minimum and maximum frequency of small total convective areas (i.e. less than 100 km^2) between the wind regimes. In the easterly regime, such range of total convective areas is least frequent near sunset, while in the westerly regime this is observed to occur in the afternoon. Regardless of wind regime, it can be seen that there is a strong diurnal cycle in the total convective area, with largest precipitation features in the afternoon during the westerly regime.

Figure 3.3a showed that there is a higher frequency of larger convective fractions in the easterly regime. Since the easterly regime is associated with smaller convective areas, the larger convective fractions imply that the stratiform precipitation areas are larger in the westerly regime. This is consistent with previous results such as Rickenbach

et al. (2002). Figure 3.3b showed that the larger fractions are more common in the late afternoon to early evening (between 16:00 and 20:00), when 30% of observations indicated that the majority of the precipitation area is convective (i.e. convective area greater than 0.5). The smaller fractions are more predominant in the late night and early morning hours.

6.2.2 Vertical Characteristics

Figure 3.5 showed that, in the easterly regime, strong reflectivities (i.e. greater than 45 dBZ) are more than twice as common as in the westerly regime. Thus, convective clouds in the easterly regime usually have more intense cores than the convective clouds in the westerly regime. These results are consistent with Petersen *et al.* (2002) and Rickenbach *et al.* (2002). Cifelli *et al.* (2002) also observed that mesoscale convective systems (MCSs) in the easterly regime have more intense cores than the MCSs in the westerly regime (Williams, 2002). Figure 3.6 showed that, in the easterly regime, convection was more intense and frequent in two periods of the day: afternoon (Figure 3.6d) and sunset (Figure 3.6e). Hourly distributions (not shown) indicated that the number of convective points and the number of high reflectivity observations peak at 16:00 in the easterly regime. Since one of the day periods used in this study begins at 16:00 (16-20) and one ends just before 16:00 (12-16) the peak results influenced both periods. Therefore, this choice of periods caused the maximum convective activity and strength to appear nearly the same in both periods. However, as mentioned earlier, the convection activity and strength is greatest late in the afternoon (around 16:00). The minimum number of convective points occurs in the morning (Figure 3.6c). The strong

diurnal cycle, observed in the horizontal structure, is also present in the reflectivity distribution. Figure 3.7 showed that, in the westerly regime, convection was more frequent and intense in the afternoon (Figure 3.7d), and weaker and least frequent in the morning. Hourly distributions (now shown) indicated that the peak in distribution occurs between 14:00 and 16:00, indicating that convection peaks earlier in the westerly regime. Thus, the strong diurnal cycle is also clearly present in the westerly regime, but the peak in convective activity and strength during the westerly regime occurs two hours before such peaks in the easterly regime.

Figure 3.8 also shows that the reflectivity heights in the easterly regime have a greater variability over the diurnal cycle than in the westerly regime. The tallest reflectivity features are observed to occur between 16:00 and 17:00 in the easterly regime, in agreement with the reflectivity distributions discussed previously. On the other hand, the westerly regime shows two distinct peaks in reflectivity heights: one at 16:00 for reflectivities greater than 10 dBZ, and another at 20:00 for the 5-dBZ reflectivity height. The first peak is consistent with the reflectivity distributions, but the second peak was not in those distributions. Cloud decks at different heights and partitioning algorithm misinterpretations could serve as possible explanations to this difference, since the averaging nature of this analysis make it more susceptible to such errors. The lowest reflectivity heights are observed to occur near 09:00 (11:00) in the easterly (westerly) regime, also in agreement with previous results.

6.2.3 Precipitation Characteristics

Figure 3.9 showed that light precipitation (i.e. rain rates less than 1 mm/h) is slightly more common in the westerly regime. We also concluded that intense rain rates (i.e. greater than 30 mm/h) in the easterly regime are over twice as frequent as in the westerly regime. This is consistent with the reflectivity distributions, which showed that large reflectivities are more frequent in the easterly regime. Figure 3.10 showed that light precipitation is more frequent in the morning in both wind regimes, but more frequent in the easterly. Light precipitation was least frequent in the afternoon in both wind regimes, but also less frequent in the easterly regime at this time of the day. In the easterly regime, very intense rain rates, such as those greater than 70 mm/h are twice as frequent as in the westerly regime. These results suggest that easterly regime days go through a more intense diurnal cycle, with an explosive growth during the afternoon, which is consistent with larger CIN and CAPE values in the easterly regime (Rickenbach *et al.*, 2002). Halverson *et al.* (2002), Petersen *et al.* (2002) and Rickenbach *et al.* (2002) found similar results indicating more intense rain rates in the easterly regime. Rickenbach *et al.* (2002) also showed that the lightest rain rates occur in the morning and the most intense occur in the afternoon over the southwest portion of the Amazon.

Figure 3.11 showed that the fraction of warm-rain-producing areas is higher in the westerly regime during most of the diurnal cycle. Maximum and minimum fractions occur approximately at the same time of the day in both wind regimes. Maximum fractions are observed late in morning (10:00-11:00) in both regimes. This indicates that at this time, the majority of the convective areas are generating rain through warm processes. This is consistent with the reflectivity distributions that showed that in the morning most of the convection is shallow. Figure 3.11b showed that the volume

associated with warm processes is small compared to the volume of rain associated with mixed processes. Figure 3.11b also showed that the fraction of warm rain volume peaks at 09:00 (04:00) in the easterly (westerly) regime. The easterly regime peak coincides with the maximum fraction of warm-rain areas, whereas the westerly regime peak does not. In the easterly regime, the maximum fraction of warm rainfall is almost directly proportional to the maximum fraction of warm-raining areas. In the westerly regime, the peaks in warm-rain area and warm-rain volume do not appear to be related. Increased warm-rain volume can be produced either by the increase in warm-producing areas or by the increase of warm rain rates. The former (latter) explanation appears to be more likely in the easterly (westerly) regime, since the warm rain areas (do not) increase at the same time as the warm-rain volume.

6.2.4 Upper Core Characteristics

Figure 3.12 showed that mean diameters of supercooled drops in the upper core are usually smaller in the easterly regime. This is probably caused by the greater ice fractions in upper core of convective clouds during the easterly regime. Greater ice fractions would lead to a significant increase in the number of small Z_{dr} values and, thus, small mean drop diameters. Figure 3.13, 3.14 and 3.15 showed that the smallest drop diameters were most (least) frequent near sunset (sunrise) in both wind regimes. Once again, this is most likely explained by the strength of convection over the diurnal cycle, and the greater ice fraction observed near sunset. Figures 3.12 through 3.15 also showed that the mean drop diameter had a larger spread of values when the Bringi and Chandra Z_{dr}- D_0 relationship was used.

Figure 3.16 showed that the easterly regime convective clouds have a higher fraction of ice in their upper cores than the convective clouds in the westerly regime. Ice fractions are highest in the afternoon and near sunset and lowest near sunrise and in the morning. Large fractions of ice in convective clouds can only be maintained in the Tropics with intense updrafts. Hence, the existence of higher (lower) ice fractions near sunset (sunrise) is consistent with the previous results shown in the study, indicating that convection intensity (a proxy for updraft intensity) is highest (lowest) at the same time of the day. These differences in ice fraction, coupled with differences in the vertical structure, would suggest that easterly convective clouds are associated with higher lightning flash rates. Halverson *et al.* (2002) observed that the peak flash rates in the easterly regime vary between 14 and 30 flashes per minute, while in the westerly regime, the peak rates do not exceed 8 flashes per minute.

6.2.5 Summary

Overall, the results presented corroborate previous studies, such as Cifelli *et al.* (2002), Halverson *et al.* (2002), Petersen *et al.* (2002) and Rickenbach *et al.* (2002), that indicated that the easterly regime is associated with more intense convective features than the westerly regime. Higher convective fractions, reflectivities, reflectivity heights, rain rates and ice fractions are more frequent in the easterly regime. Convective clouds in the westerly regime could be described as more widespread, with lower convective fractions, light precipitation, smaller ice fractions and bigger supercooled droplets in the upper core region. These results are also in agreement previous studies indicating that convection in the southwest portion of the Amazon, as it occurs with the rest of the Amazon region, is

strongly modulated by the solar radiation diurnal cycle and the onset of convection through surface heating. It is also consistent with results over other land regions as described by Nesbitt and Zipser (2003).

6.3 EPIC Intra-regional Variability Discussion

This section discusses the results shown in Chapter Four, and it is further divided into four subsections. The first three subsections present each of the three convection elements studied in the EPIC region (i.e. horizontal, vertical and precipitation characteristics). The last subsection summarizes the characteristics and the variability of convection in the Eastern Pacific region.

6.3.1 Horizontal Characteristics

Figure 4.1a showed that larger convective areas are more frequent in the southerly regime and small convective areas (i.e. less than 100 km^2) are 15% more frequent in the northerly regime. This is consistent with previous studies over the eastern Pacific region, such as Serra and Houze (2002), which suggested greater area coverage of rainfall in southerly flow behind the easterly wave through axis. Figure 4.1b shows that the convective area is largest in the late night hours and near sunrise, while the smallest convective areas are observed in the afternoon. Boccippio *et al.* (2002) also observed that the similar pattern over the diurnal cycle in the eastern Pacific region, with few precipitating cells near dusk and increased convection after nightfall. Figure 4.2 showed that small convective areas (i.e. less than 100 km^2) are very infrequent in the southerly

regime (not more than 16% of occurrences), especially between 00:00 and 04:00, when 99% of observations indicated convective areas greater than 100 km^2.

Figure 4.3a showed that the convective fractions are usually higher in the northerly regime. Since the northerly regime is associated with smaller convective areas, the larger convective fractions imply that the stratiform areas are larger in the southerly regime. This is in agreement with Petersen *et al.* (2003). Figure 4.3b showed that the larger convective fractions are more common late at night (00:00 to 04:00), when 42% of observations indicate that the majority of the precipitation area is convective (i.e. convective area greater than 0.5). The smaller fractions are more frequent in the afternoon (12:00 to 16:00). Convective fractions are lowest in the afternoon hours of the southerly regime. This is consistent with results shown over other oceanic regions (Gray and Jacobson, 1977), such as in the western Pacific region during TOGA-COARE (Petersen *et al.*, 1996).

6.3.2 Vertical Characteristics

Figure 4.5 showed that, in the northerly regime, strong reflectivities (i.e. greater than 45 dBZ) are more than three times as frequent as in the southerly regime. Thus, convective clouds in the northerly regime usually have more intense cores than the convective clouds in the southerly regime. This is consistent with Petersen *et al.* (2003), who showed that deeper and more vertically developed convection were more likely to lead the through phase of the easterly waves (i.e. northerly regime) during EPIC. Figures 4.6 and 4.7 showed that, in both regimes, convection was more intense at night (Figure 4.6a and 4.7a) and near dawn (Figure 4.6b and 4.7b). Hourly distributions (not shown)

indicated that the number of convective points and the number of high reflectivity observations peak at 01:00 in the northerly regime, but another secondary peak, and slightly less intense, is also observed at 06:00. Two peaks are also observed in the southerly regime, but they occur one or two hours later in the day. The primary peak is observed at 02:00 and the secondary peak is observed at 10:00. These results are consistent with Boccippio *et al.* (2002). These observations suggest two possible scenarios: 1) there are two independent convective cycles overnight, or 2) there is one single convective cycle overnight, which is affected between 03:00 and 04:00 by mesoscale or regional atmospheric conditions. However, Boccippio *et al.* (2002) suggested that this secondary convective peak did not appear to be directly coupled to boundary layer moist enthalpy. The primary peak in convective intensity is associated with conditional instability, which peaks just prior to midnight, and appears to be driven by surface flux moistening of the boundary layer (Boccippio *et al.*, 2002). In the northerly regime, the minimum number of convective points occurs in the afternoon (Figure 4.6d) and near sunset (Figure 4.6e). In the southerly regime, the minimum in convective intensity is concentrated in the afternoon hours (Figure 4.7d).

6.3.3 Precipitation Characteristics

Figure 4.9 showed that light precipitation (i.e. rain rates less than 1 mm/h) is slightly more common in the southerly regime. We also conclude that intense rain rates (i.e. greater than 30 mm/h) represent less than 1% of observations, regardless of wind regime. Figure 4.10a showed that, during the northerly regime periods, light precipitation is most frequent near dusk and least frequent near dawn. In the southerly regime (Figure

4.10b), light precipitation is most frequent at night (between 20:00 and 00:00) and least frequent near sunrise. This is in agreement with the previous results, which showed that convection is most intense overnight and least intense near dusk. Petersen *et al.* (2003) also indicated that heavy convective precipitation is more likely in the northerly regime. The quantitative numbers shown in Petersen *et al.* (2003) differ somewhat from those presented here. The Z-R relationship used in this study was recently determined based on information collected during EPIC, and before this information was made available, most studies, such as Petersen *et al.* (2003), chose to use the Z-R relationship from the western Pacific warm-pool region (Tokay and Short, 1996). Since the Z-R relationships from the eastern and western Pacific regions are so different, this may be a source of difference between the quantitative results presented here and those presented in Petersen *et al.* (2003).

Figure 4.11 showed that the fraction of warm-rain-producing areas is higher in the southerly regime during most of the diurnal cycle. Warm rain areas are generally associated with shallower convection, and hence, lighter precipitation. Thus, these results are in agreement with the rain rate results, which showed higher frequency of lighter rain rates in the southerly regime. Maximum and minimum warm rain fractions are approximately the same in both wind regimes. There is also a lag of two hours between the northerly and southerly curves, a feature that was also observed in other analyses discussed in this section, such as the vertical structure. Maximum fractions are observed near sunset (at night) in the northerly (southerly) regime. This is consistent with the reflectivity distributions that showed that near dusk most of the convection is shallow. Figure 4.11b showed that the volume associated with warm processes is small compared

to the volume of rain associated with mixed processes. Figure 4.11b also showed that the fraction of warm rain volume peaks at 16:00 (20:00) in the northerly (southerly) regime. The peaks in both regimes coincide with the peaks observed in Figure 4.11a showing the fraction of warm-rain areas.

6.3.4 Summary

Overall, the results presented corroborate previous studies, such as Boccippio *et al.* (2002) and Petersen *et al.* (2003), that indicated that the northerly regime usually generate more intense convective features than the southerly regime and also that the convection initiates near dusk and peaks overnight. This is consistent with other oceanic tropical regions as described by Nesbitt and Zipser (2003). Higher convective fractions, reflectivities and rain rates are more frequent at night during the northerly regime. Convective clouds in the southerly regime could be described as more widespread, with lower convective fractions, lighter precipitation.

6.4 TRMM/LBA-EPIC Inter-regional Variability Discussion

This section discusses the results shown in Chapter Five, and it is divided into four subsections. The next three subsections will discuss each of the three convection elements used compared the TRMM/LBA and EPIC regions (i.e. horizontal, vertical and precipitation characteristics). The last subsection summarizes the characteristics and the variability of convection between the southwest Amazon and the east Pacific regions.

6.4.1 Horizontal Characteristics

Figure 5.1 showed that larger convective areas are more frequent in the EPIC region, and small convective areas (i.e. less than 100 km^2) are 28% more frequent in the TRMM/LBA region. Figure 5.2 showed that there is a higher frequency of convective fractions in the EPIC region. In general, the eastern Pacific region is associated with larger precipitation features than in the southwestern portion of the Amazon.

6.4.2 Vertical Characteristics

Figure 5.3 showed that strong reflectivities (i.e. greater than 45 dBZ) were about twice as common in the TRMM/LBA region. On the other hand, we also found that the convective clouds in the EPIC region are more likely to have intermediate reflectivities (i.e. between 30 and 45 dBZ) in the three lowest vertical levels (2.5, 3.5 and 4.5 km). In the sub-freezing vertical levels (5.5 km and higher), the frequency of intermediate reflectivities is again higher in the TRMM/LBA region. Thus, convective clouds in the eastern Pacific are more likely to have a stronger core, but such cores tend to be much shallower than in the southwestern Amazon region. The convective clouds in the TRMM/LBA region are more likely to have very intense cores, and such cores more frequently extend into subfreezing temperatures, where cold cloud microphysics can also play a role in precipitation characteristics and cloud electrification. Petersen and Rutledge (2001) used LIS (lightning image sensor) data from the TRMM satellite to show differences in convection over the tropics, and they found that the lightning flash density over the Amazon region was slightly higher than over the eastern Pacific warm pool region.

6.4.3 Precipitation Characteristics

Figure 5.4 showed that light precipitation (i.e. rain rates less than 1.0 mm/h) is 19% more frequent in the TRMM/LBA region. We also showed that larger rain rates (i.e. greater than 30 mm/h) are three times more frequent in the TRMM/LBA region. The eastern Pacific region is associated with more moderate rain rates (i.e. between 1 and 15 mm/h), whereas the southwestern Amazon region is associated with more extreme rain rates (i.e. less than 1 mm/h and greater than 30 mm/h).

Figure 5.5 showed that warm-rain-producing areas are 14% more frequent in the EPIC region. This is consistent with the vertical structure results, which showed that convective clouds in the EPIC region are more likely to have shallower cores. These cores usually do not extend into the sub-freezing regions of the atmosphere, so it is more likely that a larger portion of the precipitation areas will be generating rain through warm processes only.

Figure 5.6 showed that the fraction of rainfall owed to warm rain processes is very small compared to the fraction generated by mixed (i.e. warm and cold) processes. In addition to that, fractions of the warm rainfall are almost identical in both regions: approximately 7%. Since there were more warm areas precipitating in the EPIC region, the similar amount of warm rainfall can only be explained by larger rain rates in warm clouds over the TRMM/LBA region.

6.4.4 Summary

Overall, the results presented in this thesis are consistent with previous studies, such as Nesbitt and Zipser (2003) and Petersen and Rutledge (2001). The results

indicated that, overall, the TRMM/LBA region generates more intense convective features than the EPIC region. Lower convective areas, lower convective fractions, and lighter precipitation are more frequent in the TRMM/LBA region. Intense reflectivities and rain rates are also more frequent in the southwestern portion of the Amazon. Convective clouds in the EPIC region could be described as more widespread, but with higher convective fractions, moderate precipitation and reflectivities, shallower cores and also larger areas of warm rain. The vertical structure and the precipitation characteristics vary more between easterly and westerly than between northerly and southerly. The opposite is true for the horizontal structure. In other words, the higher frequency extreme precipitation in the TRMM/LBA region is probably due to the higher frequency of light precipitation in the westerly regime and higher frequency of intense precipitation in the easterly regime. The EPIC rain rates do not vary as much between northerly and southerly, and thus the rain rates tend to be somewhere in the middle of these extremes. The rain rates and vertical structure also vary more over the diurnal cycle in the TRMM/LBA region, which also lead to more extreme values than in the EPIC region. This is consistent with previous works indicating that the diurnal cycle of rainfall over continents is larger than that over the open oceans (Gray and Jacobson, 1977).

6.5 Conclusion

In this study, radar data collected during the TRMM/LBA and EPIC campaigns were used to evaluate the variability of the characteristics of tropical convection in the southwestern Amazon and eastern Pacific regions. Some of the elements used to characterize the convection in each of these regions included: convective area, convective

fraction, vertical reflectivity distributions, rain rates, fraction of total convective area generating warm rain, fraction of convective rainfall owed to warm microphysical processes, mean diameters of supercooled droplets in the upper core region and ice fractions.

This study showed that the southwestern portion of the Amazon undergo a convective diurnal cycle that initiates in morning and peaks in the afternoon, whereas the eastern Pacific warm-pool region has a convective diurnal cycle that initiates after sunset and peaks overnight. Afternoon peaks in the diurnal cycle of convection over land, like in the Amazon, have been linked to boundary layer destabilization caused by daytime insolation (Wallace, 1975; Dai, 2001). The causes for the overnight enhancement in convection are still not well understood and remain a theme currently under discussion (Nesbitt and Zipser, 2003). Several possible mechanisms that drive the diurnal cycle over open ocean areas have been proposed and discussed in different studies, such as Gray and Jacobson (1977), Cox and Griffith (1979) Webster and Stephens (1980), Dudhia (1989), Randall *et al.* (1991), Tao *et al.* (1996), Chen and Houze (1997), Sui *et al.* (1997) and Dai (2001).

In general, convection during the easterly regime of TRMM/LBA tended to more frequently possess characteristics associated with vertically developed clouds: greater rain rates, larger reflectivities, deeper cores, higher ice fractions, smaller fraction of convective areas generating warm rain, smaller total convective areas, but higher convective fractions. Similar characteristics were also observed to be more frequent during the northerly regime over the eastern Pacific region. These results are consistent with previous studies such as Cifelli *et al.* (2002), Halverson *et al.* (2002), Petersen *et al.*

(2002), Petersen *et al.* (2003) and Rickenbach *et al.* (2002). The eastern Pacific region showed a higher fraction of warm-rain-producing areas than over the southwestern Amazon region. Nevertheless, the fraction of total rainfall owed to warm processes was approximately the same in both regions, and is significantly less than the fraction of warm-rain areas. This result suggested that warm rain areas were associated with very light rain rates. This is consistent with Cheng and Houze (1979) who found that convective clouds less than 5 km in depth (i.e. warm rain producers) were associated with a very small portion of the convective rainfall during GATE. They showed that convective clouds that extended well above the freezing level (i.e. mixed rain producers) were associated with the majority of the rain. In this study we showed that over 90% of the rainfall was generated by deep convective features, which generated rain by mixed microphysical processes.

These results point to other possible themes for future research, including the use of a different partitioning algorithm to determine the sensitivity of the results to the partitioning method. It also points to the use of a different methodology to determine the size of individual convective features. Finally, another important possible avenue for future research would be an in-depth study to determine if the eastern Pacific region undergoes two independent convective cycles overnight, or one single convective cycle that is affected between 03:00 and 04:00 by mesoscale or regional atmospheric conditions.

REFERENCES

Augstein, E., H. Riehl, F. Ostapoff, and V. Wagner, 1973: Mass and energy transports in an undisturbed Atlantic trade-wind flow. *Mon. Wea. Rev.*, **101**, 101-111.

Aydin, K., Seliga, T. A., and V. N. Bringi, 1984: Differential radar scattering properties of model hail and mixed phase hydrometeors. *Radio Sci.*, **19**, 58-66.

Aydin, K., and Y. Zhao, 1990: A computational study of polarimetric radar observables in hail. *IEEE Trans. Geosci. Remote Sens.*, **28**, 412-422.

Battan, L. J., 1973: Radar Observations of the Atmosphere. The University of Chicago Press, Chicago, IL.

Betts, A. K., 1975: Parametric interpretation of trade-wind cumulus budget studies. *J. Atmos. Sci.*, **32**, 1934-1945.

Bjerknes, J., 1969: Atmospheric teleconnections from the equatorial Pacific. *Mon. Wea. Rev.*, **97**, 163-172.

Boccippio, D. J., W. A. Petersen, R. Cifelli, and S. A. Rutledge. 2002: Diurnal cycle of convection in the east Pacific ITCZ during EPIC-2001. *Preprints, 25th Conference on Hurricanes and Tropical Meteorology*, San Diego, CA, Amer. Meteor. Soc., 523-524.

Bringi, V.N., and V. Chandrasekar, 2001: Polarimetric Doppler Weather Radar: Principles and Applications, Cambridge University Press, Cambridge, United Kingdom, 636 pp.

Carey, L. D., and S. A. Rutledge, 1996: A multiparameter radar case study of the microphysical and kinematic evolution of a lightning-producing storm. *Meteor. Atmos. Phys.*, **59**, 33-64.

Carey, L. D., and S. A. Rutledge, 2000: The relationship between precipitation and lightning in tropical island convection: A C-band polarimetric radar study. *Mon. Wea. Rev.*, **128**, 2687-2710.

Chen, S. S., and R. A. Houze Jr., 1997: Diurnal variation and life-cycle of deep convective systems over the Pacific warm pool. *Quart. J. Roy. Meteor. Soc.*, **123**, 357-388.

Cheng, C.-P., and R. A. Houze, 1979: The distribution of convective and mesoscale precipitation in GATE radar echo patterns. *Mon. Wea. Rev.*, **107**, 1370–1381.

Cifelli, R., W. A. Petersen, L. D. Carey, and S. A. Rutledge, 2002: Radar observations of the kinematic, microphysical and precipitation characteristics of two MCSs in TRMM-LBA. *J. Geophys. Res.*, **107**, 10.1029/2000JD000264.

Cohen, J. C. P., M. A. F. Silva Dias, and C. A. Nobre, 1995: Environmental conditions associated with Amazonian squall lines: A case study. *Mon. Wea. Rev.*, **123**, 3163–3174.

Conway, J. W., and D. S. Zrnić, 1993: A study of embryo production and hail growth using dual-Doppler and multiparameter radars. *Mon. Wea. Rev.*, **121**, 2511–2528.

Cox, S. K., and K. T. Griffith, 1979: Estimates of radiative divergence during phase III of the GARP Atlantic Tropical Experiment: Part II. Analysis of phase III results. *J. Atmos. Sci.*, **36**, 586-601.

Cressman, G. P., 1959: An operational objective analysis system. *Mon. Wea. Rev.*, **87**, 367--374.

Dai, A., 2001: Global precipitation and thunderstorm frequencies. Part II: Diurnal variations. *J. Climate*, **14**, 1112-1128.

DeMaria, M., 1985: Linear response of a stratified tropical atmosphere to convective forcing. *J. Atmos. Sci.*, **42**, 1944-1959.

DeMott, C. A., and S. A. Rutledge, 1998a: The vertical structure of TOGA COARE convection. Part I: Radar echo distributions. *J. Atmos. Sci.*, **55**, 2730-2747.

DeMott, C. A., and S. A. Rutledge, 1998b: The vertical structure of TOGA COARE convection. Part II: Modulating influences and implications for diabatic heating. *J. Atmos. Sci.*, **55**, 2748–2762.

Dudhia, J., 1989: Numerical study of convection observed during the Winter Monsoon Experiment using a mesoscale two-dimensional model. *J. Atmos. Sci.*, **46**, 3077-3107.

Golestani, Y., V. Chandrasekar, and V. N. Bringi, 1989: Intercomparison of multiparameter radar measurements. *Preprints, 24th Conference on Radar Meteorology*, Tallahassee, FL, Amer. Meteor. Soc., 309-314.

Gray, W. M., and R. W. Jacobson Jr, 1977: Diurnal variation of deep cumulus convection. *Mon. Wea. Rev.*, **105**, 1171-1188.

Greco, S., R. Swap, M. Garstang, S. Ulanski, M. Shipham, R. C. Harriss, R. Talbot, M. O. Andreae, and P. Artaxo, 1990: Rainfall and surface kinematic conditions over central Amazonia during ABLE 2B. *J. Geophys. Res.*, **93**, 17001-17014.

Halverson, J. B., T. M. Rickenbach, B. Roy, H. Pierce, and E. Williams, 2002: Environmental characteristics of convective systems during TRMM-LBA. *Mon. Wea. Rev.*, **130**, 1493–1509.

Herzegh, P. H., and A. R. Jameson, 1992: Observing precipitation through dual-polarization radar measurements. *Bull. Amer. Meteor. Soc.*, **73**, 1365–1376.

Holland, J. Z., and E.M. Rasmusson, 1973: Measurements of the atmospheric mass, energy and momentum budgets over a 500-kilometer square of tropical ocean. *Mon. Wea. Rev.*, **101**, 44-55.

Horel, J. D., A. N. Hahmann, and J. E. Geisler, 1989: An investigation of the annual cycle of convective activity over the tropical Americas. *J. Climate*, **2**, 1388-1403.

Hubbert, J. H., Bringi, V. N., Carey, L. D., and S. Bolen, 1998: CSU-CHILL polarimetric radar measurements from a severe hailstorm in eastern Colorado. *J. Appl. Meteor.*, **37**, 749-775.

Johnson, R. H., T. M. Rickenbach, S. A. Rutledge, P. E. Ciesielski, and W. H. Schubert, 1999: Trimodal characteristics of tropical convection. *J. Climate*, **12**, 2397-2418.

Krishnamurti, T. N., 1971: Tropical east-west circulations during the northern summer. *J. Atmos. Sci.*, **28**, 1342-1347.

Krishnamurti, T. N., M. Kanamitsu, W. J. Koss, and J. D. Lee, 1973: Tropical east-west circulations during the northern winter. *J. Atmos. Sci.*, **30**, 780-787.

Kummerow, C., J. Simpson, O. Thiele, W. Barnes, A. T. C. Chang, E. Stocker, R. F. Adler, A. Hou, R. Kakar, F. Wentz, P. Ashcroft, T. Kozu, Y. Hong, K. Okamoto, T. Iguchi, H. Kuroiwa, E. Im, Z. Haddad, G. Huffman, B. Ferrier, W. S. Olson, E. Zipser, E. A. Smith, T. T. Wilheit, G. North, T. Krishnamurti, and K. Nakamura, 2000: The status of the tropical rainfall measuring mission (TRMM) after two years in orbit. *J. Appl. Meteor.*, **39**, 1965-1982.

Leary, C. A., 1984: Precipitation structure of the cloud clusters in a tropical easterly wave. *Mon. Wea. Rev.*, **112**, 313–325.

LeMone, M. A., and E. J. Zipser, 1980: Cumulonimbus vertical velocity events in Gate. Part I: Diameter, intensity and mass flux. *J. Atmos. Sci.*, **37**, 2444-2457.

Liebmann, B., G. N. Kiladis, J. A. Marengo, T. Ambrizzi, and J. D. Glick, 1999: Submonthly convective variability over South America and the South Atlantic Convergence Zone. *J. Climate*, **12**, 1877-1891.

Lin, X., and R. H. Johnson, 1996: Kinematic and thermodynamic characteristics of the flow over the western Pacific warm pool during TOGA COARE. *J. Atmos. Sci.*, **53**, 695-715.

Lucas, C., E. J. Zipser, and M. A. LeMone, 1994: Vertical velocity in oceanic convection off tropical Australia. *J. Atmos. Sci.*, **51**, 3183-3193.

Madden, R. A., and P. R. Julian, 1994: Observations of the 40-50-day tropical oscillation – A review. *Mon. Wea. Rev.*, **122**, 814-837.

Nesbitt, S. W., and E. J. Zipser, 2003: The diurnal cycle of rainfall and convective intensity according to three years of TRMM measurements. *J. Climate*, in press

Nesbitt, S. W., E. J. Zipser, and D. J. Cecil, 2000: A census of precipitation features in the tropics using TRMM: radar, ice scattering and lightning observations. *J. Climate*, **13**, 4087-4106.

Nitta, T., and S. Esbensen, 1974: Heat and moisture budget analyses using BOMEX data. *Mon. Wea. Rev.*, **102**, 17-28.

Pereira Filho, A. J., M. A. F. Silva Dias, R. I. Albrecht, L. G. Paiva Pereira, A. W. Gandu, O. Massambani, A. Tokay, and S. Rutledge, 2002: Multi-Sensor Analysis of a Squall Line in the Amazon Region. *J. Geophys. Res.*, **107**, 10.1029/2000JD000305.

Petersen, W. A., R. Cifelli, D. J. Boccippio, S. A. Rutledge, and C. Fairall, 2003: Convection and easterly wave structure observed in the eastern Pacific warm-pool during EPIC 2001. *J. Atmos. Sci.*, submitted.

Petersen, W. A., and S. A. Rutledge, 2001: Regional variability in tropical convection: Observations from TRMM. *J. Climate*, **14**, 3566-3585.

Petersen, W. A., S. A. Rutledge, and R. E. Orville, 1996: Cloud-to-ground lightning observations in TOGA COARE: Lightning location algorithms and selected results. *Mon. Wea. Rev.*, **124**, 602-620.

Petersen, W. A., S. W. Nesbitt, R. J. Blakeslee, R. Cifelli, P. Hein, and S. A. Rutledge, 2002: TRMM observations of intraseasonal variability in convective regimes over the Amazon. *J. Climate*, **15**, 1278–1294.

Pruppacher, H. R., and K. V. Beard, 1970: A wind tunnel investigation of the internal circulation and shape f water drops falling at terminal velocity in air. *Quart. J. Roy. Metor. Soc.*, **96**, 247-256.

Pruppacher, H. R., and J. D. Klett, 1997: Microphysics of Clouds and Precipitation. 2nd Ed. Kluwer Academic, 954 pp.

Randall, D. A., Harshvardhan, and D. A. Dazlich: 1991: Diurnal variability of the hydrologic cycle in a general ciculation model. *J. Atmos. Sci.*, **48**, 40-62.

Rao, V. B., and K. Hada, 1990: Characteristics of rainfall over Brazil: annual variations and connections with the southern oscillation. *Theor. Appl. Climatol.*, **42**, 81-91.

Reed, R. J., and E. E. Recker, 1971: Structure and properties of synoptic-scale wave disturbances in the equatorial western Pacific. *J. Atmos. Sci.*, **28**, 1117–1133.

Rickenbach, T.M., R. Nieto Ferreira, J. B. Halverson, D. L. Herdies and M. A. F. Silva Dias, 2002: Modulation of convection in the southwestern Amazon basin by extratropical stationary fronts. *J. Geophys. Res.*, **107**, 10.1029/2000JD000263.

Rickenbach, T. M., and S. A. Rutledge, 1998: Convection in TOGA-COARE: Horizontal scale, morphology, and rainfall production. *J. Atmos. Sci.*, **55**, 2715-2729.

Riehl, H., and J. S. Malkus, 1958: On the heat balance in the equatorial trough zone. *Geophysica*, **6**, 503-538.

Riehl, H., T. C. Yeh, J. S. Malkus, and N. E. LaSeur, 1951: The northeast trade of the Pacific Ocean. *Quart. J. Roy. Meteor. Soc.*, **77**, 598-626.

Rutledge, S. A., E. R. Williams, and T. D. Keenan, 1992: The down under doppler and electricity experiment (DUNDEE): Overview and preliminary results. *Bull. Amer. Meteor. Soc.*, **73**, 3-16.

Serra, Y. L., and R. A. Houze Jr., 2002. Observations of variability on synoptic timescales in the east Pacific ITCZ. *J. Atmos. Sci.*, **59**, 1723–1743.

Silva Dias, M. A. F., S. Rutledge, P. Kabat, P. L. Silva Dias, C. Nobre, G. Fisch, A. J. Dolman, E. Zipser, M. Garstag, A. O. Manzi, J. Fuentes, M. O. Andreae, P. Artaxo, R. Gielow, and L. Gatti, 2002: Cloud and rain processes in a biosphere-atmosphere interaction context in the Amazon region. *J. Geophys. Res.*, **107**, 10.1029/2000JD000335.

Silva Dias, P. L., W. H. Schubert, and M. DeMaria, 1983: Large-scale response of the tropical atmosphere to transient convection. *J. Atmos. Sci.*, **40**, 2689-2707.

Steiner, M., and R. A. Houze Jr., 1993: Three-dimensional validation at TRMM ground truth sites: Some early results from Darwin, Australia, *Preprints, 26th Conference on Radar Meteorology*, Norman, OK, Amer. Meteor. Soc., 417-420.

Steiner, M., R. A. Houze, and S. E. Yuter, 1995: Climatological characteristics of three-dimensional storm structure from operational radar and rain gauge data. *J. Appl. Meteor.*, **34**, 1978-2007.

Sui, C.-H., K.-M. Lau, Y. N. Takayabu, and D. A. Short, 1997: Diurnal variations in tropical oceanic cumulus convection during TOGA-COARE. *J. Atmos. Sci.*, **54**, 639-655.

Szoke, E. J., E. J. Zipser, and D. P. Jorgensen, 1986: A radar study of convective cells in mesoscale systems in GATE. Part I: Vertical profile statistics and comparison with hurricanes. *J. Atmos. Sci.*, **43**, 181-197.

Takahashi, T., 1978: Riming electrification as a charge generation mechanism in thunderstorms. *J. Atmos. Sci.*, **35**, 1536-1548.

Tao, W.-K., S. Lang, J. Simpson, C.-H. Sui, B. Ferrier, and M.-D. Chou, 1996: Mechanisms of cloud-radiation interaction in the tropics and midlatitudes. *J. Atmos. Sci.*, **53**, 2624-2651.

Tokay, A., A. Kruger, W. Krajewski, and A. Pereira Filho, 2002: Measurements of drop size distribution in southwestern Amazon region, *J. Geophys. Res.*, **107**, 10.1029/2001JD000355.

Tokay, A., and D. A. Short, 1996: Evidence from tropical raindrop spectra of the origin of rain from stratiform versus convective clouds. *J. Appl. Meteor.*, **35**, 355–371.

Ulbrich, C. W., 1983: Natural variations in the analytical form of the raindrop size distribution. *J. Appl. Meteor.*, **22**, 1764–1775.

Wallace, J. M., 1975: Diurnal variations in precipitation and thunderstorm frequency over the conterminous United States. *Mon. Wea. Rev.*, **103**, 406-419.

Webster, P. J., and R. Lukas, 1992: TOGA COARE: The coupled ocean-atmosphere response experiment. *Bull. Amer. Meteor.*, **72**, 1481-1505.

Webster, P. J., and G. L. Stephens, 1980: Tropical upper-tropospheric extended clouds: Interferences from winter MONEX. *J. Atmos. Sci.*, **37**, 1521-1541.

Weller, B., B. Albrecht, S. Esbensen, C. Eriksen, A. Kumar, R. Mechoso, D. Raymond, D. Rogers, and D. Rudnick, 1999: A science and implementation plan for EPIC 2001: An eastern Pacific investigation of the climate processes in the coupled ocean-atmosphere system. Available at http://www.atmos.washington.edu/gcg/EPIC/EPIC_rev.pdf.

Williams, A. G., 2002: Kinematic, microphysical and latent heating aspects of two mesoscale convective systems observed during TRMM/LBA. M.S. thesis, Colorado State University, 111 pp.

Williams, E., 1989: The tripole structure of thunderstorms. *J. Geophys. Rev.*, **94**, 13151-13167.

Williams, E. R., D. Rosenfeld, N. Madden, J. Gerlach, N. Gears, L. Atkinson, N. Dunnemann, G. Frostrom, M. Antonio, B. Biazon, R. Camargo, H. Franca, A. Gomes, M. Lima, R. Machado, S. Manhaes, L. Nachtigall, H. Piva, W. Quintiliano, L. Machado, P. Artaxo, G. Roberts, N. Renno, R. Blakeslee, J. Bailey, D. Boccippio, A. Betts, D. Wolff, B. Roy, J. Halverson, T. Rickenbach, J. D. Fuentes, and E. Avelino, 2002: Contrasting convective regimes over the Amazon: Implications for cloud-electrification. *J. Geophys. Res.*, **107**, 10.1029/2001JD00380.

Williams, E., R. Zhang, and D. Boccippio, 1994: Microphysical growth state of ice particles and large-scale electrical structure of clouds. *J. Geophys. Rev.*, **99**, 10787-10792.

Zipser, E. J., and M. A. LeMone, 1980: Cumulonimbus vertical velocity events in GATE. Part II: Synthesis and model core structure. *J. Atmos. Sci.*, **37**, 2458-2469.

Zrnić, D. S., V. N. Bringi, N. Balakrishnan, K. Aydin, V. Chandrasekar, and J. Hubbert, 1993: Polarimetric measurements in a severe hailstorm. *Mon. Wea. Rev.*, **121**, 2223-2238.